The City College
City University of New York
New York, N. Y. 10031

Technical Report

The Effect of Surface Boundary Conditions on the Climate Generated by a Coarse-Mesh General Circulation Model

Charles Cohen

June 1981

NASA, Goddard Space Flight Center
Grant NGR 33-016-086

J. Spar, Principal Investigator

Abstract

An attempt was made to compute the contributions of various surface boundary conditions to the monthly mean states generated by the 7-layer, 8 x 10 GISS climate model. A hierarchy of experiments was run, starting with an all water planet with zonally symmetric sea surface temperatures, then adding, one at a time, flat continents, mountains, surface physics, and realistic sea surface temperatures. The model was run with the sun fixed at a perpetual January.

Ensemble means and standard deviations were computed and the t-test was used to determine the statistical significance of the results.

In addition to subjective examination of maps, the results were evaluated using spherical harmonic analysis.

This paper begins with a comparison of the "flat continents" experiment and the "mountain" experiment. It was found that, although the effects of mountains on the model climatology are generally qualitatively correct, the resulting climate is not always a better simulation of nature.

The addition of realistic surface physics does not affect the model climatology to as large an extent as does the addition of mountains.

Departures from zonal symmetry of the SST field result in a better simulation of the real atmosphere.

Contents

Figures

1a. Observed sea level pressure (SLP)
1b. Observed 500 milliber (mb) height
1c. Observed surface air temperature
1d. Observed precipitation

2a. Mean SLP for run #2
2b. Mean 500 mb height for run #2
2c. Mean surface air temperature for run #2
2d. Mean precipitation for run #2
2e. Mean temperature between 850 mb and 700 mb for run #2
2f. Zonally averaged mean temperature for run #2
2g. Zonally averaged mean zonal wind for run #2
2h. Zonally averaged mean meridional wind for run #2
2i. Zonally averaged mean vertical velocity for run #2

3a. Mean SLP for run #3
3b. Mean 500 mb height for run #3
3c. Mean surface air temperature for run #3
3d. Mean precipitation for run #3
3e. Mean temperature between 850 mb and 700 mb for run #3
3f. Zonally averaged mean temperature for run #3
3g. Zonally averaged mean zonal wind for run #3
3h. Zonally averaged mean meridional wind for run #3
3i. Zonally averaged mean vertical velocity for run #3

4a. Mean SLP for run #4
4b. Mean 500 mb height for run #4
4c. Mean surface air temperature for run #4
4d. Mean precipitation for run #4
4e. Mean temperature between 850 mb and 700 mb for run #4
4f. Zonally averaged mean temperature for run #4
4g. Zonally averaged mean zonal wind for run #4
4h. Zonally averaged mean meridional wind for run #4
4i. Zonally averaged mean vertical velocity for run #4

5a. Mean SLP for run #5
5b. Mean 500 mb height for run #5
5c. Mean surface air temperature for run #5
5d. Mean precipitation for run #5
5e. Mean temperature between 850 mb and 700 mb for run #5
5f. Zonally averaged mean temperature for run #5
5g. Zonally averaged mean zonal wind for run #5
5h. Zonally averaged mean meridional wind for run #5
5i. Zonally averaged mean vertical velocity for run #5

6a. Sea surface temperature (SST) for runs #0 through #4
6b. SST for run #5
6c. SST difference: run #5 - run #4

7a. Mean SLP for run #3 - run #2
7b. Mean 500 mb height for run #3 - run #2
7c. Mean surface air temperature for run #3 - run #2
7d. Mean precipitation for run #3 - run #2
7e. Mean temperature between 850 mb and 700 mb for run #3 - run #2
7f. Zonally averaged mean temperature for run #3 - run #2
7g. Zonally averaged mean zonal wind for run #3 - run #2
7h. Zonally averaged mean meridional wind for run #3 - run #2
7i. Zonally averaged mean vertical velocity for run #3 -

run #2

8a. Mean SLP for run #4 - run #3
8b. Mean 500 mb height for run #4 - run #3
8c. Mean surface air temperature for run #4 - run #3
8d. Mean precipitation for run #4 - run #3
8e. Mean temperature between 850 mb and 700 mb for run #4 - run #3
8f. Zonally averaged mean temperature for run #4 - run #3
8g. Zonally averaged mean zonal wind for run #4 - run #3
8h. Zonally averaged mean meridional wind for run #4 - run #3
8i. Zonally averaged mean vertical velocity for run #4 - run #3

9a. Mean SLP for run #5 - run #4
9b. Mean 500 mb height for run #5 - run #4
9c. Mean surface air temperature for run #5 - run #4
9d. Mean precipitation for run #5 - run #4
9e. Mean temperature between 850 mb and 700 mb for run #5 - run #4
9f. Zonally averaged mean temperature for run #5 - run #4
9g. Zonally averaged mean zonal wind for run #5 - run #4
9h. Zonally averaged mean meridional wind for run #5 - run #4
9i. Zonally averaged mean vertical velocity for run #5 - run #4

10a. Significance level of differences of means for mean SLP for run #2 and run #3
10b. Significance level of differences of means for mean 500 mb height for run #2 and run #3
10c. Significance level of differences of means for mean surface air temperature for run #2 and run #3
10d. Significance level of differences of means for mean precipitation for run #2 and run #3
10e. Significance level of differences of means for mean temperature between 850 mb and 700 mb for run #2 and run #3
10f. Significance level of differences of means for zonally averaged mean temperature for run #2 and run #3
10g. Significance level of differences of means for zonally averaged mean zonal wind for run #2 and run #3
10h. Significance level of differences of means for zonally averaged mean meridional wind for run #2 and run #3
10i. Significance level of differences of means for zonally averaged mean vertical velocity for run #2 and run #3

11a. Significance level of differences of means for mean SLP for run #3 and run #4
11b. Significance level of differences of means for mean 500 mb height for run #3 and run #4
11c. Significance level of differences of means for mean surface air temperature for run #3 and run #4
11d. Significance level of differences of means for mean precipitation for run #3 and run #4
11e. Significance level of differences of means for mean temperature between 850 mb and 700 mb for run #3 and run #4
11f. Significance level of differences of means for zonally averaged mean temperature for run #3 and run #4
11g. Significance level of differences of means for zonally

averaged mean zonal wind for run #3 and run #4

11h. Significance level of differences of means for zonally averaged mean meridional wind for run #3 and run #4

11i. Significance level of differences of means for zonally averaged mean vertical velocity for run #3 and run #4

12a. Significance level of differences of means for mean SLP for run #4 and run #5

12b. Significance level of differences of means for mean 500 mb height for run #4 and run #5

12c. Significance level of differences of means for mean surface air temperature for run #4 and run #5

12d. Significance level of differences of means for mean precipitation for run #4 and run #5

12e. Significance level of differences of means for mean temperature between 850 mb and 700 mb for run #4 and run #5

12f. Significance level of differences of means for zonally averaged mean temperature for run #4 and run #5

12g. Significance level of differences of means for zonally averaged mean zonal wind for run #4 and run #5

12h. Significance level of differences of means for zonally averaged mean meridional wind for run #4 and run #5

12i. Significance level of differences of means for zonally averaged mean vertical velocity for run #4 and run #5

Introduction

General circulation models, including the GISS coarse mesh climate model (Hansen et. al., 1980), are often used to perform "prescribed change" experiments in which some alteration in solar radiation, surface boundary conditions, or atmospheric composition is specified and the atmospheric response, i.e. the effect of the prescribed change on the weather or climate, is calculated. In such experiments, the specified change is usually some small perturbation of the basic constraints on the system, and the computed response of the model may be weaker than the background noise. The analysis of these experiments would undoubtedly be aided by a better understanding of the ways in which the primary climatological controls combine to generate the basic climatic state. In this study, an attempt is made to compute the contributions of various surface boundary conditions to the monthly mean states generated by the 7-layer, 8 x 10 GISS climate model.

For the purposes of the study, such obvious climatic controls as the shape and rotation of the earth, the solar radiation, and the dry composition of the atmosphere are fixed, and only the surface boundary conditions are altered in the various simulations. The model (version 660) is operated at a fixed solar declination, specifically that of January 15, initialized on January 1, and allowed to simulate 25 successive Januaries without going through the annual cycle. Monthly means are computed for each January and for ensembles of all but five Januaries, the first five months being discarded as transients.

The first two experiments in this study, e0 and e1, in which all land is eliminated and zonally uniform sea surface

temperature (SST) and ice coverage patterns are specified, are described in detail in Spar (1981). Briefly, experiment #0 is a water planet spin up, in which the model is initialized with globally uniform mean values of sigma- level specific humidities and temperatures, as well as a constant surface pressure and zero winds.

This paper will begin with experiment #2, in which flat continents are placed on the earth, with zero elevation above sea level, zero water storage capacity, and uniform surface albedo, in order to assess the thermal influence of the land, while the zonal distribution of sea ice and SST remain unchanged over the oceans. The model is again initialized with the same state of rest as in the water planet spin up experiment, and is again run for a period of 25 Januaries, the first five months being discarded. The initial surface albedo of Greenland and Antarctica is that of glacial ice, but snow is allowed to alter both the sea ice and continental albedos as computed by the model.

The effect of mountains on the global model climatology is computed by repeating the last run, but with the correct model terrain elevation restored at each grid point. However, in the "mountain" experiment (run #3) the model is initialized not only with a state of rest, but also with a completely dry and isothermal atmosphere, so that it is required to generate its own humidity and temperature distribution. The ground albedo is still kept uniform over the continents, except where snow is calculated, and the water storage capacity is zero in this mountain run.

The climatic effects of variable surface albedo and water storage capacity over the continents are investigated

through a second perpetual January mountain experiment (run #4) in which realistic surface physics is added, and then the influence of departures from zonal symmetry of the SST field is examined by comparing the results of the previous run with the perpetual January climatology generated by the complete model (run #5) using the actual January climatological SST's.

Model description

The GISS model of the global atmosphere is a three-dimensional primitive equation model using spherical geometry. The model numerically solves the simultaneous equations for conservation of mass, energy, and momentum, and the equation of state. The numerical differencing schemes for the dynamics are based on the work of Arakawa, with a time step of 15 minutes. Radiative heating and cooling are computed with a semi-implicit spectral integration which is accurate throughout the troposphere and stratosphere and includes all significant atmospheric gases, aerosols, and cloud particles. Cloud cover is computed by the model. Convection mixes moisture, sensible heat, and horizontal momentum in the vertical direction based on a model which permits penetration to an arbitrary height. The ground temperature is computed with a method which provides realistic simulation of both the diurnal variation of temperature and seasonal heat storage. Ground moisture is computed with a two layer model; the wetness of the upper layer responds rapidly to evaporation and precipitation while the deeper layer has a water holding capacity appropriate for the root zone of the regional vegetation.

Snow depth is computed over land and ice with a simple mass budget model. Fluxes of sensible heat, moisture, and momentum between the surface and atmosphere are obtained from a drag-law formulation which employs a parameterization of the Monin-Obukhov similarity functions. Sea surface temperature and sea ice coverage are specified seasonally-varying boundary conditions.

The model uses a grid of 24 points of latitude by 36 points of longitude, or about 8 x 10 degrees. This coarse horizontal resolution results in computing times an order of magnitude less than normally employed in general circulation models, allowing simulations of long time periods. To compensate for the great distance between grid points, the specified surface condition for each grid point represents appropriate fractions of land and ocean. Interactions between the surface and the atmosphere (radiation, momentum transfer, and latent and sensible heat fluxes) are computed separately for each surface type.

The seven vertical layers use a sigma coordinate, so that the ground is a coordinate surface. The top of the dynamically active portion of the atmosphere is fixed at 10 mb; the atmosphere above is radiatively interactive with the lower levels, with the temperature profile above 10 mb determined by radiative equilibrium.

Methods of data analysis

The fields we have selected for examination are the horizontal maps of 500 millibar (mb) height, sea level pressure (SLP), the average temperature in the layer between 850 mb and 700 mb, precipitation and surface temperature, and meridional cross sections of zonal means of temperature and the three components of the wind.

To supplement the subjective analysis of these fields, the spectral components of the first three horizontal maps listed above are examined using the method of spherical harmonic analysis described in Christidis and Spar (1981). Table 1 lists the degree (n) and order (m) of the ten leading harmonics (with the exception of the 0,0 component, which represents the global mean value) of SLP, layer temperature, and 500 mb height for runs #2, #3, #4, and #5. For the n,m-th harmonic, m is the zonal (longitudinal) wave number, while n-m represents the number of nodal parallels. Also tabulated are the amplitude (A), in physical units, and the phase angle (b), in degrees, of each harmonic.

As in Chervin (1980a and 1980b), the results are analyzed by computing, for each experiment, ensemble means and ensemble standard deviations of the 20 Januaries. These statistics are then used to calculate, with the standard Student's t-test, the confidence levels at which the ensemble means of each pair of experiments can be judged to be significantly different.

The test variate, t, is defined, as in Chervin and Schneider (1976), to be

Table 1

Comparison of dominant spherical harmonic components
(See text for details)

SLP (mb)

run #2				run #3				run #4				run #5			
n	m	A	b	n	m	A	b	n	m	A	b	n	m	A	b
4	0	10.0	180	1	0	11.4	0	1	0	11.8	0	1	0	10.1	0
2	0	5.9	180	4	0	7.5	180	4	0	7.6	180	4	0	10.0	180
1	1	5.4	155	1	1	7.0	167	2	0	5.2	0	2	0	6.6	0
3	2	5.2	230	2	0	6.9	0	8	0	4.4	0	3	2	4.7	217
4	4	4.2	306	3	2	5.1	234	3	2	4.3	219	2	1	4.4	96
5	4	3.6	136	4	4	4.7	296	3	0	4.0	0	4	2	4.0	171
3	3	3.6	286	3	0	4.7	0	1	1	3.9	152	3	1	3.8	108
2	2	3.6	154	5	4	4.6	124	2	1	3.6	87	2	2	3.3	167
2	1	3.3	96	5	2	4.5	127	5	2	3.4	143	8	0	3.2	0
3	0	3.2	180	8	0	4.3	0	4	2	3.3	159	5	2	3.2	159

temperature between 850 mb and 700 mb (K)

run #2				run #3				run #4				run #5			
n	m	A	b	n	m	A	b	n	m	A	b	n	m	A	b
2	0	39.9	180	2	0	42.1	180	2	0	40.4	180	2	0	40.4	180
1	0	14.1	180	1	0	16.6	180	1	0	16.4	180	1	0	16.7	180
8	0	3.4	180	6	0	4.0	0	8	0	3.1	180	6	0	4.8	0
3	2	3.1	55	8	0	3.7	180	3	2	2.7	42	3	1	3.5	311
1	1	3.1	341	1	1	3.6	4	6	0	2.7	0	2	1	3.2	327
6	0	2.3	0	3	2	3.5	62	6	2	2.7	33	3	2	3.0	60
4	4	2.2	127	6	2	2.8	27	7	0	2.7	180	6	2	2.7	46
2	2	2.2	339	4	1	2.8	283	4	1	2.6	289	8	0	2.6	180
7	0	2.0	180	5	4	2.7	308	4	2	2.5	3	4	1	2.5	328
2	1	2.0	278	4	4	2.6	116	3	0	2.5	180	5	2	2.4	30

500 mb height (meters)

run #2				run #3				run #4				run #5			
n	m	A	b	n	m	A	b	n	m	A	b	n	m	A	b
2	0	886	180	2	0	836	180	2	0	830	180	2	0	819	180
1	0	293	180	1	0	264	180	1	0	262	180	1	0	286	180
4	0	96	180	4	0	96	180	4	0	96	180	4	0	93	180
8	0	55	180	6	0	74	0	6	0	60	0	6	0	87	0
7	0	49	180	8	0	44	180	7	0	56	180	4	1	56	1
6	0	49	0	7	0	43	180	6	2	41	42	3	1	51	330
3	0	34	180	6	2	39	38	5	2	41	44	2	1	51	351
15	0	25	0	5	2	34	31	4	2	38	20	5	1	47	357
4	2	24	21	7	2	32	48	8	0	37	180	5	2	46	54
7	1	23	85	5	3	32	237	3	0	33	180	6	2	46	58

$$t = \left[\frac{1}{n_1}\sum_{i=1}^{n_1} x_i - \frac{1}{n_2}\sum_{i=1}^{n_2} y_i\right] \Big/ \left[s^2\left(\frac{1}{n_1} + \frac{1}{n_2}\right)\right]^{1/2}$$

with the combined estimate of variance s^2 given by

$$s^2 = \left[\sum_{i=1}^{n_1}(x_i-\bar{x})^2 + \sum_{i=1}^{n_2}(y_i-\bar{y})^2\right] / (n_1+n_2-2),$$

where

$$\bar{x} = \sum_{i=1}^{n_1} x_i / n_1, \quad \bar{y} = \sum_{i=1}^{n_2} y_i / n_2,$$

x_i and y_i are monthly averages at a particular grid point, and n_1 and n_2 are the number of Januaries in the experiments.

The number of degrees of freedom, v, is defined by

$$v = n_1 + n_2 - 2.$$

The level of significance, Q, is calculated from

$$Q = 1 - \int_{-t}^{t} f(z)\,dz$$

where

$$f(z) = \frac{\Gamma\left(\frac{v+1}{2}\right)}{\sqrt{\pi v}\,\Gamma\left(\frac{v}{2}\right)} \cdot \left(1 + \frac{z^2}{v}\right)^{-\frac{v+1}{2}} \qquad \text{for } -\infty < z < \infty$$

The gamma function is defined by

$$\Gamma(v) = \int_0^\infty z^{v-1} e^{-z}\,dz$$

Contour maps and cross-sections of Q are then plotted with contour lines for Q=.01, .05, and multiples of 0.10. On these maps and cross-sections, large continuous areas where the differences between the ensemble means are significant at the 1% level appear as clear areas, and areas where the differences are not significant --where the "signal" cannot be seen through the "noise"-- are generally covered with closely spaced contour lines for Q in multiples of 0.10. In a few cases small clear areas appear in regions that show no statistically significant difference, necessitating numerical labels on the contour lines.

The maps and cross-sections of significance levels should be examined in conjunction with the maps of differences between ensemble means, since there can, of

course, be no statistical significance where the means are exactly equal. Statistical significance is a result of a difference between two ensemble means that is large compared to the ensemble standard deviations; therefore, there can be some cases where differences too small to be physically interesting are nevertheless statistically significant, and some cases where very large differences are not significant.

1. The effects of mountains: differences between run #2 and run #3

a. Horizontal fields

In run #2 the SLP map (fig. 2a) shows highs over Northern Hemisphere continents and lows over those in the Southern Hemisphere, except for Antarctica, where the SLP of 1005 mb is about the same as on the surrounding oceans. Pressure gradients are generally small and on the Northern Hemisphere continents pressures are weaker than observed (fig. 1a). The Siberian and Canadian highs are centered around 35 N, the Aleutian low is at the Bering Strait, and for the Icelandic low the 995 mb isobar stretches from Scandinavia almost to Greenland.

In run #3 (fig. 3a) SLP gradients are larger and the pattern is more cellular. The pressure is increased over the Arctic Ocean and the Northern Hemisphere continents, particularly over Greenland, where the elevated glacier generates extremely low temperatures and, hence, excessively high sea-level pressures due to the method of reducing station pressures to sea level.

In the SLP field of run #3, the Icelandic low is shifted toward the southwest, south of Greenland, relative to that of run #2, in agreement with the observed climatology, and the Aleutian low is similarly shifted to the southern end of the Kamchatka peninsula. Thus, the two lows are blocked by the mountainous continents from affecting the atmosphere above the Arctic Ocean, in contrast to run #2, where the SLP in the Arctic is too low. The westward shift of the Aleutian low in run #3 allows the Canadian high to extend, correctly, northwest towards Alaska. (Compare figs. 2a and 3a with fig. 1a.)

In run #3 the Siberian high is intensified and shifted northward by the terrain effect, as in Manabe and Terpstra (1974), allowing the increase, noted below, in the precipitation in eastern China. This is qualitatively realistic but excessive in magnitude. (Compare figs. 2a and 3a with fig. 1a.)

In the Southern Hemisphere, SLP is decreased over Africa and South America, and lows appear over the highest mountains of Antarctica, between about 20 E and 90 E. West of Chile the high pressure cell is intensified, while east of Argentina the high covers a smaller area in run #3 than run #2.

The 500 mb map for run #2 (fig. 2b) shows patterns that are generally zonally symmetric outside of the tropics. In run #3 (fig. 3b) the ridge at northwestern Europe and the trough north of Japan are clearly visible, in agreement with the observed climatology. Over Antarctica, on the other hand, the 500 mb pattern has become excessively cellular in run #3. (Compare fig. 3b with fig. 1b.)

In the Southern Hemisphere the 500 mb heights show small differences in middle latitudes when mountains are included (fig. 7b), in agreement with the results of Manabe and Terpstra (1974).

The 500 mb map for run #3 shows flow around the Himalayas which is absent in run #2.

Errors in the 500 mb heights of the model compared to the observed climatology similar to those noted in Christidis and Sper (1981) (i.e. a contour pattern that is too cellular over southern Asia and too diffluent in the

eastern North Atlantic) appear in run #3 but are not seen in run #2.

The increased intensity of the high sea-level pressure cell west of Chile in run #3 can also be seen in the shorter wavelengths at the same location on the 500 mb map (figs. 3a and 3b).

The surface temperature map for run #2 (fig. 2c) shows warm areas centered around 25 S on the continents and low temperatures on the Northern Hemisphere continents. Temperatures on the oceans are zonally symmetric, in accordance with the sea surface temperatures which are fixed boundary conditions (fig. 6a). The map for run #3 (fig. 3c) shows changes over the continents that are mainly in magnitude. An exception is the zonal gradients that appear on Antarctica in run #3.

For both runs, the maps of temperature in the layer between 850 mb and 700 mb (figs. 2c and 3c) show warm air over South America, Africa, and Australia. For the Northern Hemisphere in run #2 gradients are small and the continental lows are weak compared to those of run #3.

The air at the surface of the southern hemisphere continents is generally colder in run #3 than in run #2 (fig. 7c) as a result of the higher altitude. However the layer temperature (fig. 7a) is higher over all the continents of the summer hemisphere,except for a small part of Antarctica, due to the elevation of the continental heat source.

The excessively large gradients of temperature in the lower troposphere south of the Himalayas in run #3 (fig. 3a) are absent in run #2 (fig. 2a). The difference map (fig.

7e) shows colder air in run #3 over the highest part of the Himalayas and warmer air in the surrounding areas.

In high latitudes over Eurasia and Canada the temperature at the surface (fig. 7c) and in the lower troposphere (fig. 7e) is lower in run #3 due to both the higher altitude and the dry initialization; over the Arctic Ocean, without the altitude effect, the temperature is lower by a smaller amount. Therefore, over the Arctic Ocean, in run #3, with its very high SLP relative to run #2 (fig. 7a) and its only slightly lower temperature, the 500 mb height (fig. 7b) remains higher than in run #2, whereas over the surrounding continents where the SLP difference is not as great (fig. 7a), the very low temperature causes a large pressure decrease with height, so that the 500 mb level is lower.

Precipitation in both run #2 (fig. 2d) and run #3 (fig. 3d) is concentrated on the continents in the tropics; nearly all of North America and Asia have less than 2 mm per day of precipitation. An exception is the precipitation maximum in eastern China in run #3, already explained in connection with the SLP pattern.

In run #3, the area of maximum precipitation in South America is intensified, shifted southward, and expanded in longitudinal extent. Two different factors combine to explain this.

In run #3 the subtropical high in the South Atlantic is made unrealistically small (figs. 3a and 1a), with a consequently decreased effect on the southeastern part of South America. This allows the ITCZ to move too far south and the precipitation to be excessive (figs. 3d and 1d).

In addition, as explained in Manabe and Holloway (1970), the Andes act as a barrier preventing dry air originating in the subtropical high off the coast of Chile from penetrating into the interior of the continent. Maps of the surface winds verify this, showing the moist northeast trades in run #3 covering a larger area over the continent, bringing rain west of 60 W.

The area of maximum rainfall in the southern half of Africa is intensified and tilted towards a southwest-northeast orientation in run #3 (fig. 3d), in line with the mountains.

Over the northern part of Australia the area of maximum rainfall is shifted toward the plateau in the western half of the continent; the narrow eastern highlands, which cause an actual rainfall maximum, are not resolved by the coarse grid of this model.

Orographic precipitation is also present in New Guinea.

Areas of statistical significance are generally scattered. The largest continuous area of significance is in the tropics, Asia, and high northern latitudes for SLP (fig. 10a). Surface air temperature differences are generally significant only on the continents (fig. 10c), as might be expected since sea surface temperatures are a fixed boundary condition. Otherwise, large differences in regional climatology that result from the addition of mountains to the model are statistically significant over all or part of each region in question (Compare figs. 7b and 10b, figs. 7d and 10d, figs. 7e and 10e.)

It is interesting to notice here the isolated area in the northwest Pacific, where the Aleutian low is located in

run #3 (fig. 3a), for which there is no statistically significant difference. The large scale increase in pressure (fig. 7a) combines with the shifted high and low centers (figs. 2a and 3a) to result in no net change.

b. spherical harmonic analysis

For all fields the dominance of a few large-scale harmonics is greatly decreased in run #3, reflecting the more cellular patterns. None of the mean values are changed.

For SLP run #3 shows a dominant 1,0 harmonic which does not appear among the leading harmonics of run #2, indicating the correct excess of mass in the winter hemisphere in run #3, but also the SLP reduction from elevated terrain. The appearance of the 1,0 harmonic in run #3 combined with the higher magnitude and reversal of phase of the 2,0 harmonic reflects the unrealistically low pressure in the Arctic in run #2, with no corresponding gradient in the southern hemisphere. The higher pressure in high northern latitudes and the lower pressure in mid-latitudes and subtropics is reflected in the stronger 3,0 harmonic in run #3. This pressure gradient can also be seen in the decreased magnitude of the 4,0 harmonic with its 180 phase, which signifies highs over mid-latitudes and lows at the equator and at the poles.

Larger east-west differences in run #3 are reflected in the stronger 1,1 harmonic. Finally, for SLP, the 3,2 harmonic does not change, while the 4,4 increases in magnitude.

For the 500 mb height, the first three harmonics, 2,0,

1,0, and 4,0, are nearly the same for both runs. The main difference in the next three, 6,0, 7,0, and 8,0, is the larger amplitude for the 6,0 harmonic which reflects the lower elevation over Canada and Siberia and the higher elevation over the Arctic and the Himalayas.

Increased effects of the continents in run #3 are shown by more dominant 5,2, 6,2, and 7,2 harmonics for the 500 mb height. The 1,0 and 3,0 harmonics for the 500 mb height are weaker, indicating a decreased difference between the north and south poles; in addition, a weaker 2,0 harmonic reflects a smaller polar-equatorial contrast. The 4,0 harmonic remains the same.

For the 850 mb to 700 mb layer temperature the 1,1 harmonic has a larger magnitude in run #3, representing the greater contrast between the continents and the Pacific Ocean; also larger in run #3 is the 4,1 harmonic, corresponding to the higher temperatures in run #3 over Greenland, southern Asia, South America, and the eastern half of Antarctica.

The larger 1,0 and slightly larger 2,0 harmonics in the layer temperature for run #3 combine to reveal a north-south temperature gradient in the winter hemisphere, possibly due to the dry initialization.

For the 850 mb to 700 mb layer temperature run #3 shows a larger 6,0 harmonic, reflecting the warmer air at 30 N and 30 S and the colder air at 60 N. Also, the 8,0 and 3,2 harmonics are larger in magnitude but they have moved down in rank.

c. meridional cross-sections

The meridional cross-sections of zonal means of zonal wind for run #2 (fig. 2g) and run #3 (fig. 3g) are qualitatively similar. One difference is the weaker mid-latitude westerlies in run #3 in the Northern Hemisphere, but not in the Southern Hemisphere, in accordance with the exchange of angular momentum between the earth and the atmosphere due to the torque exerted by mountain ranges, explained by White (1949). This is negated somewhat below 200 mb by the excessively cold air at high latitudes over the continents, according to the thermal wind equation. Even larger in magnitude is the difference in the Arctic stratospheric westerlies, which are weaker in run #3 (fig. 7g), due to the deviation of the jet stream from an otherwise almost symmetric pattern as a result of flow around the mountains, in agreement with the results of Kasahara et. al. (1973).

The tropical easterlies are stronger in run #3, especially around 200 mb, due to the convective heating that results from the intensified Southern Hemisphere Hadley cell.

The cross-sections of temperature are similar for run #2 (fig. 2f) and run #3 (fig. 3f); throughout most of the atmosphere the differences are less than 2 degrees (fig. 7f). Larger differences occur in the stratosphere, particularly over the Arctic, where run #3 is as much as 10 degrees warmer. The atmosphere of run #3 is also warmer in the Southern Hemisphere, especially over Antarctica, due to the elevation of the continental heat source. The pattern of temperature differences in the stratosphere results in the temperature gradients required by the thermal wind relationship for consistency with the differences in zonal

wind discussed above. (Compare figs. 7f and 7g.)

The stronger Southern Hemisphere Hadley cell in run #3 is evident in the cross-sections of meridional wind (figs. 2h and 3h), which show a more intense circulation for run #3 than for run #2. Above about 800 mb, run #3 shows a southward shift of the ITCZ and of the corresponding divergence zone in the upper atmosphere, consistent with the earlier discussion of the precipitation in South America. The higher Arctic SLP for run #3, also noted above, can be inferred from the appearance of southerly winds at the surface centered around 70 N.

The cross-section of vertical velocity for run #2 (fig. 2i) shows two distinct Hadley cells with the ascending branches equal in intensity but with the Northern Hemisphere descending branch stronger than its southern counterpart. In run #3 (fig. 3i) the Southern Hemisphere Hadley cell has grown while the ascending branch of the northern cell has weakened. This intensification of the southern branch of the Hadley circulation is a result of the indirect role of the Andes mountains in increasing the precipitation in South America, as discussed above, since the highest part of the Andes is between 10 S and 30 S, where the difference cross-section shows an increase in vertical velocity.

The descending air in the northern hemisphere has broken into two cells in run #3, extending further north. This combines with the appearance of an area of subsidence over the Arctic in run #3, consistent with the higher surface pressure, to cause a narrowing and strengthening of the ascending cell centered at 67 N. There is also a large increase in the subsidence over Antarctica, especially in

the upper atmosphere (fig. 7i), due to the outflow from the high pressure area created by the heating from the elevated continent. This can also be seen on the difference cross-section for meridional wind (fig. 7h).

All the differences in temperature are statistically significant; the areas of insignificance on the significance cross-section (fig. 10f) follow the zero isopleths on the difference cross-section (fig. 7f).

The correspondence between the areas of insignificance for zonal wind (fig. 10g) and the zero isopleth on the difference cross-section for zonal wind (fig. 7g) is not as close. Differences are significant north of 30 S in the stratosphere, and in the troposphere only where the differences are larger than about 1.5 or 3.0 meters per second.

The major differences in meridional wind and vertical velocity are statistically significant (figs. 10h and 10i), except for parts of the increase in subsidence over Antarctica.

II. The effects of surface physics: differences between run #3 and run #4

a. horizontal maps

The warm areas on the Southern Hemisphere continents on the surface temperature map for run #3 (fig. 3c) are greatly weakened in run #4 (fig. 4c), due to the increased evaporation, resulting in smaller zonal temperature gradients. The difference map (fig. 8c) shows colder air on all the continents between 45 S and 45 N, warmer air on the continents between about 45 N and 70 N, and colder air over the Arctic.

The snow cover in run #4 reaches further south than in run #3; the colder area near Afghanistan in run #4 (fig. 8c) is caused by the higher albedo resulting from the more extensive snow cover.

Several different factors combine to influence the temperature over the continents north of 45 N. The numerous but small differences in humidity, precipitation, and cloudiness, which effect the radiation balance and the convective heating, and in the exchange of heat with the earth's surface, are not sufficient to explain the differences in temperature, and in some areas indicate an influence opposite to the net difference in temperature. It is likely, therefore, that the differences in temperature at high latitudes result from a greater transport of heat from low and middle latitudes.

The SLP pattern is qualitatively similar in run #4 (fig. 4a) and run #3 (fig. 3a), with the highs and lows remaining at nearly the same locations. The largest differences are in the magnitudes of the Southern Hemisphere continental lows (fig. 8a), which show higher pressure in

run #4, closer to the observed values (fig. 1a), due to the smaller differences in temperature between land and sea at this latitude resulting from evaporative cooling on the continents. Southern Hemisphere zonal SLP gradients have generally decreased, with the high pressure cells slightly weaker. The high west of Chile, however, has somewhat larger meridional pressure gradients.

Similarly, in the Northern Hemisphere, the Aleutian low, which is slightly weaker in run #4, is located in an area of smaller zonal land-sea temperature gradients. The Siberian high in run #4 (fig. 4a) is more concentrated at its center near 40 N than in run #3 (fig. 3a), coinciding with the area of lower surface temperature (fig. 8c).

The map of temperature, for run #4, in the layer between 850 mb and 700 mb (fig. 4a) shows the same weakening of the Southern Hemisphere continental warm areas as does the surface temperature map (fig. 4c). The difference map for the layer temperature (fig. 8a) also resembles the surface temperature map (fig. 8c) except that the warm belt around 60 N is weaker over Eurasia and more concentrated at the western side of the continent.

The 500 mb map for run #4 (fig. 4b) shows generally the same pattern as in run #3 (fig. 3b). Noticeable changes include the slightly less diffluent pattern in the North Atlantic and the greater zonal symmetry over southern Asia, partial reversals of the unrealistic features in run #3 that were noted in the previous section. Also showing a somewhat greater zonal symmetry is the short wave pattern west of Chile. However, the stronger low in eastern Europe, north of the Black Sea, is not in agreement with observation (fig.

1b).

The large areas of lower elevation on the 500 mb difference map (fig. 8b) are due to the colder air in the lower troposphere (fig. 8a). Lower elevation occurs over the Southern Hemisphere continents in a belt near 25 S, over the Arctic, and over most of Asia, coinciding with the lower temperature in the layer from 850 mb to 700 mb. Similarly, the elevation is higher over northern Europe and western Canada, where the air is warmer.

The map of precipitation for run e4 (fig. 4d) shows maximums close to those of run e3 (fig. 3d), with an additional maximum at Indonesia. Increased evaporation over land is the dominant cause of the greater precipitation in run e4. Over Australia the higher evaporation more than compensates for the higher albedo, in contrast to New Guinea where a lower albedo accompanies the increased precipitation.

In run e4 the tropical Pacific shows a stronger and more concentrated belt of precipitation around 4 N. This is caused by the higher humidity the northeast trades gain in their passage over Mexico and Central America, where the evaporation is much larger in run e4 than in run e3, resulting in greatly enhanced cumulus convection downwind in the tropical Pacific. Since the southeast trades of the Southern Hemisphere have no such warm continental moisture source, the ITCZ is shifted northward over the ocean.

In South America the map for run e3 shows two precipitation maximums; in run e4 the eastern maximum has weakened while the western maximum has strengthened and moved southward. Because of the weaker subtropical high pressure cells east and west of South America, the southeast

trades are weaker, allowing the northeast trades to penetrate further into the continent, moving the ITCZ toward the southwest in South America. In addition, precipitation has generally increased in the northern half of the continent (fig. 8d), due to the higher evaporation.

The area of maximum precipitation in Africa has moved southward and eastward in run #4. The precipitation in run #3 is orographic in Africa, caused by the converging monsoon winds; in run #4, where the winds are weaker due to the weaker high pressure cells, the greatly increased evaporation over land, especially at the southeast part of the continent, is a controlling factor.

The large differences in temperature between run #3 and run #4 at the surface and in the layer between 850 mb and 700 mb are all statistically significant except for the higher temperature north of 45 N in run #4, which is significant only in small areas. (Compare fig. 11c with fig. 8c, and fig. 11e with fig. 8e.)

Similarly, the differences in SLP and 500 mb height are statistically significant in low latitudes, but only in scattered areas at higher latitudes. (Compare fig. 11a with fig. 8a, and fig. 11b with fig. 8b.)

The large differences in precipitation are generally statistically significant. (Compare fig. 11d with fig. 8d.)

b. spherical harmonic analysis

For SLP the first two harmonics, the 1,0 and the 4,0, are nearly the same for runs #3 and #4; all the others are weaker, indicating generally smaller gradients. The 1,1 harmonic shows the greatest decrease in magnitude in run #4

because of the smaller contrast between the tropical continental lows and the Pacific Ocean. The higher pressure on the continents in the tropics also results in a smaller difference between the equator and the poles, reflected in the weaker 2,0 harmonic in run #4.

The 5,4 and 4,4 harmonics appear among the leading components of run #3 but not of run #4, indicating smaller zonal gradients in run #4. Similarly, the weaker land-sea contrast is shown by the weaker 3,2 and 5,2 harmonics in run #4. The 4,2 harmonic has moved up in rank but down in magnitude.

The 3,0 harmonic is also weaker in run #4, reflecting the decreased difference between the Northern and Southern Hemispheres.

The first two harmonics for temperature in the layer between 850 mb and 700 mb, the 2,0 and the 1,0, are about the same for runs #3 and #4, and the others are weaker, but to a lesser extent than for SLP. As in SLP, the 1,1 harmonic for the layer temperature shows the greatest decrease in magnitude in run #4, reflecting the smaller contrast between the warm air over the tropical continents and the cooler air over the Pacific.

The 6,0 and 8,0 harmonics are weaker in run #4, reflecting the lower temperature around 25 N and the higher temperature around 60 N. The 7,0 and 3,0 harmonics, on the other hand, are stronger in run #4, their phase of 180 indicating colder air over the North Pole and in low southern latitudes.

The 3,2 harmonic is weaker in run #4, reflecting the smaller zonal gradients in the Southern Hemisphere, while

the stronger 4,2 harmonic indicates the relatively colder air over the tropical continents in run #4 compared to run #3, and the relatively warmer air to the north over Canada and Europe.

As in SLP, the 5,4 and 4,4 harmonics do not appear among the leading components of run #4, as they do in run #3, indicating smaller zonal temperature gradients in run #4.

Since the larger differences in 500 mb height are due to the warmer air in the lower troposphere, many of the same features can be seen in the harmonic components for 500 mb height and for temperature in the layer from 850 mb to 700 mb. For 500 mb height the first three harmonics, the 2,0, 1,0, and 4,0 are the same; the 6,0 and 8,0 are weaker in run #4, and the 7,0, 3,0, and 4,2 are stronger.

The 5,2 harmonic is larger in magnitude in run #4, as is the 6,2, but by a smaller amount, reflecting the higher elevation over Canada and northern Europe, and to the south, a high over the Pacific and lows over Asia and the United States.

The 5,3 is weaker in run #4, reflecting the smaller contrast between the low latitude continents and oceans.

c. vertical cross-sections

Although the cross-sections of zonally averaged temperature for runs #3 (fig. 3f) and run #4 (fig. 4f) appear almost identical, there are warmer and colder areas that are visible on the difference cross-section (fig. 8f). In the lower troposphere many of the features are the same as those of the horizontal temperature maps discussed above, which are generally zonally symmetric.

Between about 40 N and 45 S greater evaporation over the continents in run #4 cools the atmosphere up to about 700 mb, while above that level increased convective heating results in warmer air.

The warmer area between 43 N and 65 N at the surface, weakening upwards to about 300 mb, and the colder air north of 65 N in the lower troposphere are the result of the combination of factors discussed in connection with the horizontal maps. Above 300 mb the air is colder north of 35 N and, by a smaller amount, south of 51 S.

The cross-section of zonally averaged vertical velocity for run #4 (fig. 4i) shows two distinct Hadley cells centered at 4 N and 20 S as in run #3 (fig. 3i), but in run #4 the two ascending branches are equal in intensity, in contrast to run #3, where the southern branch is stronger. The Northern Hemisphere descending branch centered at 20 N is also stronger in run #4. This is a consequence of the northward shift of the ITCZ over the ocean noted on the horizontal maps.

A comparison of the difference maps for vertical velocity (fig. 8i) and for temperature (fig. 8f) reveals that in high northern latitudes where the temperature is lower at around 35 N near the surface up to 51 N in the upper troposphere, the subsidence is more intense, and further north, where the air is warmer, the ascent is stronger, indicating that the stronger circulation is thermally driven.

The cross-section of meridional wind for run #4 (fig. 4h) shows the same pattern of north and south winds as in run #3 (fig. 3h) except for a northward shift from 16 S to

the equator of the southerly winds at the surface. The Hadley circulation for run #4 shows smaller meridional gradients near 20 S, indicating less speed convergence and divergence, while the reverse is true near the equator, consistent with the movement of the ITCZ over the ocean noted above.

The cross-section of zonal wind for run #4 (fig. 4g) shows weaker equatorial easterlies compared to run #3 (fig. 3g), and stronger Northern Hemisphere westerlies. The differences in zonal wind between run #3 and run #4 (fig. 8g) can be understood as a result of the differences in temperature, according to the thermal wind equation. For example, the strongest evaporative cooling is at 20 S in the lower troposphere, which is the border between the weaker easterlies centered at 8 S and the weaker westerlies at 31 S. Both of these effects decrease in the upper atmosphere, where the convective heating reverses the meridional gradient on the temperature difference cross-section (fig. 8f). Similarly, the increased intensity of the westerlies in the Northern Hemisphere is strongest at high levels, between the colder air at middle latitudes and the warmer air in the tropics.

The differences in temperature and vertical velocity are statistically significant in the tropics but generally not at high latitudes. The lower temperature and increased subsidence in middle northern latitudes are statistically significant. (Compare fig. 11f with fig. 8f, and fig. 11i with fig. 8i.)

The largest differences in zonal wind and in meridional wind are significant at low latitudes but only partly so at

higher latitudes. (Compare fig. 11g with fig. 8g, and fig. 11h with fig. 8h.)

III. The effects of non-zonally symmetric SST: differences between run #4 and run #5

a. horizontal maps

The map of realistic SST of run #5 (fig. 6b) shows the effects of ocean currents, in contrast to run #4 in which the SST is zonally symmetric (fig. 6a). The ocean is warmer in run #5 (fig. 6c) from the Caribbean northeast to the coast of northern Europe by the influence of the Gulf Stream and colder on the northeast coast of North America as a result of the Labrador Current. Similarly, the warm Kuroshio Current extends its influence to the Gulf of Alaska, while the northwest Pacific is colder in run #5 because of the Oyashio Current. In the subtropics the currents flowing towards the equator on the west coasts of the continents result in lower temperatures in run #5. South of 30 S the oceans are generally warmer in the Pacific and colder in the Atlantic and Indian Oceans.

Most of the differences in surface air temperature coincide with those of SST. The zero degree isotherm is shifted northeast in the North Atlantic in run #5 (fig. 5c) along with the large temperature gradient to the north, producing temperatures as much as 45 degrees warmer north of Scandinavia (fig. 9c). There are a number of mechanisms responsible for the greatly increased temperature. Increased evaporation from the open ocean, which was frozen in run #4 at this location, results in a greater cloud cover at all levels, trapping the greater long wave radiation from the ocean which is warmer in run #5 by as much as 6 degrees (fig. 6c). This is in addition to the increased transfer of sensible heat from the ocean and by advection from the south (cf. SLP maps, below). This effects the whole Arctic region,

so that temperatures are generally warmer north of about 70 N (fig. 9c).

The colder areas on the continents and oceans to the south are dominated by the ice-covered Bering Sea, Sea of Okhotsk, and Hudson's Bay, which are not frozen in run #4. Temperatures are also lower by 2.5 degrees over the oceans west of the continents at 20 N and 20 S, and south and southwest of Africa around 50 S, in accordance with the lower SST. The air is warmer over a large part of the Pacific south of 30 N, particularly southwest of New Zealand.

In run #5 the Aleutian low has decreased in size and deepened, while the opposite changes have occurred in the Icelandic low (fig. 5a). However, in both cases, which are in better agreement with the observed climatology (fig. 1a), the differences in pressure are caused by the differences in temperature (figs. 9a and 9c). The colder air over the ice-covered areas north and west of the Aleutian low result in higher SLP, causing the low pressure center to shrink on its western side. The greatest decrease in pressure occurs north of Iceland and Scandinavia, where the surface temperature is much higher. This allows a northeastward expansion of the Icelandic low and of the area influenced by the warm southwesterly winds on its eastern side.

Throughout most of the globe south of 45 N, SLP differences are small (fig. 9a). An increase in pressure from 995 mb to 1000 mb on the west coast of South America (figs. 4a and 5a) is caused by the lower temperatures (fig. 9c). Southwest of southern Africa the high pressure cell is stronger where the temperature is lower.

The map of temperature in the layer from 850 mb to 700 mb for run #5 (fig. 5a) resembles the map of surface air temperature for run #5 (fig. 5c). The difference map shows the same areas of difference between runs #4 and #5 for layer temperature (fig. 9a) and surface temperature (fig. 9c) but the magnitude of the differences are much less further from the surface.

The map of 500 mb height for run #5 (fig. 5b) compared to that of run #4 (fig. 4b) shows a much more diffluent pattern over the North Atlantic and northern Europe and Asia and a higher amplitude long wave pattern in the Northern Hemisphere, higher than the observed (fig. 1b). A closed low appears over the Arctic around 150 E. A comparison of the 500 mb map with the layer temperature map for run #4 (figs. 4b and 4a) and run #5 (figs. 5b and 5a) shows, for each run, the same long wave patterns in high northern latitudes on both maps, and in run #5 the closed low around 150 E on both maps. The 500 mb map for run #4 (fig. 4b) shows a high in the eastern Atlantic west of Europe and a low at the east coast of Asia. The realistic SST pattern that is included in run #5 (fig. 6b) has a similar structure, resulting in an amplification of the wave in high northern latitudes on the 500 mb map for run #5 (fig. 5b).

In the Southern Hemisphere a slightly higher amplitude wave which can be seen around 60 S on the 500 mb map for run #5 appears to have a similar cause; the surface air temperature maps show a higher amplitude wave for run #5 (fig. 5c) than for run #4 (fig. 4c) at this latitude.

In the Northern Hemisphere the difference map for 500 mb height (fig. 9b) shows a pattern similar to that of the

difference map for temperature between 850 mb and 700 mb (fig. 9e). Over most of the Southern Hemisphere run #5 has higher elevations than run #4, the largest difference being 60 meters southwest of South America, in conjunction with the higher amplitude wave. The generally higher elevation is due to the warmer temperatures in the Southern Hemisphere that can be seen most easily on the vertical cross-section of zonally averaged temperature discussed below.

The precipitation maximum in run #4 on the east coast of South America around 20 S (fig. 4d) has been replaced in run #5 by one on the equator at the central part of the continent (fig. 5d), resulting in smaller meridional gradients. The precipitation over the eastern Pacific is more uniform in run #5 than in run #4, where it is concentrated in a band north of the equator. Other features are qualitatively similar for both runs, except for an extension of the precipitation over the North Atlantic toward the northeast along with the Icelandic low.

Areas of higher SST in run #5 (fig. 6c) result in higher evaporation from the oceans and lower stability of the atmosphere above, with colder SST showing the opposite effects. Precipitation has decreased in run #5 (fig. 9d) on the west coast of South America, the east coast of Asia, and on the Somali Peninsula, where the SST is lower, and has increased over the western Pacific, the Indian Ocean, the Arctic north of Scandinavia, and the West African coast, where SST has increased. An exception is the east coast of South America, where the precipitation has moved northward as a result of the stronger circulation around the high pressure cell in the South Atlantic, which limits the

influence of the moist northeast trades to the northern part of the continent.

The precipitation is less in southern Africa in run #5 (fig. 9d). This, and the decrease in precipitation at the Somali Peninsula, result from the fact that in run #5 there is a realistic monsoon circulation (not shown), which appears to be caused by the changes in SST (fig. 6c), an influence suggested by Saha (1970). Around 60 E on the equator, winds are from the southeast in run #4, whereas in run #5 they turn from northeast to northwest as they cross the equator. This has the effect of diverting the rain from the African continent to the Indian Ocean. In addition, the winds over the Somali Peninsula originate over the Indian Ocean in run #4 while in run #5, in agreement with observation, they come from the northeast over Asia.

Differences in surface air temperature from run #4 to run #5 of 2.5 degrees or more are statistically significant except for a few areas at high northern latitudes. (Compare fig. 12c with fig. 9c.) The few areas where SLP is different by 4 mb or more or where precipitation has changed by 2.5 mm/day or more all show statistical significance. (Compare fig. 12a with fig. 9a, and fig. 12d with fig. 9d.)

Differences in temperature between 850 mb and 700 mb are statistically significant. (Compare fig. 12e with fig. 9e.) The only area where differences in 500 mb height are not significant is in the Arctic north of 75 N from Siberia eastward to northern Canada. (Compare fig. 12b with fig. 9b.)

b. spherical harmonic analysis

The lower SLP at the Arctic in run #5 compared to run #4 and the higher pressure around 60 N are reflected in the

changes in the zonally symmetric harmonics. The 1,0 harmonic has decreased in magnitude and the 3,0 is no longer among the leading components in run e5, reflecting the lower pressure at the Arctic, while the increase in magnitude of the 4,0 harmonic indicates a greater contrast between middle latitudes and the pole in the Northern Hemisphere. The 2,0 harmonic has grown at the expense of the 8,0, indicating that the meridional gradients of SLP are dominated by long wavelengths to a greater degree than in run e4. To a lesser extent this is also reflected in the stronger 3,2 and 4,2 harmonics in contrast to the weaker 5,2. The stronger 2,1 and 3,1 harmonics similarly reflect long wavelength meridional gradients in contrast to the weaker 1,1 harmonic.

The stronger 2,2 harmonic reflects the more extensive continental highs and the lower pressure on the oceans in middle latitudes in the Northern Hemisphere.

The two leading components for temperature between 850 mb and 700 mb, the 2,0 and the 1,0, are nearly the same for runs e4 and e5, the 180 phase of both indicating low temperatures in the Arctic. The warmer air in the Arctic in run e5 decreases the short wave meridional temperature gradients, reflected in the smaller magnitude of the 8,0 and 7,0 harmonics. The difference map shows warmer air at 30 S and 30 N, colder air at 60 N, and warmer air at 90 N in run e5, reflected in the higher magnitude of the 6,0 harmonic with a phase of 0 and the lower magnitude of the 3,0 harmonic with a phase of 180.

The largest differences in temperature in the layer between 850 mb and 700 mb are the warmer area around northern Europe and the colder area centered at the Bering

See, reflected in the stronger 3,1 and 2,1 harmonics in run #5.

The 3,2, 6,2, and 4,2 harmonics have moved down in rank in run #5 and the 5,2 has moved up, but the only considerable changes in magnitude are a small increase of the 3,2 and a small decrease of the 4,2.

The major change in the spherical harmonic components for 500 mb height is the appearance among the leading components in run #5 of the 4,1, 3,1, 2,1, and 5,1 harmonics, reflecting the higher elevations in high northern latitudes from 60 W eastward to 120 E and the lower elevations from 120 E eastward to 60 W.

The stronger 1,0 harmonic in run #5 indicates generally higher elevations in the Southern Hemisphere. The stronger 6,0 with a phase of 0 and the weaker 3,0 with a phase of 180, similar to the 850 mb to 700 mb temperature components described above, reflect the differences in 500 mb height that are generated by the warmer air between 850 mb and 700 mb. The leading component, the 2,0, which indicates lows at the poles and a high at the equator, is the same in run #4 and run #5, as in the layer temperature, while the higher elevation at the Arctic is reflected in the smaller magnitude of the 7,0 and 8,0 harmonics, indicating decreased short wave meridional gradients.

The 6,2, 5,2, and 4,2 harmonics have moved down in rank, but the 6,2 and 5,2 have increased in magnitude, reflecting the higher amplitude of the dominant wave number 2 in the Northern Hemisphere. The 4,2 shows only a small increase in magnitude. The small decrease in magnitude of the 4,0 harmonic indicates the lesser importance of the

zonally symmetric harmonics in run e5.

c. vertical cross-sections

The vertical cross-section of temperature for run e5 (fig. 5f) shows a smaller meridional gradient near the surface at 70 N than in run e4 (fig. 4f), and a larger meridional gradient in the stratosphere north of 45 N, but these features are more easily seen on the difference cross-section (fig. 9f). Near the surface the warmer air centered at 74 N and the colder air just to the south have already been seen on the horizontal maps. The reason for the much warmer air above 300 mb at middle northern latitudes will be given below in connection with the cross-sections of vertical velocity and meridional wind.

South of 40 N the entire troposphere is warmer in run e5 than in run e4 by less than 1.5 degrees. The net result of the increases in evaporation in run e5 where the SST is higher and decreases where the SST is lower is a greater evaporation in the Southern Hemisphere, which causes a greater heating by large-scale condensation sufficient to increase the average temperature of a large part of the atmosphere.

In run e4 air is descending over the Arctic (fig. 4i), in agreement with nature. This is replaced in run e5 (fig. 5i) by strong ascending motion which is a result of the heating and lower pressure at the surface seen on the horizontal maps. This ascending motion, together with the greater evaporation at the surface, results in a release of latent heat north of 70 N that is 123% higher in run e5 than in run e4.

The descending air in middle northern latitudes extends further north, past 60 N at 900 mb, in run #5 due to the colder air and higher SLP seen on the horizontal maps at this latitude.

The Hadley circulation in run #5 is more uniformly distributed between 12 N and 27 S than in run #4, where there are two distinct cells of ascending air. This reflects the more uniform pattern of precipitation in run #5 noted above.

The vertical cross-section of meridional wind for run #5 (fig. 5h) shows inflow to the Arctic at the surface and northerly flow aloft, in contrast to the cross-section for run #4 (fig. 4h) which shows outflow at the surface. This is the reversal of the Arctic circulation that results in the warmer air above 300 mb at mid-latitudes that was discussed above.

The southerly flow above 500 mb in the Northern Hemisphere Hadley circulation reaches a smaller maximum in run #5, in agreement with the less concentrated ascending air noted above. Otherwise the meridional winds are similar for both runs (fig. 9h).

The cross-section of zonal wind for run #5 (fig. 5g) shows a weakening and a northward shift above 150 mb of the maximum westerlies in the Northern Hemisphere. This can be seen, by comparing the difference cross-sections of zonal wind (fig. 9g) and of temperature (fig. 9f), to be due to the warmer air in mid-latitudes, according to the thermal wind equation. Similarly, the westerly maximum in the upper troposphere at 70 N in run #4 (fig. 4g) is nearly absent in run #5 (fig. 5g), a result of the warmer air over the Arctic

(fig. 9f).

The equatorial easterlies above 200 mb in run #5 (fig. 5g) are stronger and cover a larger area compared to run #4 (fig. 4g), but the magnitude of the difference is much less than for the Northern Hemisphere mid-latitude westerlies. Because of the weaker westerlies there is a larger northward transport of angular momentum above 200 mb in run #5, resulting in the stronger equatorial easterlies.

The differences in temperature are almost all statistically significant; where they are not, the differences are generally less than 1.5 degrees. (Compare fig. 12f with fig. 9f.) Differences in vertical velocity, meridional wind, and zonal wind are similarly statistically significant except where they are very small. (Compare fig. 12i with fig. 9i, fig. 12h with fig. 9h, and fig. 12g with fig. 9g.)

Summary and conclusions

In run #3 the addition of mountains influences the climate in two ways: temperatures are effected by the elevated heat and cold sources resulting from the general uplift of the continents above sea level; the mountains also act as barriers, diverting or slowing the winds. At both sea level and 500 mb, mountains cause more cellular patterns and Northern Hemisphere highs and lows are moved closer to their correct positions, but in some cases these changes are excessive in magnitude. The mountain barriers also have a considerable effect on the precipitation patterns. Additional differences between runs #2 and #3 are due to the dry isothermal initialization in run #3, in contrast to the horizontally, but not vertically, uniform moist initialization of run #2.

Although the effects of mountains on the model climatology are generally qualitatively correct, the resulting climate is not always a better simulation of nature.

In run #4 realistic ground water storage and surface albedo are added. The former is the dominant feature, influencing surface temperatures and precipitation patterns over land due to the increased evaporation from the ground. The smaller zonal land-sea temperature differences result in weaker Southern Hemisphere continental lows and oceanic highs. In the tropics the greater evaporative cooling near the surface in run #4 changes to a greater convective heating at higher levels.

The addition of realistic surface physics does not effect the model climatology to as large an extent as the addition of mountains.

With realistic SST's and sea ice coverage added in run #5, the influences of zonal SST gradients on climate are simulated. The largest differences between runs #4 and #5 are the surface air temperatures in areas where the Northern Hemisphere sea ice boundary has changed. These and other changes in temperature, and the resulting changes in SLP and 500 mb height, bring the model climatology closer to the observed, but in some cases the changes are excessive.

Precipitation is influenced by the changes in evaporation from the oceans and in the stability of the atmosphere above which result from changes in SST. The zonal SST gradient in the Indian Ocean in run #5 results in a realistic monsoon circulation.

The only major change in run #5 that is not at least qualitatively realistic is the reversal of the circulation at high northern latitudes, with air ascending over the Arctic in run #5. Otherwise, the departures from zonal symmetry of the SST field result in a better simulation of the real atmosphere.

Acknowledgements

This research was supported by the National Aeronautics and Space Administration (NASA), Goddard Space Flight Center, through Grant No. NGR 33-013-086 to the City College (Prof. Jerome Spar, Principal Investigator), and the work was carried out entirely at the Goddard Institute for Space Studies (GISS) in New York. The author gratefully acknowledges the support and assistance of the GISS staff under Dr. Robert Jastrow, Director, and Dr. James Hansen, head of the climate research group, and their permission to use the GISS climate model and computer system for this investigation.

References

Chervin, R. M., 1980a: Estimates of first- and second-moment climate statistics in GCM simulated climate ensembles. J. Atmos. Sci., 37, 1889-1902.

Chervin, R. M., 1980b: On the simulations of climate and climate change with general circulation models. J. Atmos. Sci., 37, 1903-1913.

Chervin, R. M. and S. H. Schneider, 1976: On determining the statistical significance of climate experiments with general circulation models. J. Atmos. Sci., 33, 405-412.

Christidis, Z. D. and J. Spar, 1981: Spherical harmonic analysis of a model-generated climatology. Mon. Wea. Rev., 109, 215-229.

Hansen, J., G. Russell, D. Rind, P. Stone, A. Lacis, L. Travis, S. Lebedeff, and R. Ruedy, 1980: An efficient three-dimensional global model for climate studies. I. Model I. NASA, Goddard Institute for Space Studies, Goddard Space Flight Center, New York, N. Y. 10025.

Kasahara, A., T. Sasamori, and W. M. Washington, 1973: Simulation experiments with a 12-layer stratospheric global circulation model. I. Dynamical effects of the earth's orography and thermal influence of continentality. J. Atmos. Sci., 30, 1229-1251.

Kasahara, A., and W. M. Washington, 1971: General circulation experiments with a six-layer NCAR model, including orography, cloudiness and surface temperature calculations. J. Atmos. Sci., 28, 657-701.

Manabe, S. and J. L. Holloway, Jr., 1970: Climate modification and a mathematical model of atmospheric circulation. A Century of Weather Progress, Boston, Amer. Meteor. Soc., 157-164.

Manabe, S. and T. B. Terpstra, 1974: The effects of mountains on the general circulation of the atmosphere as identified by numerical experiments. J. Atmos. Sci., 31, 3-42.

Saha, K., 1970: Zonal anomaly of sea surface temperature in equatorial Indian ocean and its possible effect upon monsoon circulation. Tellus, 22, 403-409.

Schlesinger, M. E. and W. L. Gates, 1979: Numerical simulation of the January and July global climate with the OSU two-level atmospheric general circulation model. Report No. 9, Climatic Research Institute, Oregon State University, Corvallis, Oregon 97331.

Spar, J., 1981: Investigation of models for large-scale meteorological prediction experiments. NASA, Goddard Institute for Space Studies, Goddard Space Flight Center, New York, N.Y. 10025.

White, R. M., 1949: The role of mountains in the angular-momentum balance of the atmosphere. J. Meteor., 6, 353-355.

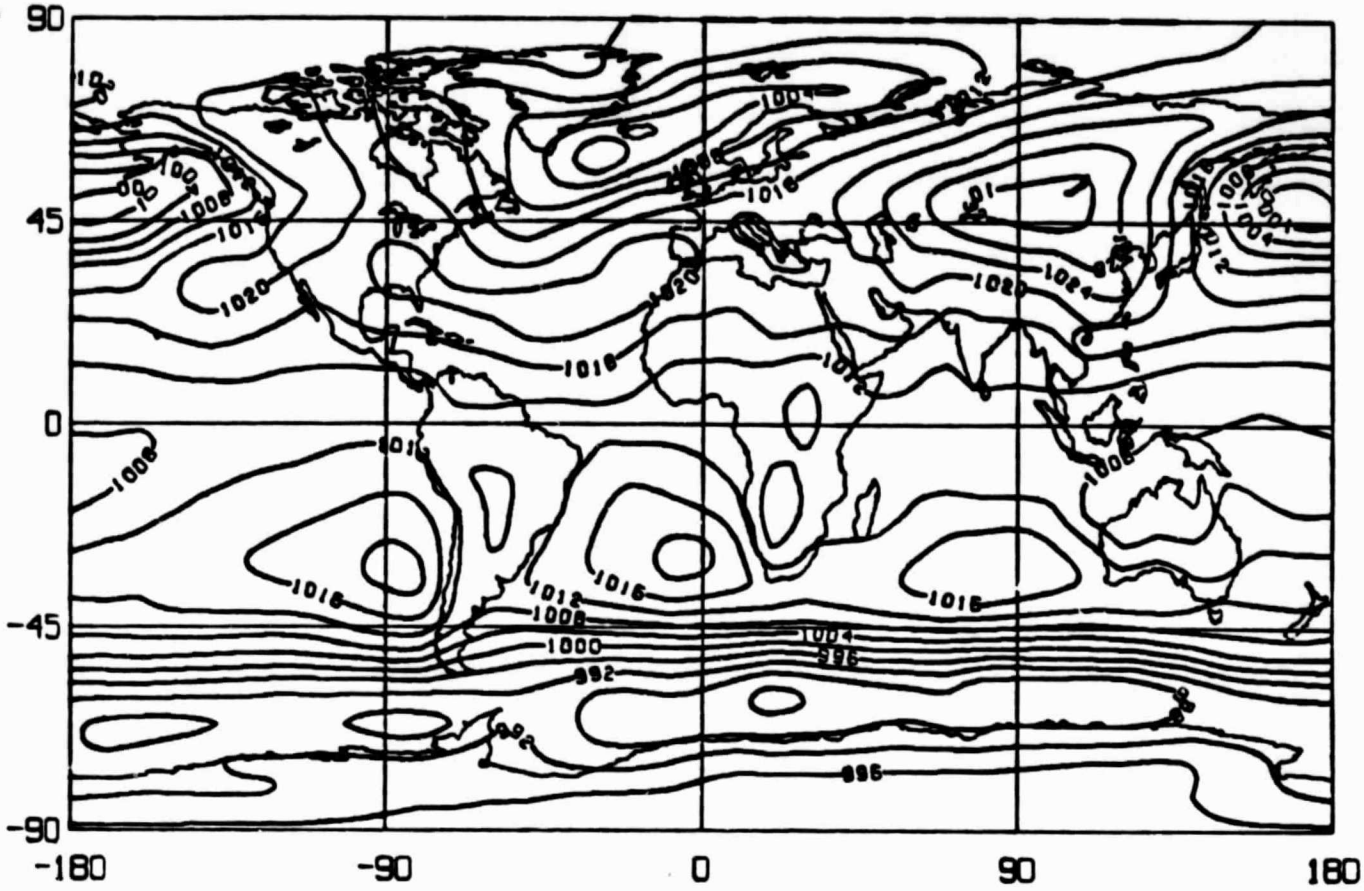

Fig. 1a Observed January climatology, SLP (mb)

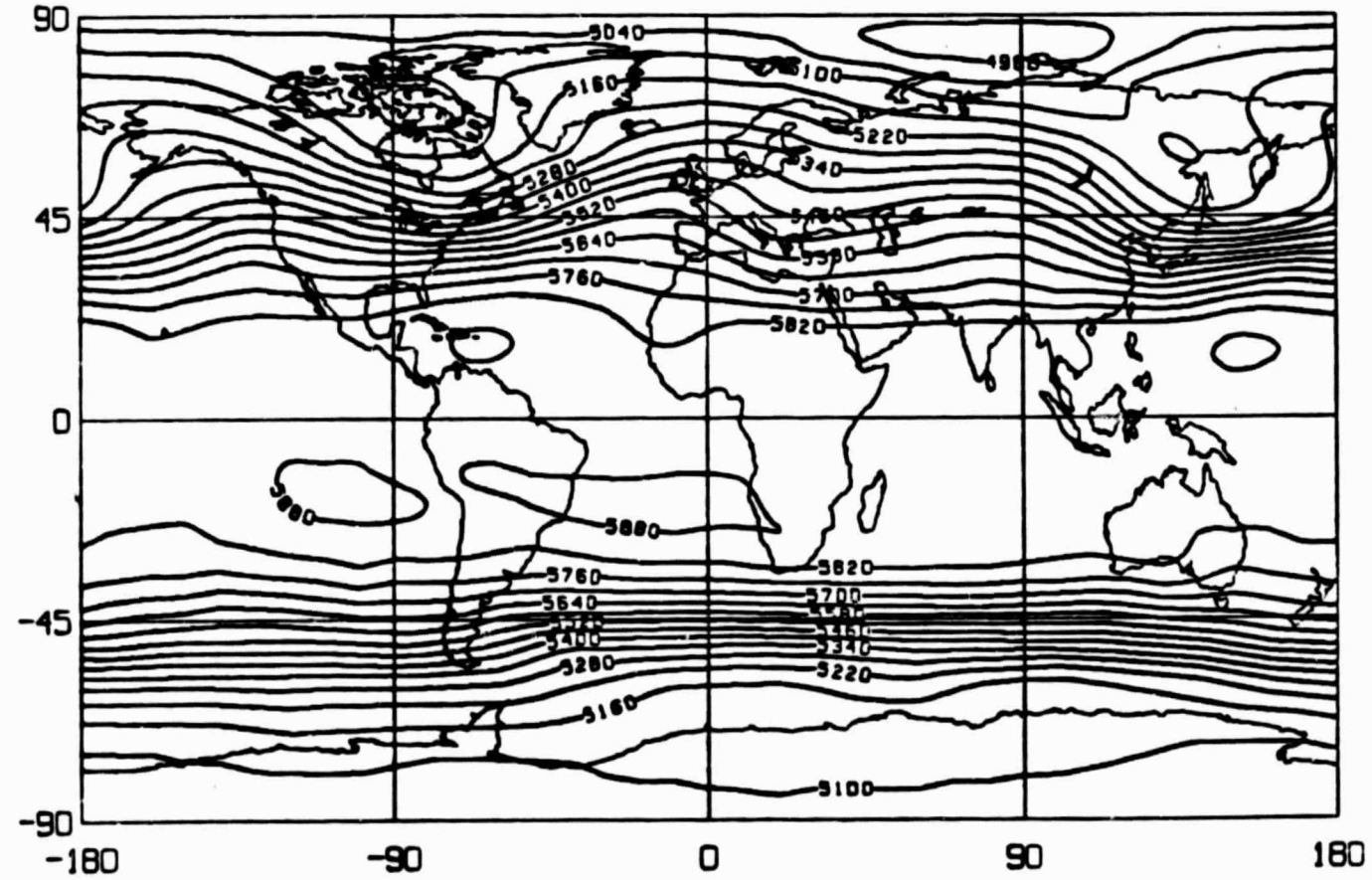

Fig. 1b Observed January climatology, 500 mb height (meters)

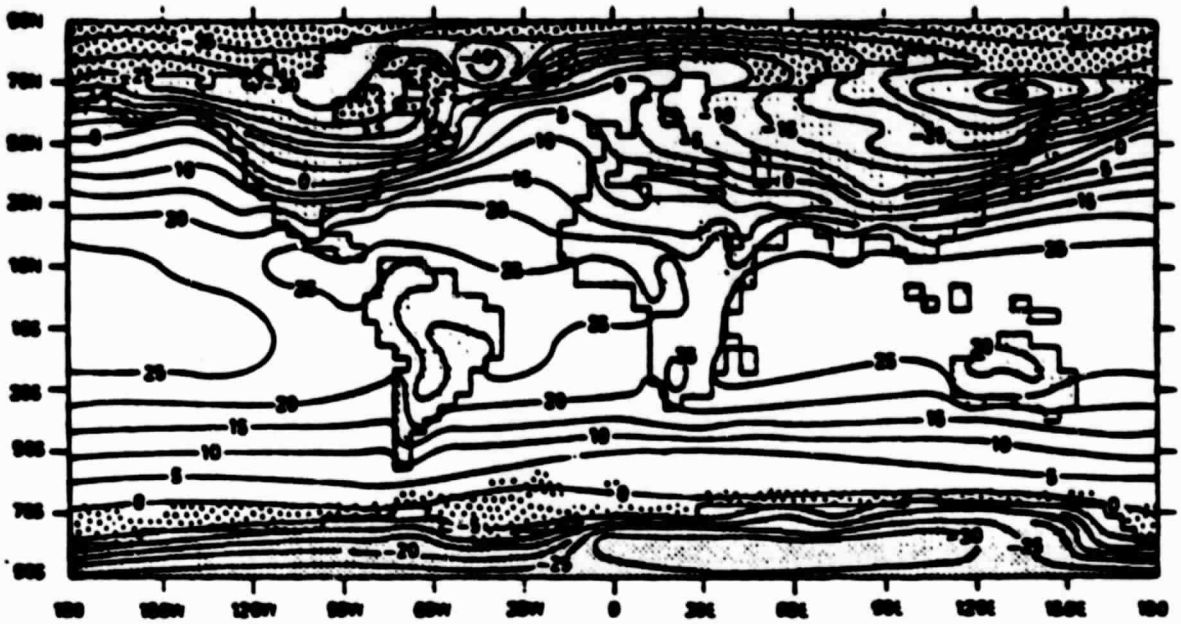

Fig. 1c Observed surface air temperature (Celsius) for January, from Schlesinger and Gates (1979)

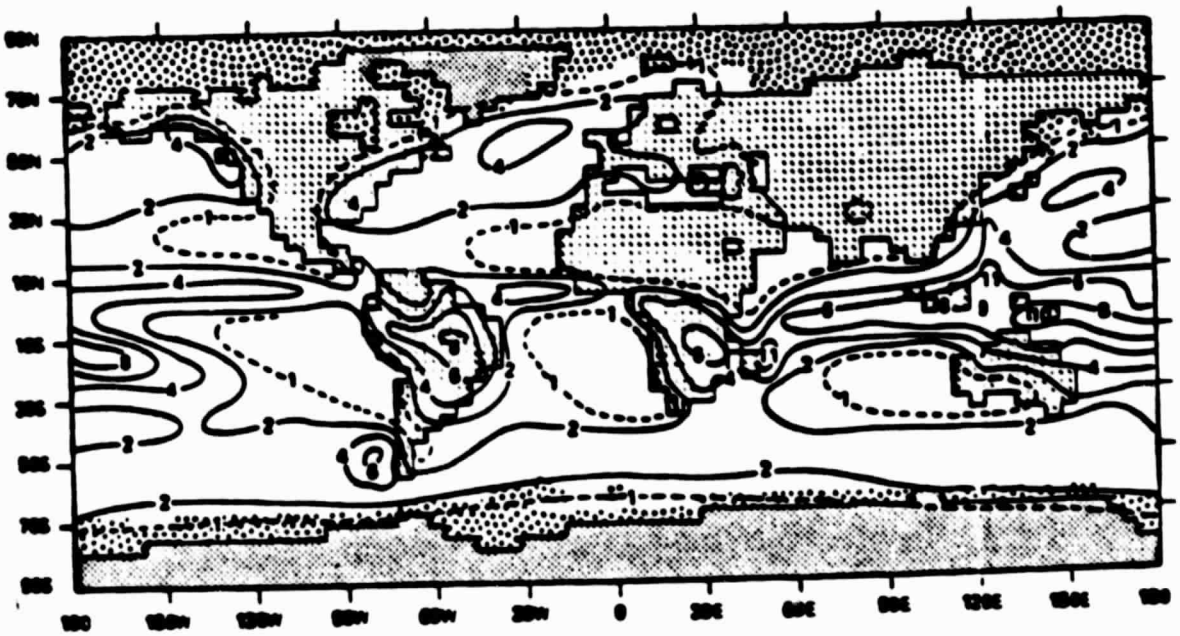

Fig. 1d Observed precipitation rate (mm/day) for December, January, and February, from Schlesinger and Gates (1979)

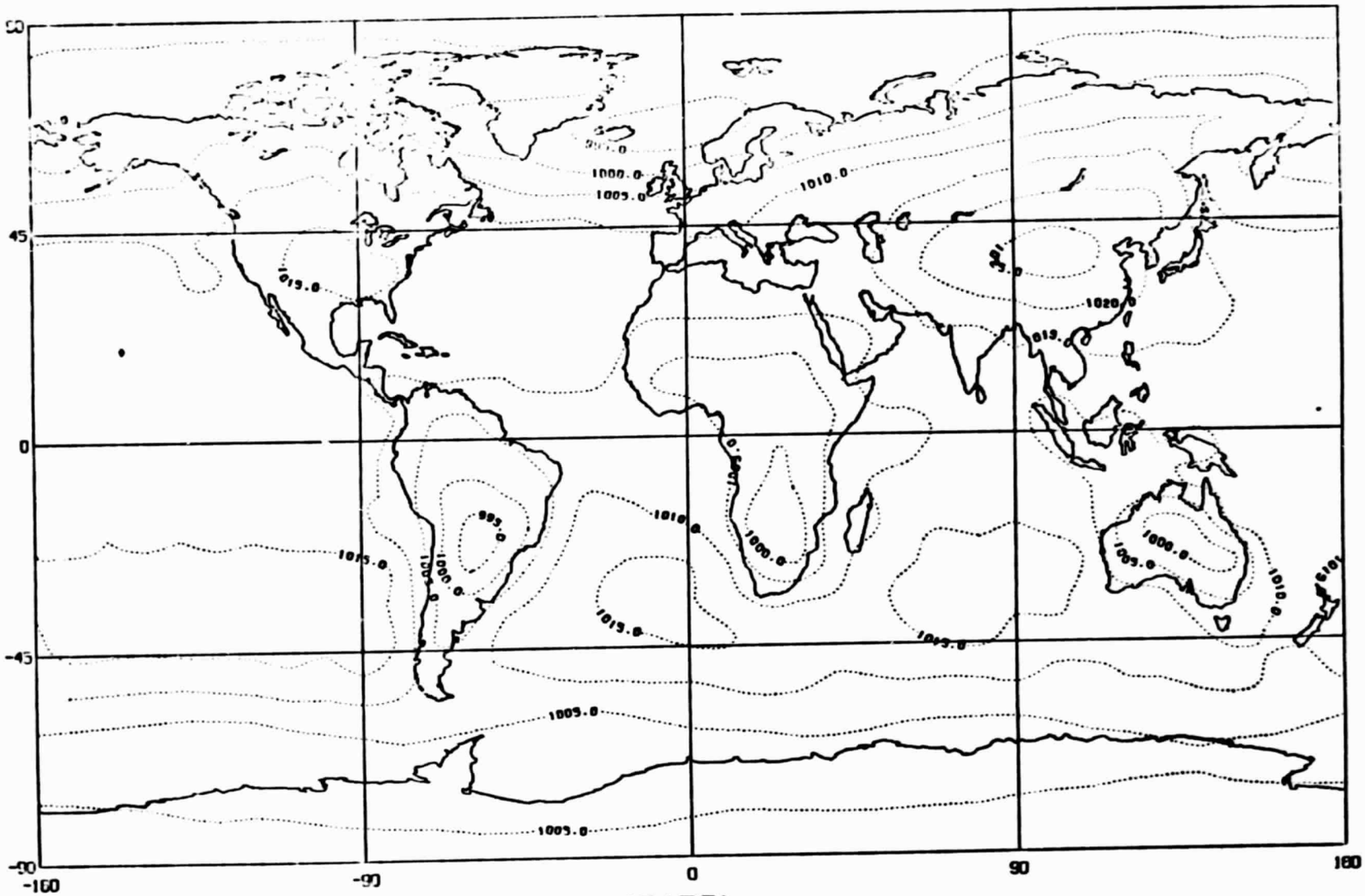

SEA LEVEL PRESSURE (IN MILLIBARS)

THE AVERAGE OF THE LAST 20 MONTHS OF RUN 002

Fig. 2a

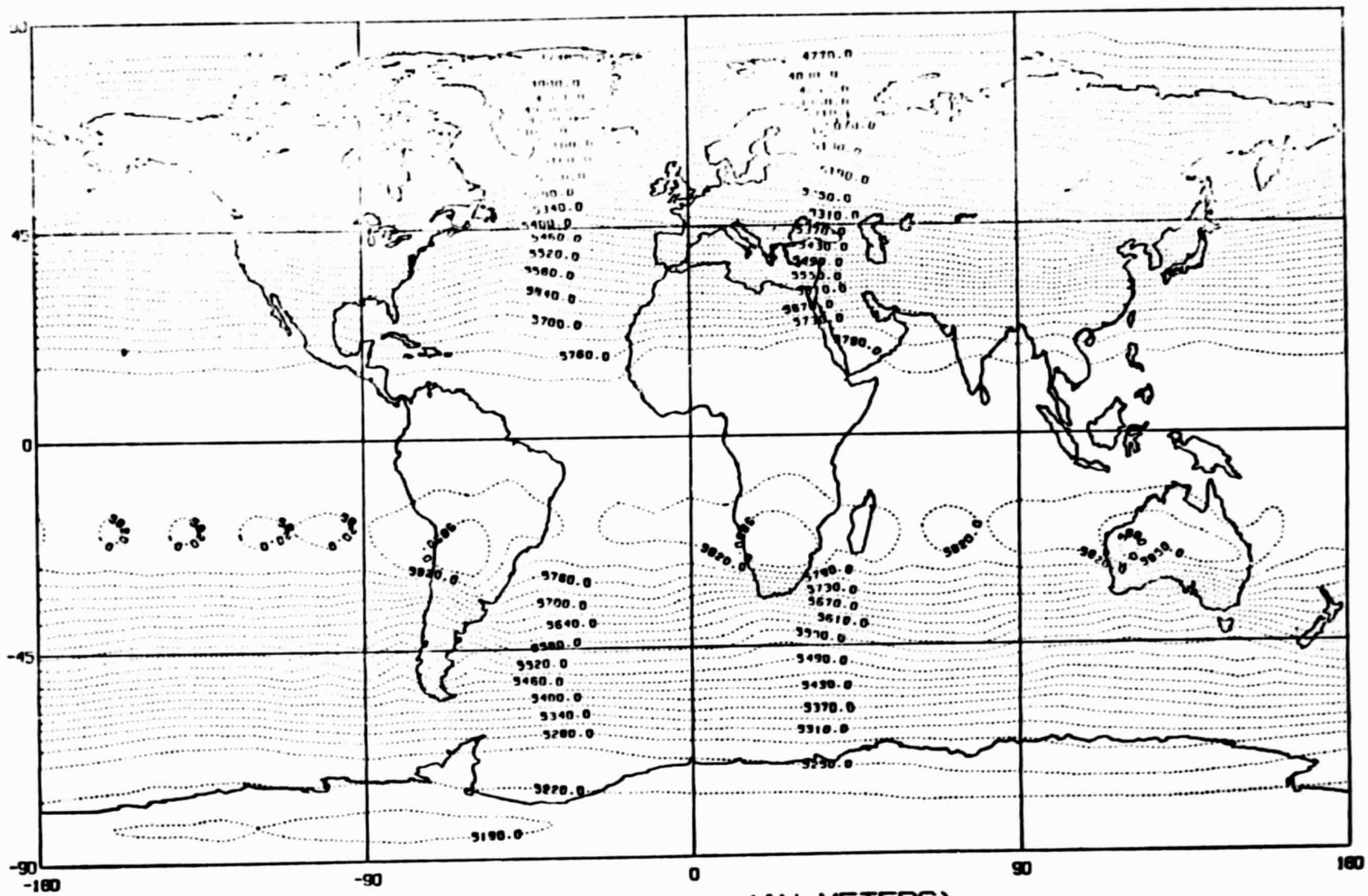

500 MB GEOPOTENTIAL HEIGHT (IN METERS)

THE AVERAGE OF THE LAST 20 MONTHS OF RUN 002

Fig. 2b

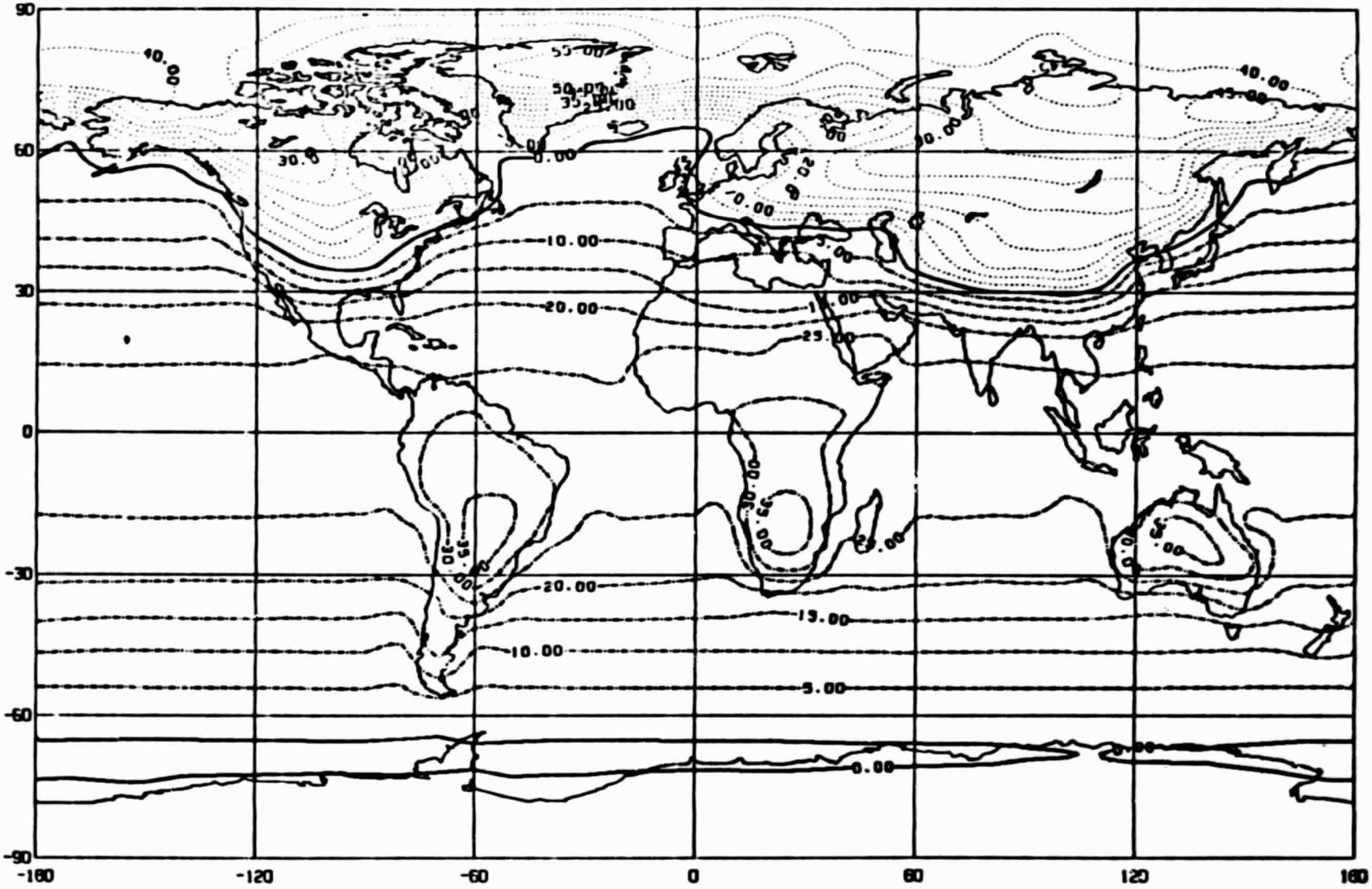

MEAN SURFACE AIR TEMPERATURE (IN DEGREES CENTIGRADE)

THIS IS RUN002

Fig. 2c

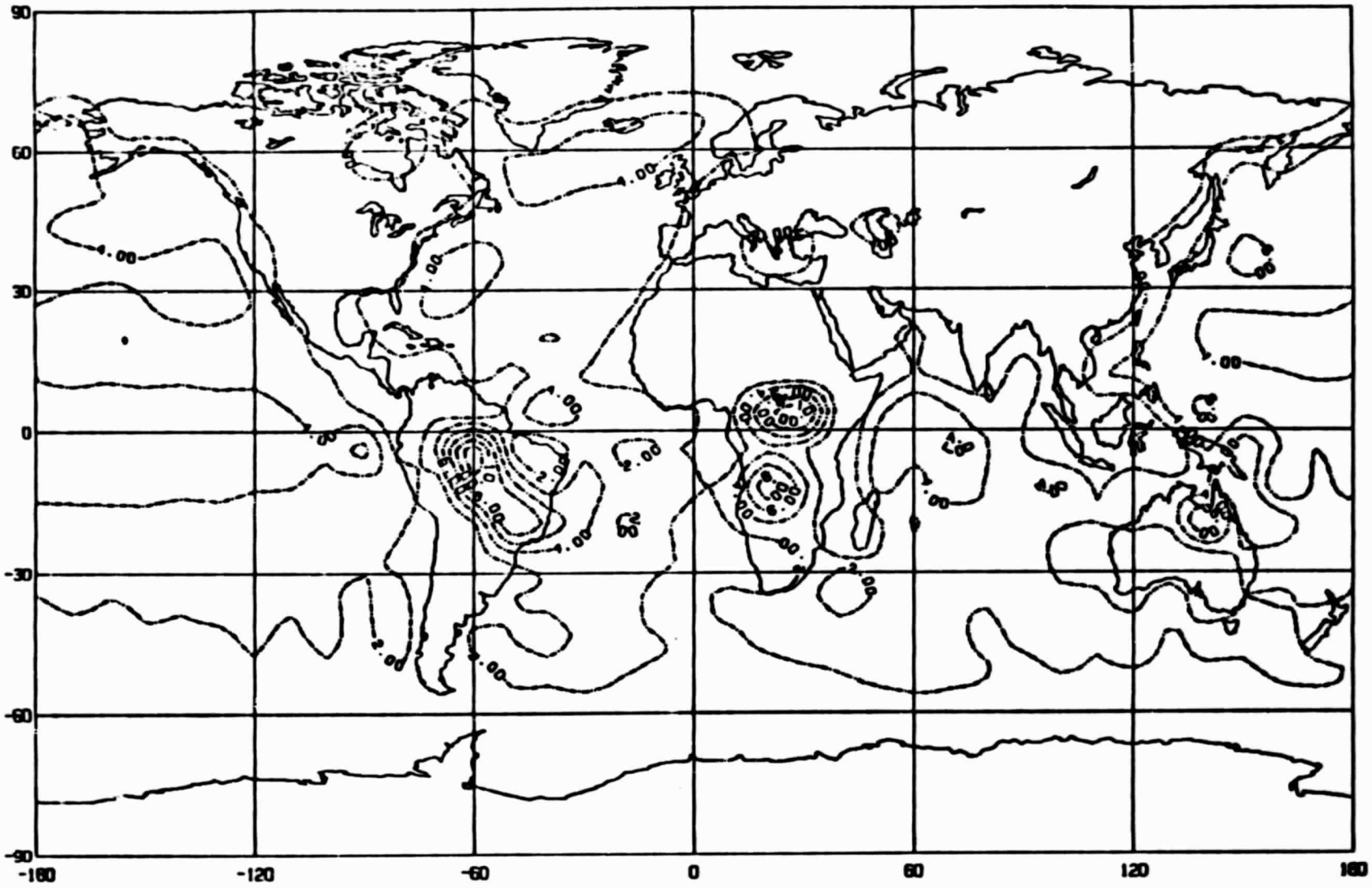

PRECIPITATION IN (MM/DAY)

THIS IS RUN002

Fig. 2d

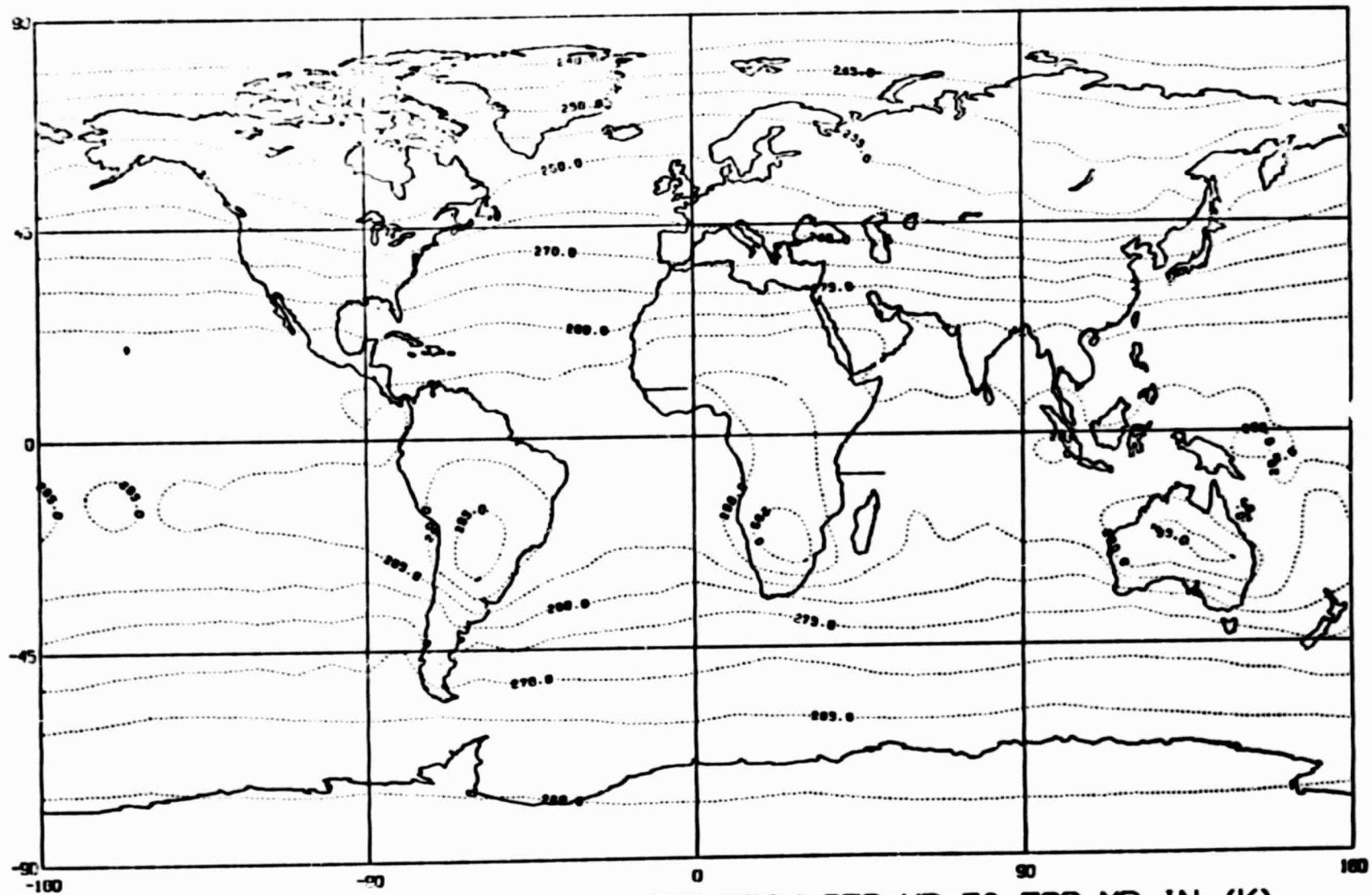

THE MEAN THICKNESS TEMPERATURES FROM 850 MB TO 700 MB IN (K)

THE AVERAGE OF THE LAST 20 MONTHS OF RUN 002

Fig. 2e

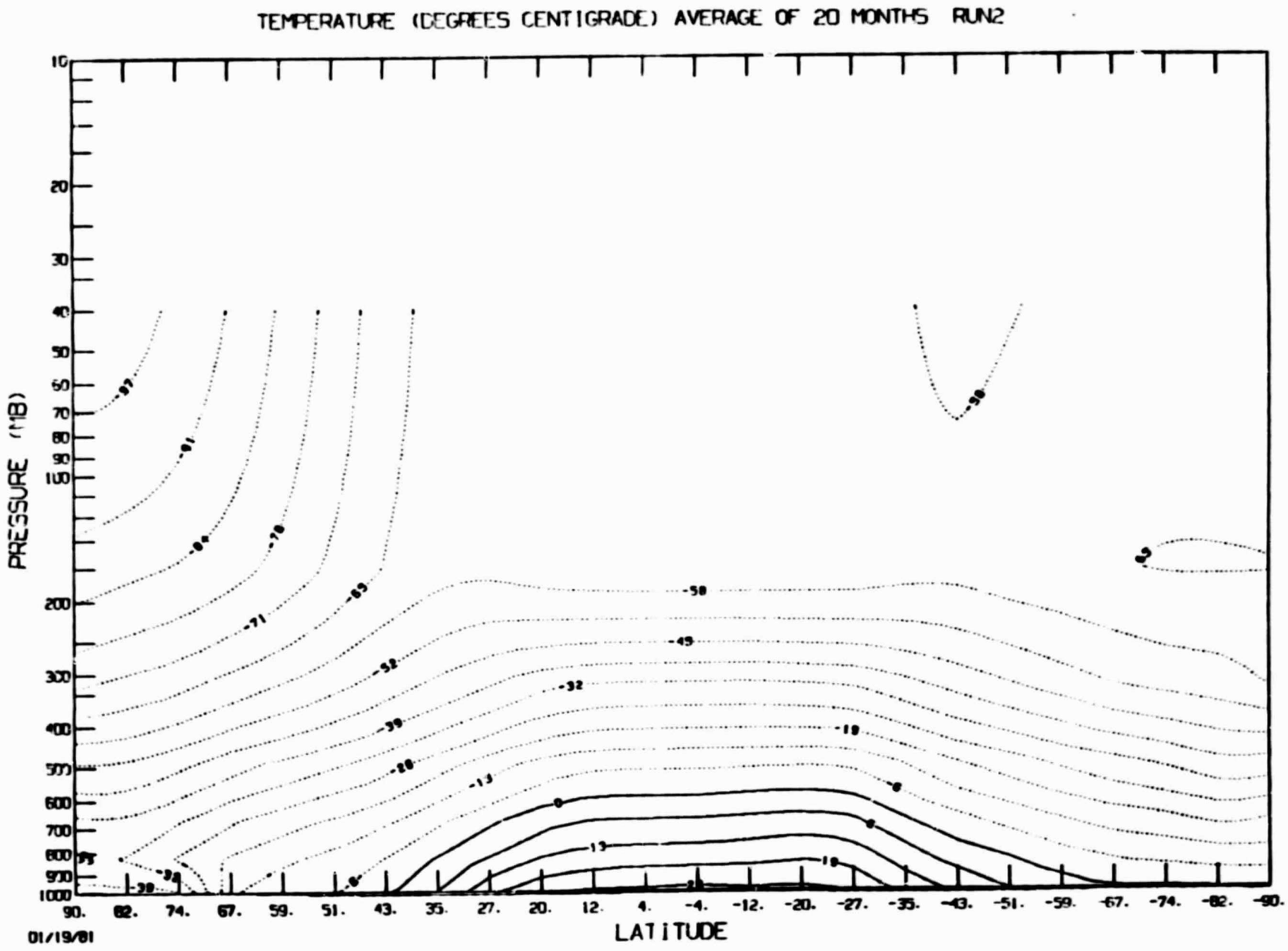
TEMPERATURE (DEGREES CENTIGRADE) AVERAGE OF 20 MONTHS RUN2
PRESSURE (MB)
10
20
30
40
50
60
70
80
90
100
200
300
400
500
600
700
800
900
1000
-92
-81
-64
-18
-71
-65
-58
-45
-32
-19
-6
0
13
18
-52
-39
-26
-13
-39
90. 82. 74. 67. 59. 51. 43. 35. 27. 20. 12. 4. -4. -12. -20. -27. -35. -43. -51. -59. -67. -74. -82. -90.
LATITUDE
01/19/81

Fig. 2f

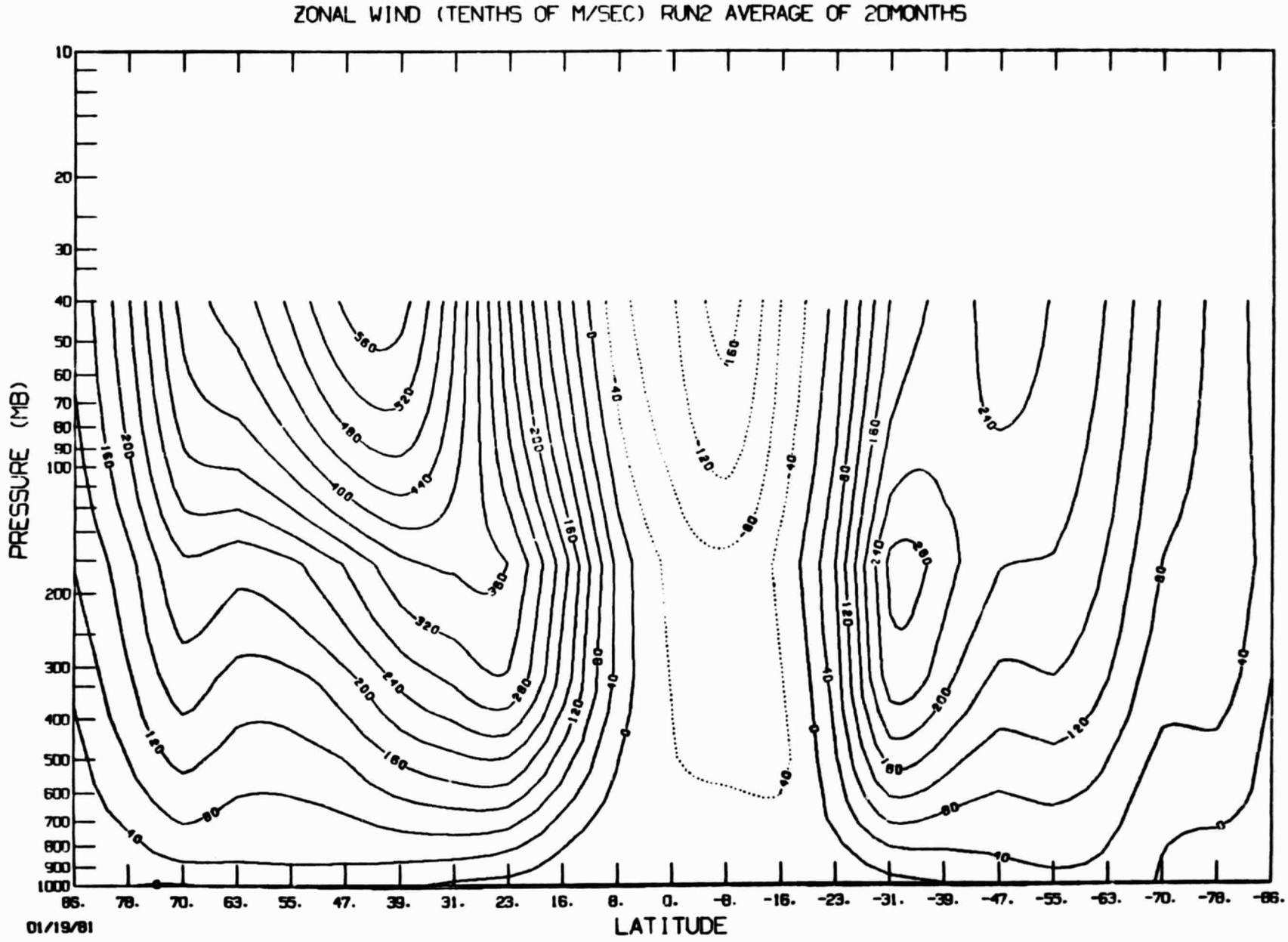
ZONAL WIND (TENTHS OF M/SEC) RUN2 AVERAGE OF 20MONTHS
PRESSURE (MB)
10
20
30
40
50
60
70
80
90
100
200
300
400
500
600
700
800
900
1000
85. 78. 70. 63. 55. 47. 39. 31. 23. 16. 8. 0. -8. -16. -23. -31. -39. -47. -55. -63. -70. -78. -86.
LATITUDE
01/19/81

Fig. 2g

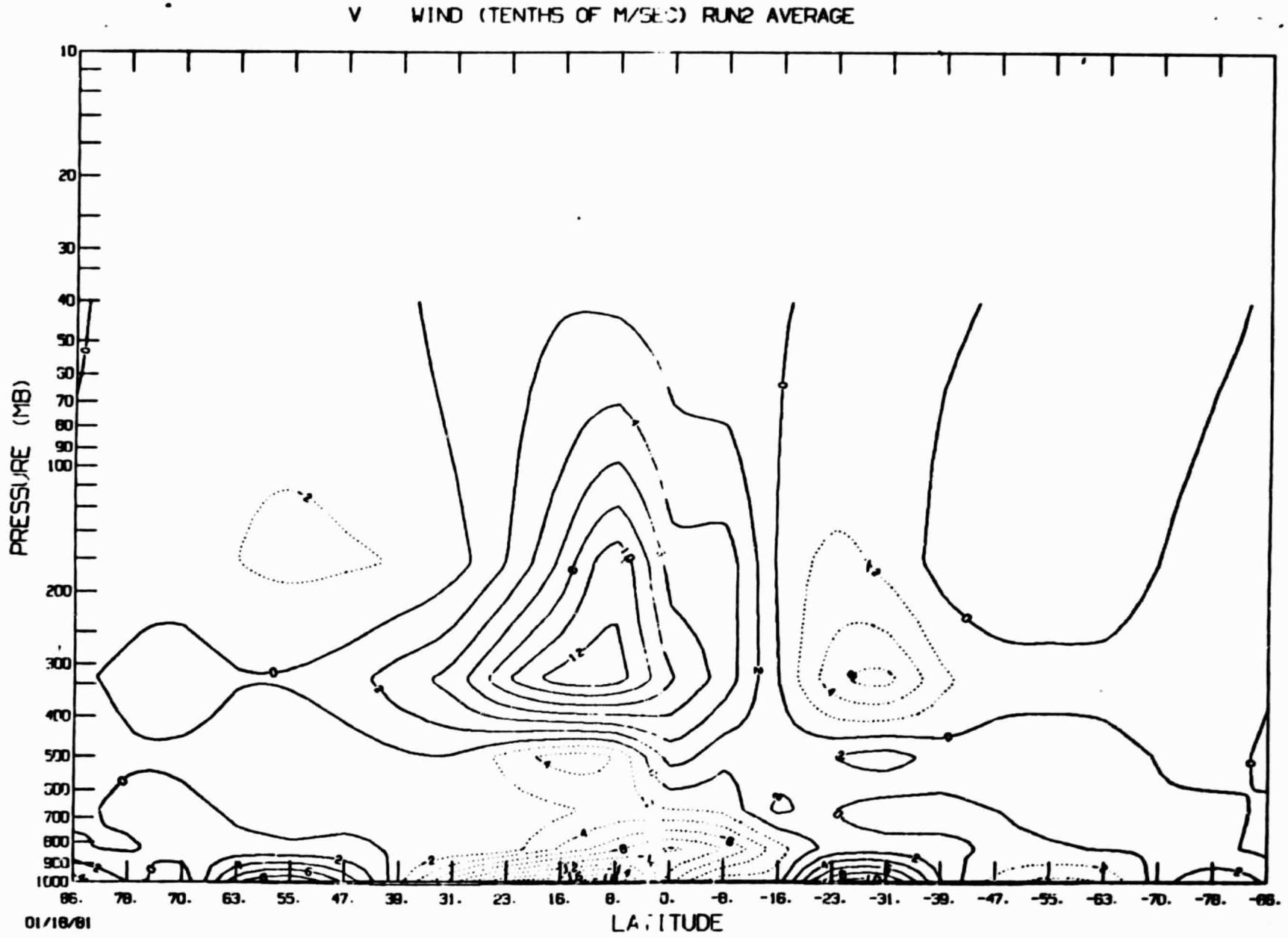
V WIND (TENTHS OF M/SEC) RUN2 AVERAGE
PRESSURE (MB)
10
20
30
40
50
60
70
80
90
100
200
300
400
500
600
700
800
900
1000
86. 78. 70. 63. 55. 47. 39. 31. 23. 16. 8. 0. -8. -16. -23. -31. -39. -47. -55. -63. -70. -78. -86.
LATITUDE
01/18/81

Fig. 2h

**********FLAT*CONTINENTS**********SPAR.WU.COHEN:RUN#2

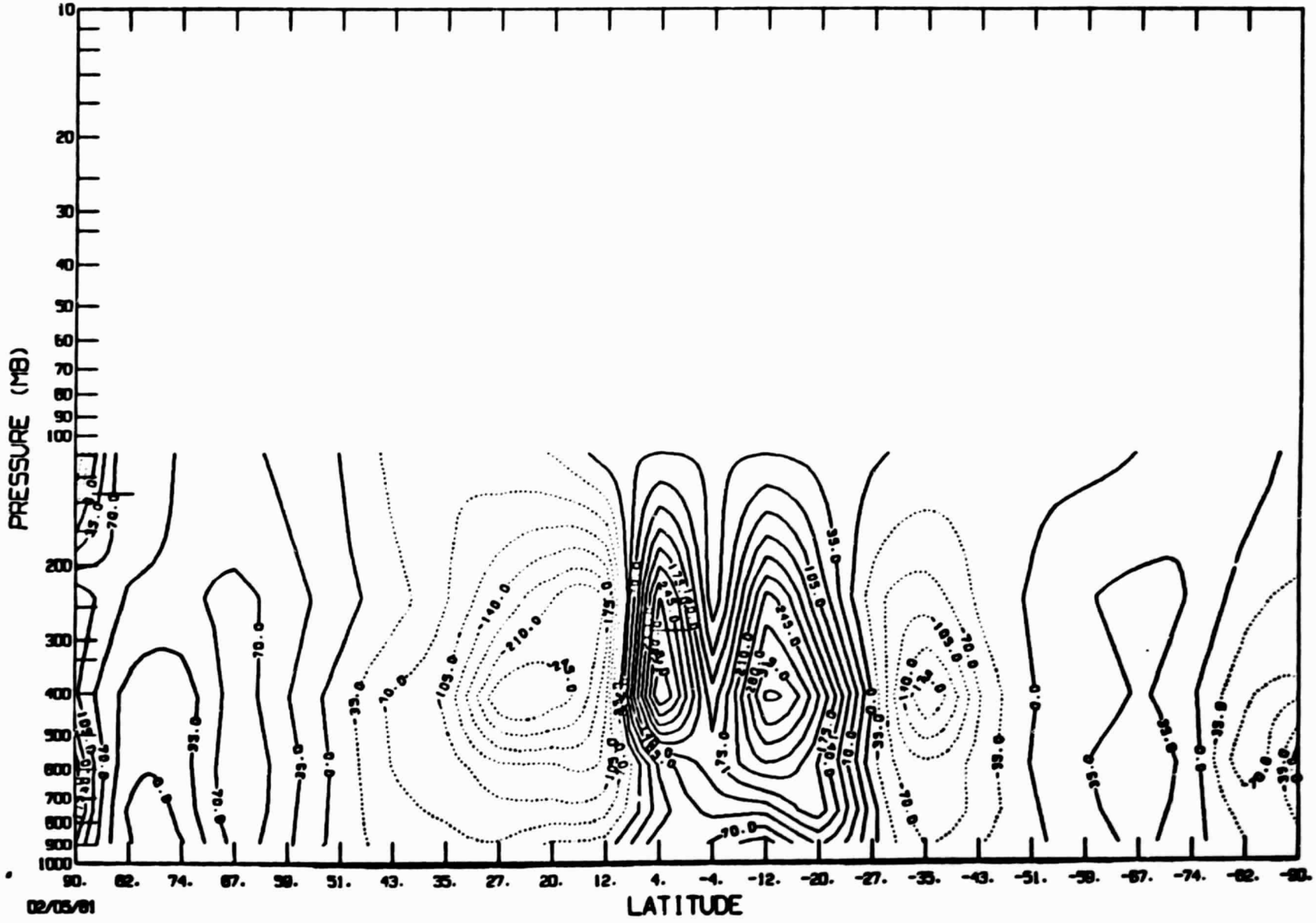

Fig. 21

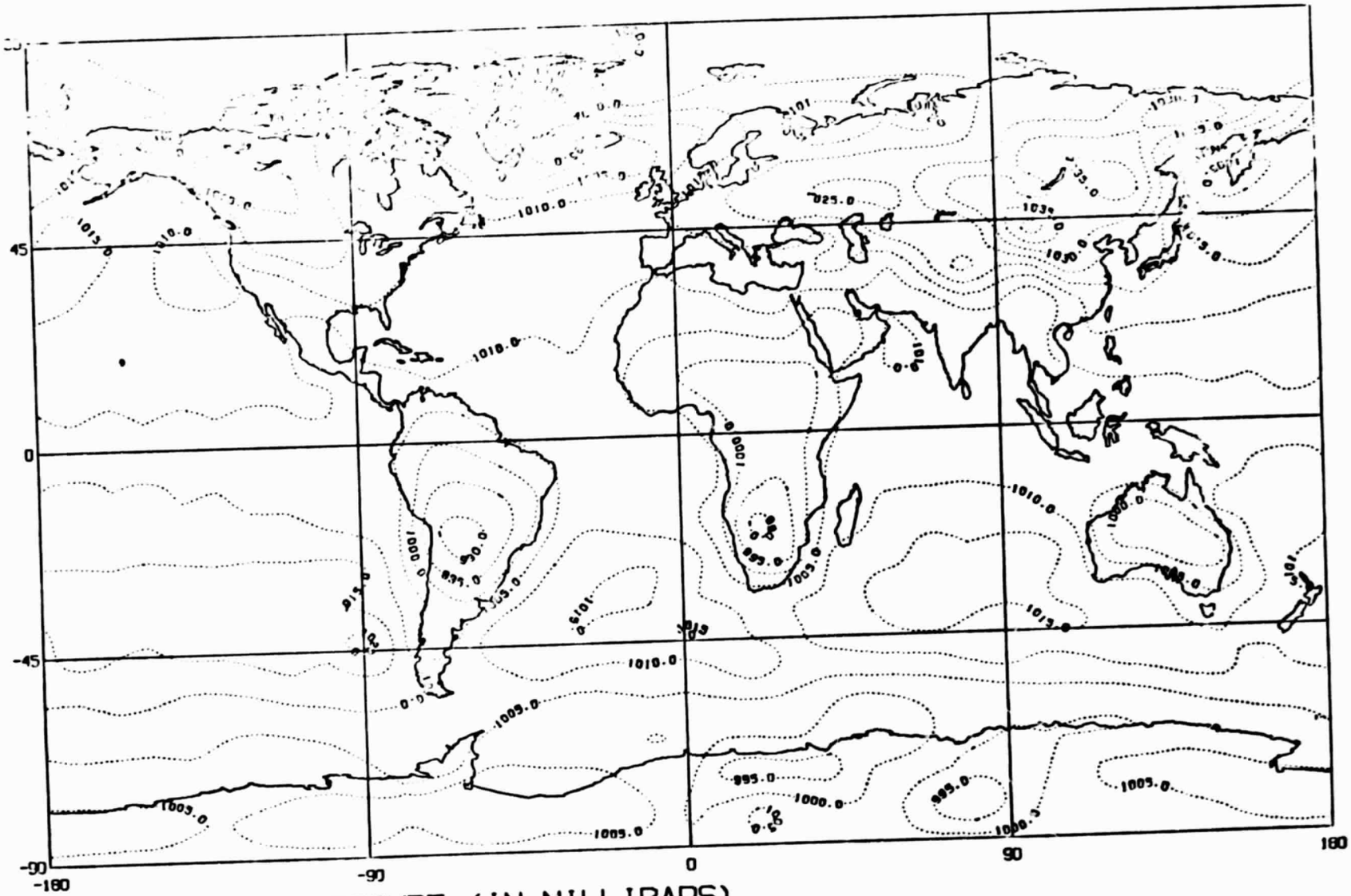

SEA LEVEL PRESSURE (IN MILLIBARS)

Fig. 3a

THE AVERAGE OF THE LAST 20 MONTHS OF RUN 003

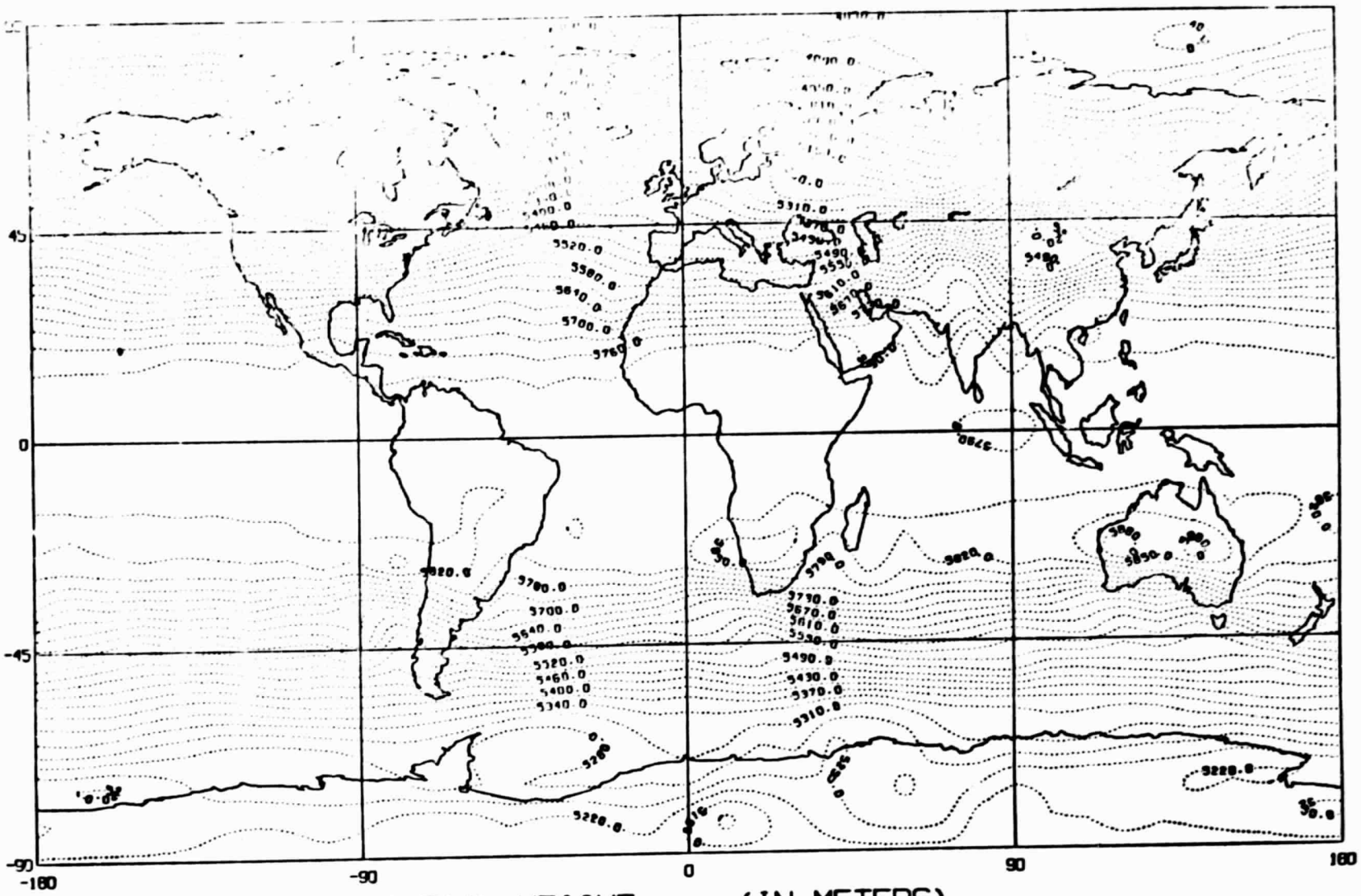

500 MB GEOPOTENTIAL HEIGHT (IN METERS)

THE AVERAGE OF THE LAST 20 MONTHS OF RUN 003

Fig. 3b

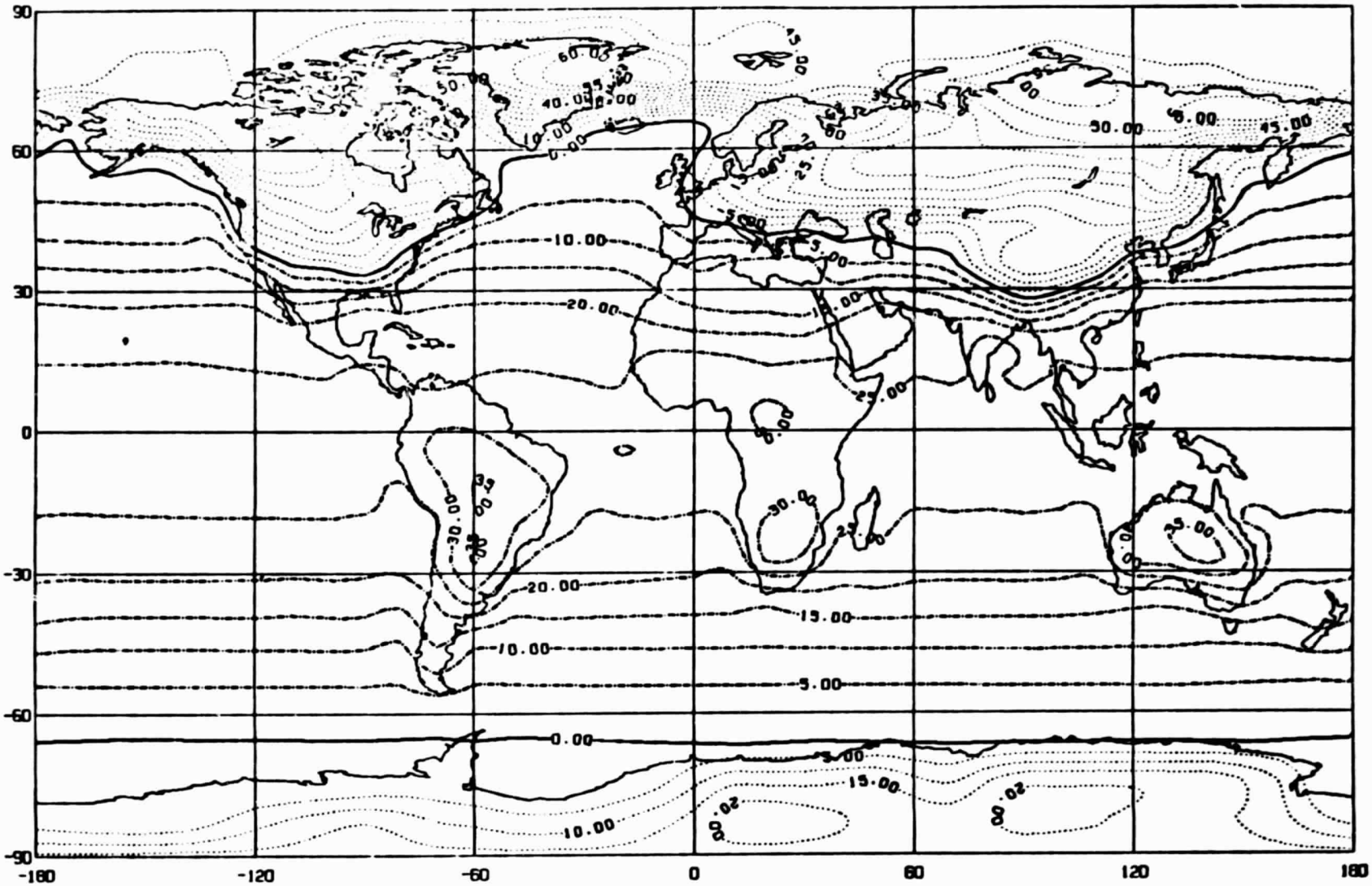

MEAN SURFACE AIR TEMPERATURE (IN DEGREES CENTIGRADE)

THIS IS RUN003

Fig. 3c

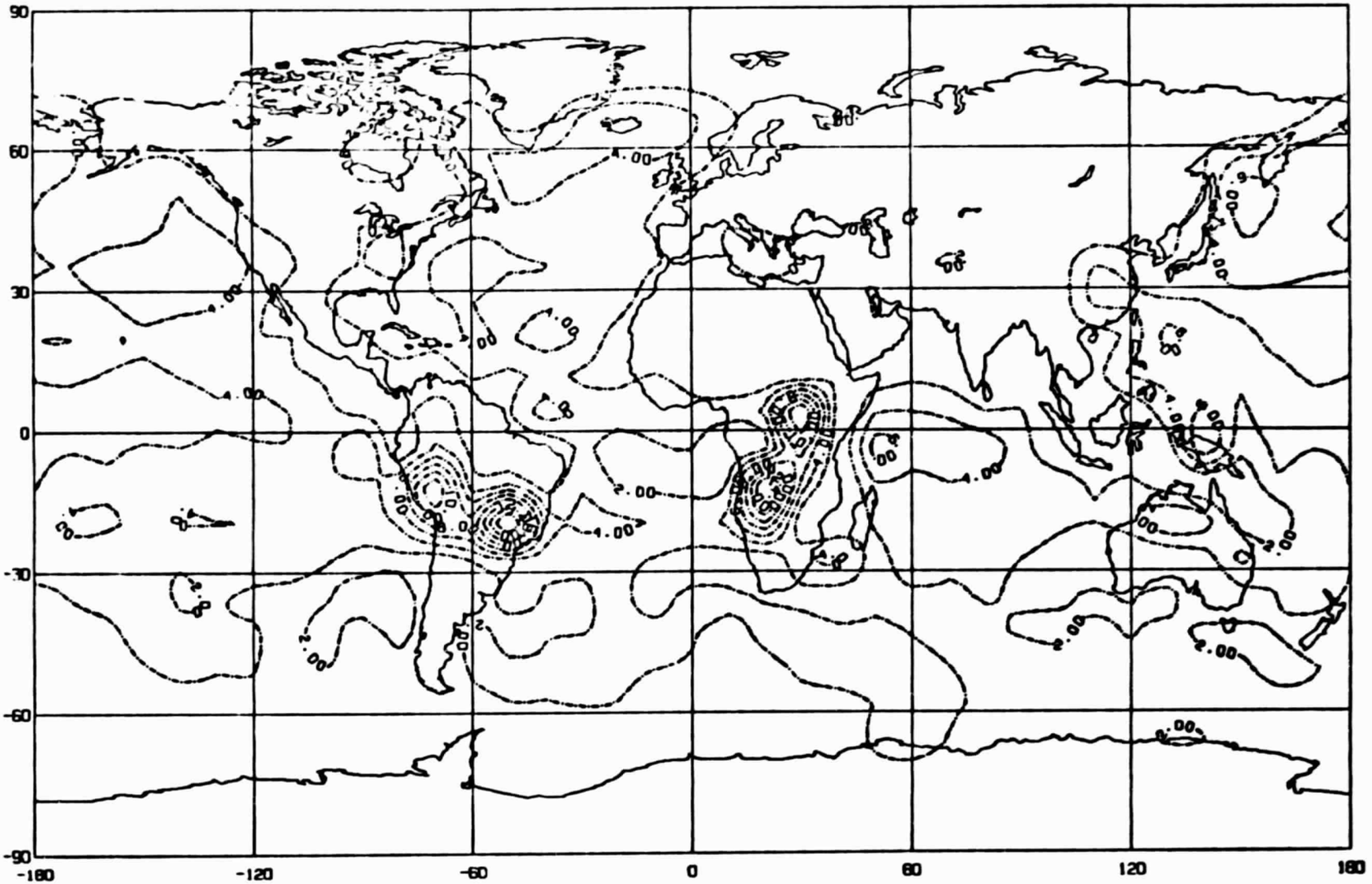

PRECIPITATION IN (MM/DAY)

THIS IS RUN003

Fig. 3d

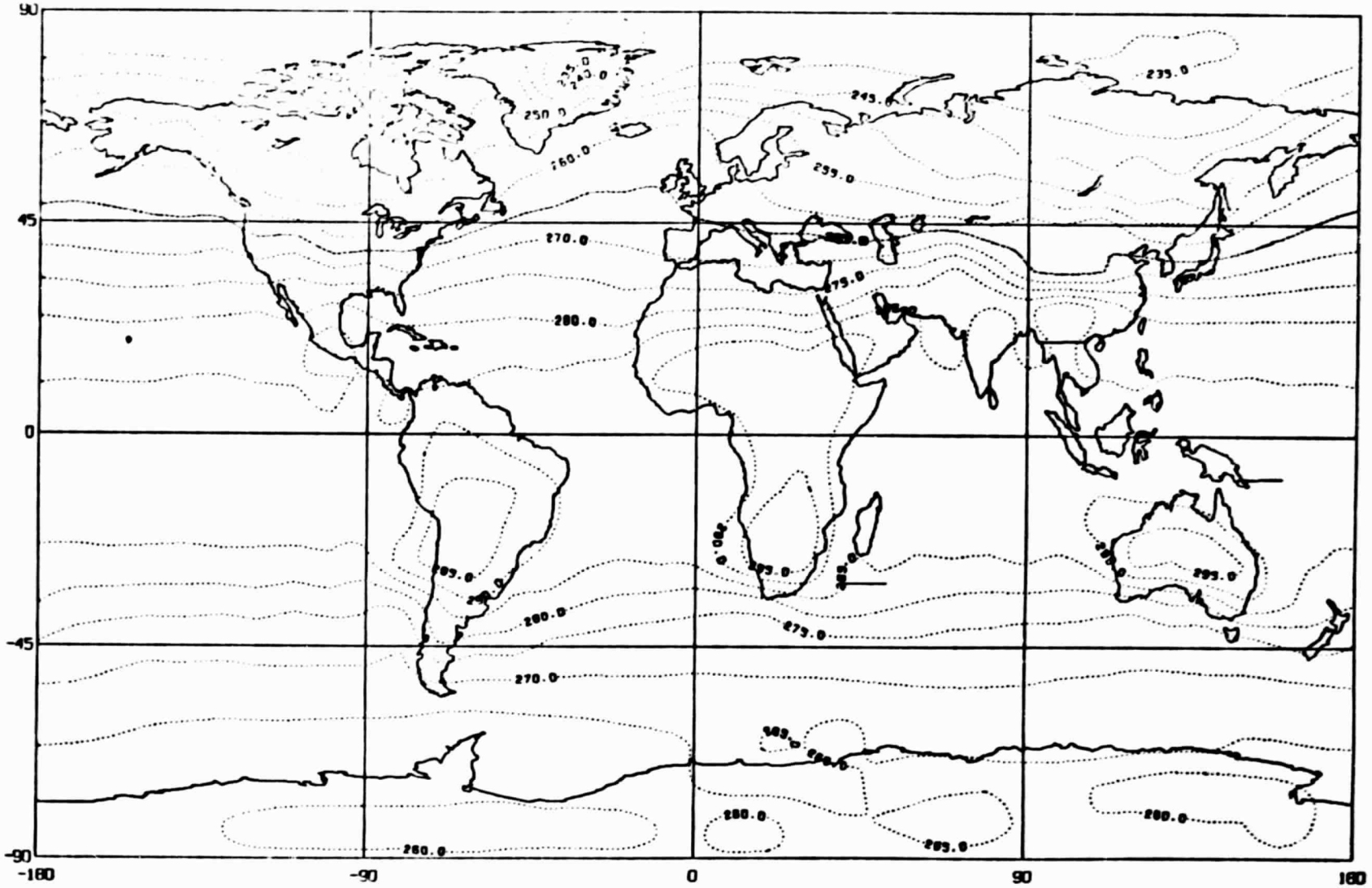

THE MEAN THICKNESS TEMPERATURES FROM 850 MB TO 700 MB IN (K)

THE AVERAGE OF THE LAST 20 MONTHS OF RUN 003

Fig. 3e

*****RUN003*SPIN UP WITH ISOTHERMAL ATMOSPHERE INCLUDING MOUNTIAN*ZERO GROUND WETNESS SPAR.COHEN.W

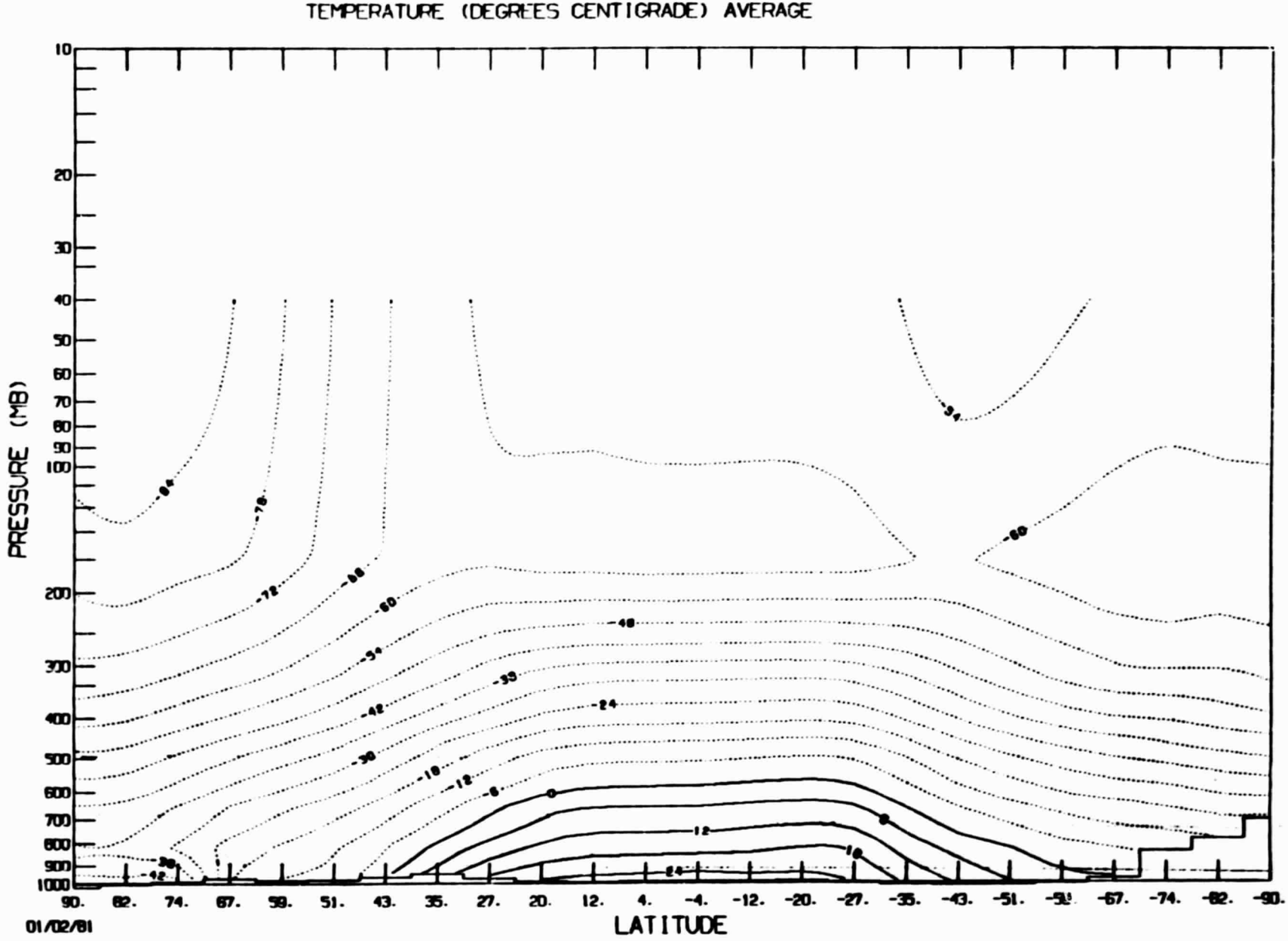

Fig. 3f

*****RUN003*SPIN UP WITH ISOTHERMAL ATMOSPHERE INCLUDING MOUNTIAN*ZERO GROUND WETNESS SPAR.COHEN.W

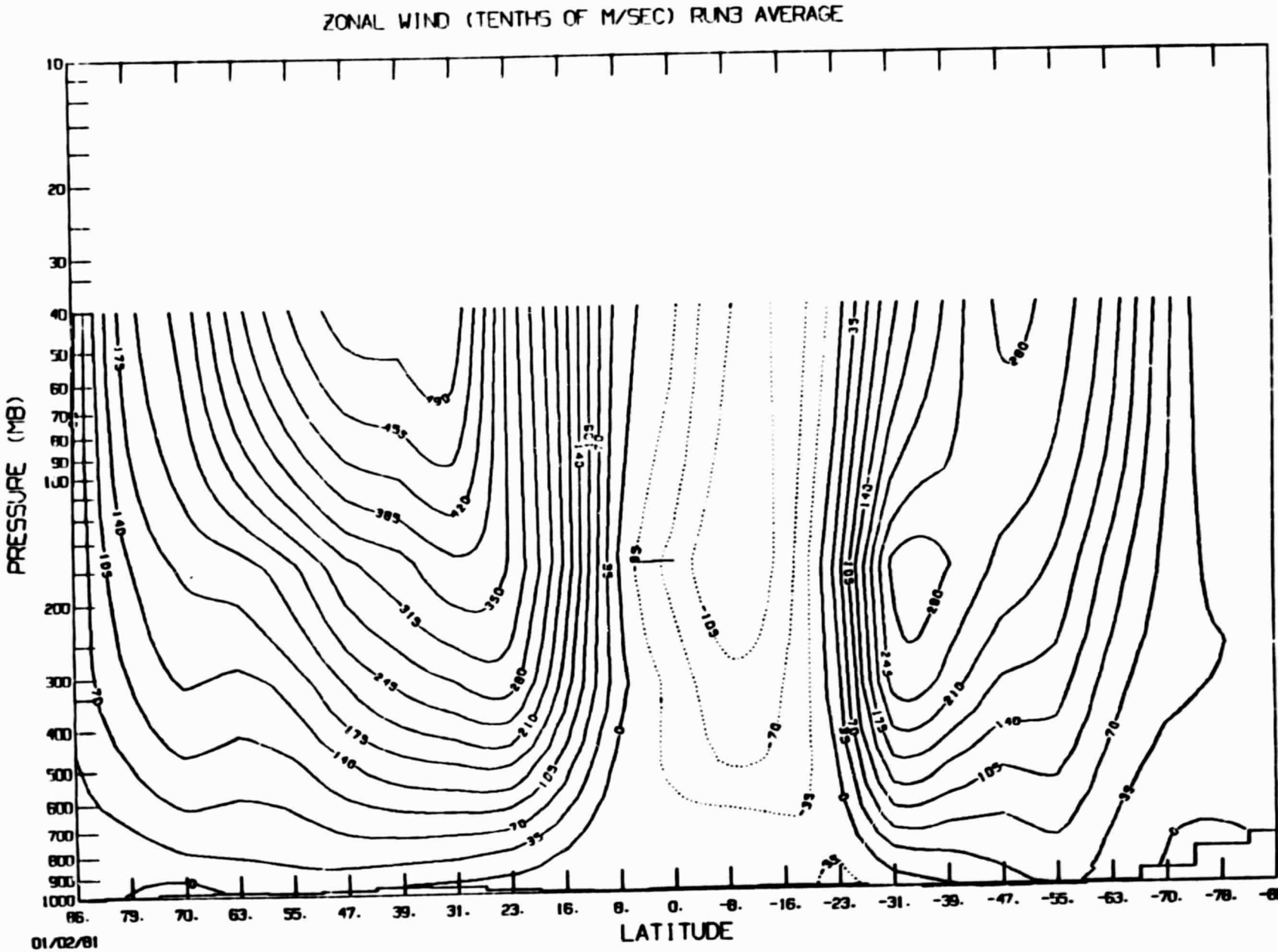

Fig. 3g

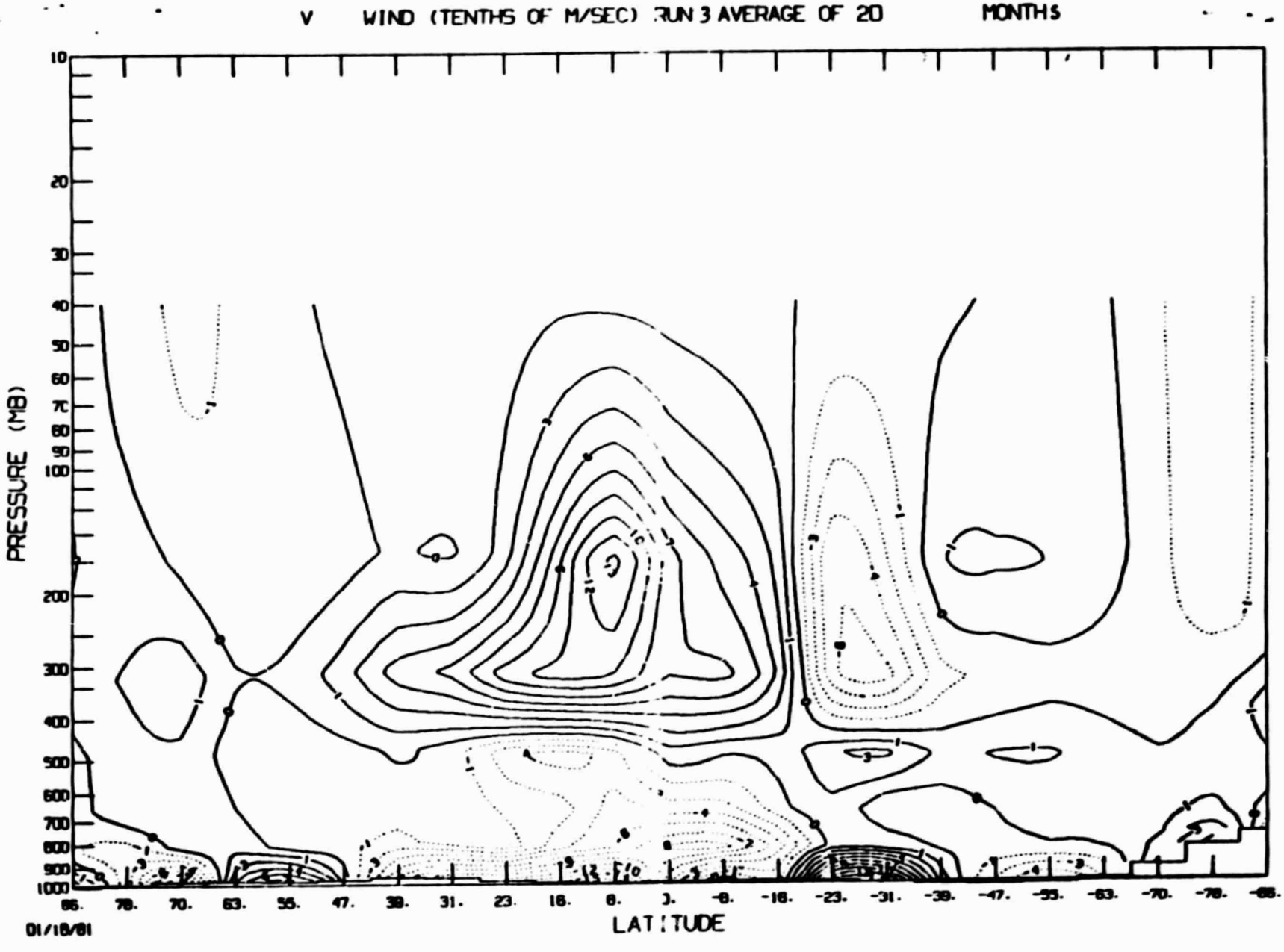
V WIND (TENTHS OF M/SEC) RUN 3 AVERAGE OF 20 MONTHS
PRESSURE (MB)
10
20
30
40
50
60
70
80
90
100
200
300
400
500
600
700
800
900
1000
86. 78. 70. 63. 55. 47. 39. 31. 23. 16. 8. 0. -8. -16. -23. -31. -39. -47. -55. -63. -70. -78. -86.
LATITUDE
01/18/81

Fig. 3h

*****RUN003*SPIN UP WITH ISOTHERMAL ATMOSPHERE INCLUDING MOUNTIAN*ZERO GROUND WETNESS SPAR.COHEN.W

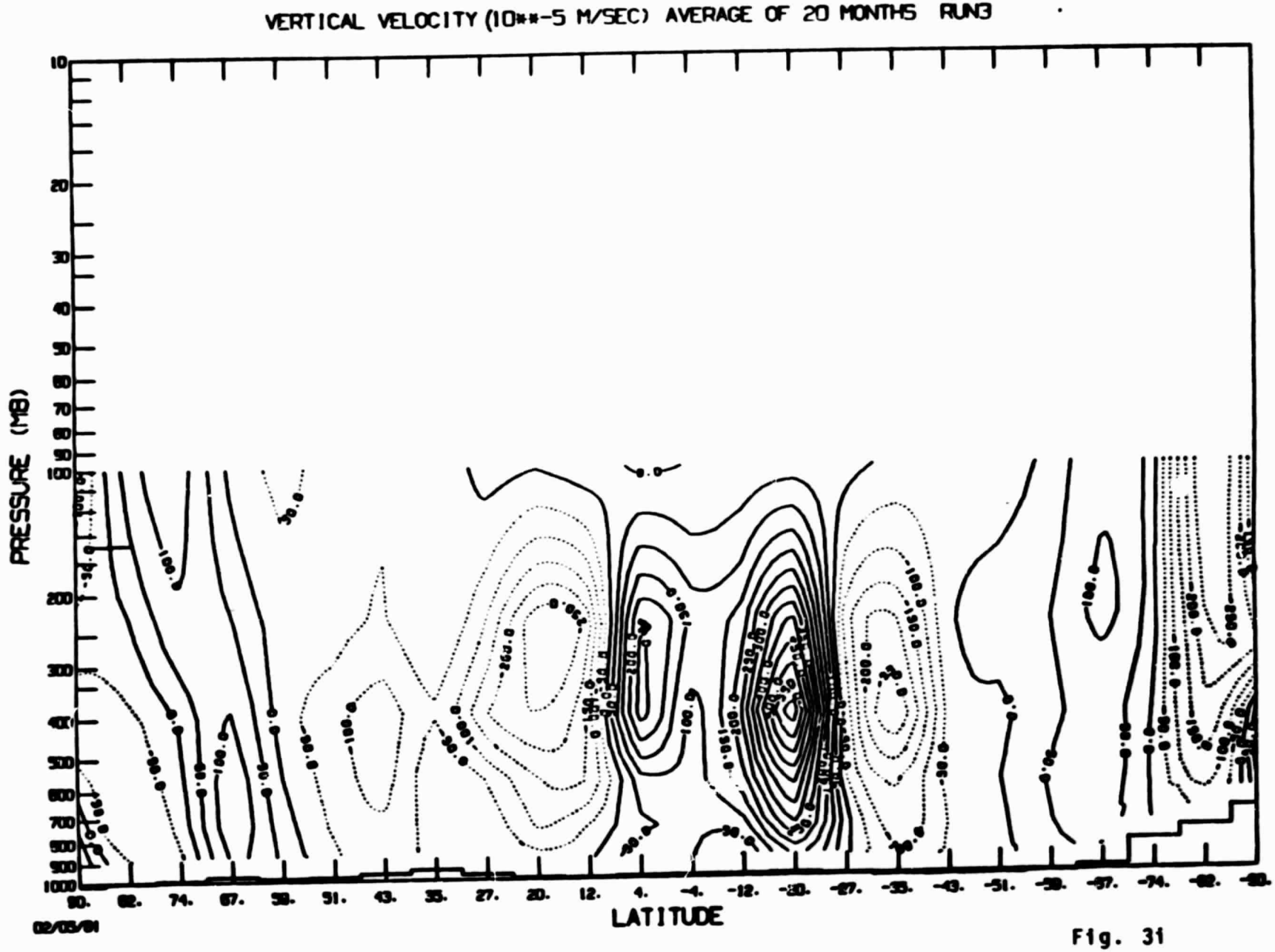

Fig. 31

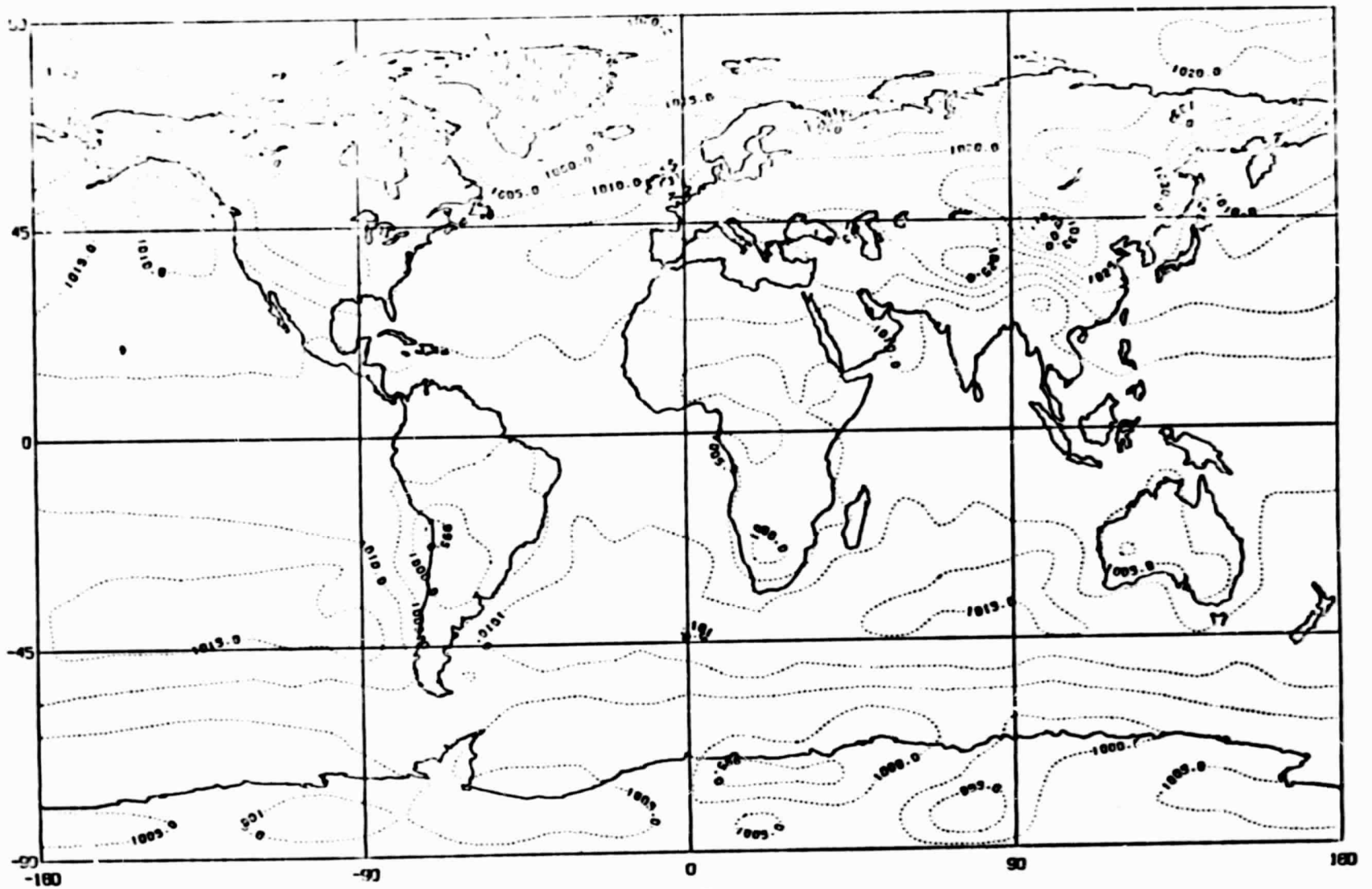

SEA LEVEL PRESSURE (IN MILLIBARS)

Fig. 4a

THE AVERAGE OF THE LAST 20 MONTHS OF RUN 004

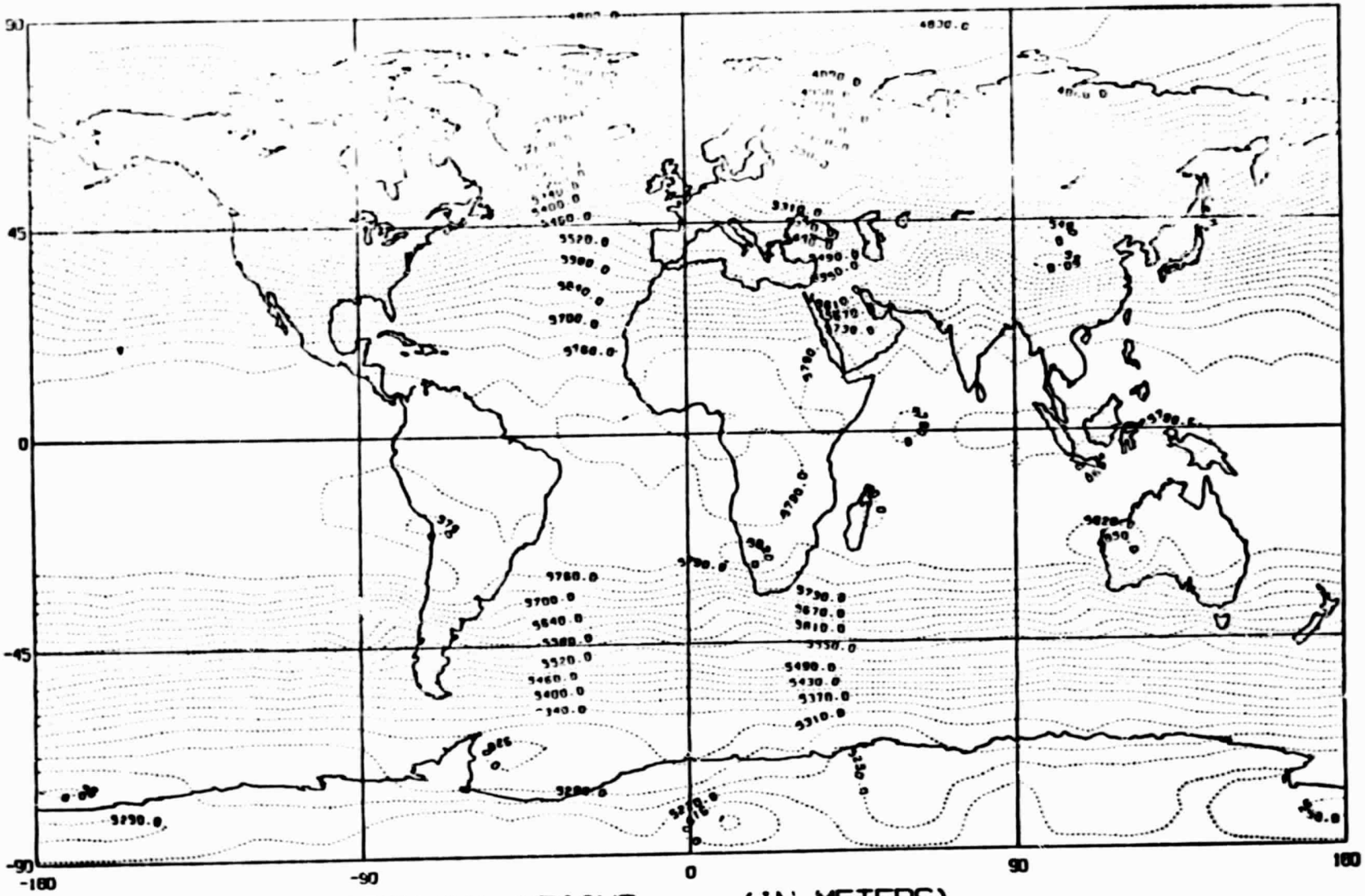

500 MB GEOPOTENTIAL HEIGHT (IN METERS)

THE AVERAGE OF THE LAST 20 MONTHS OF RUN 004

Fig. 4b

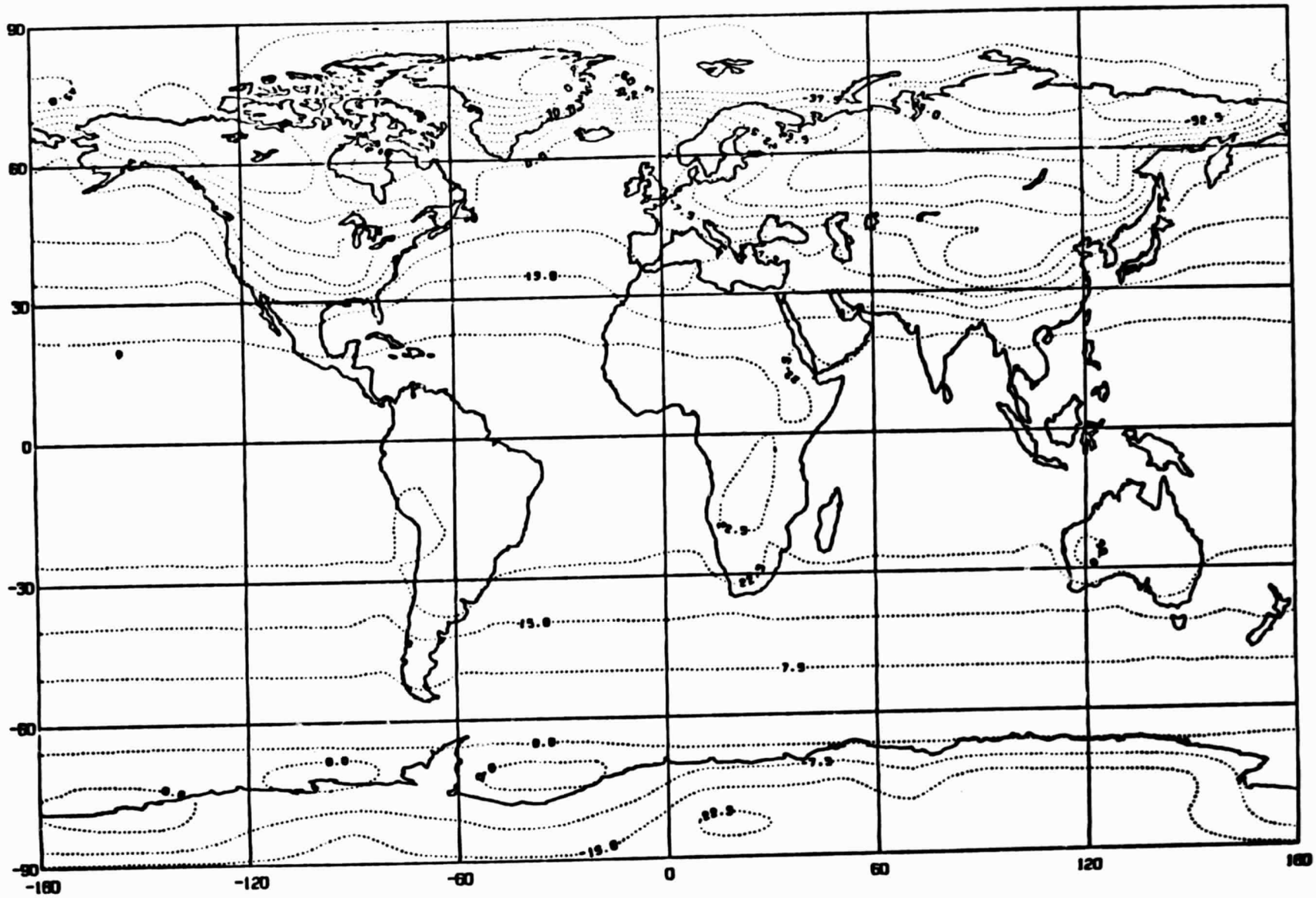

MEAN SURFACE AIR TEMPERATURE OF RUN004 (IN DEGREES CENTIGRADE)

Fig. 4c

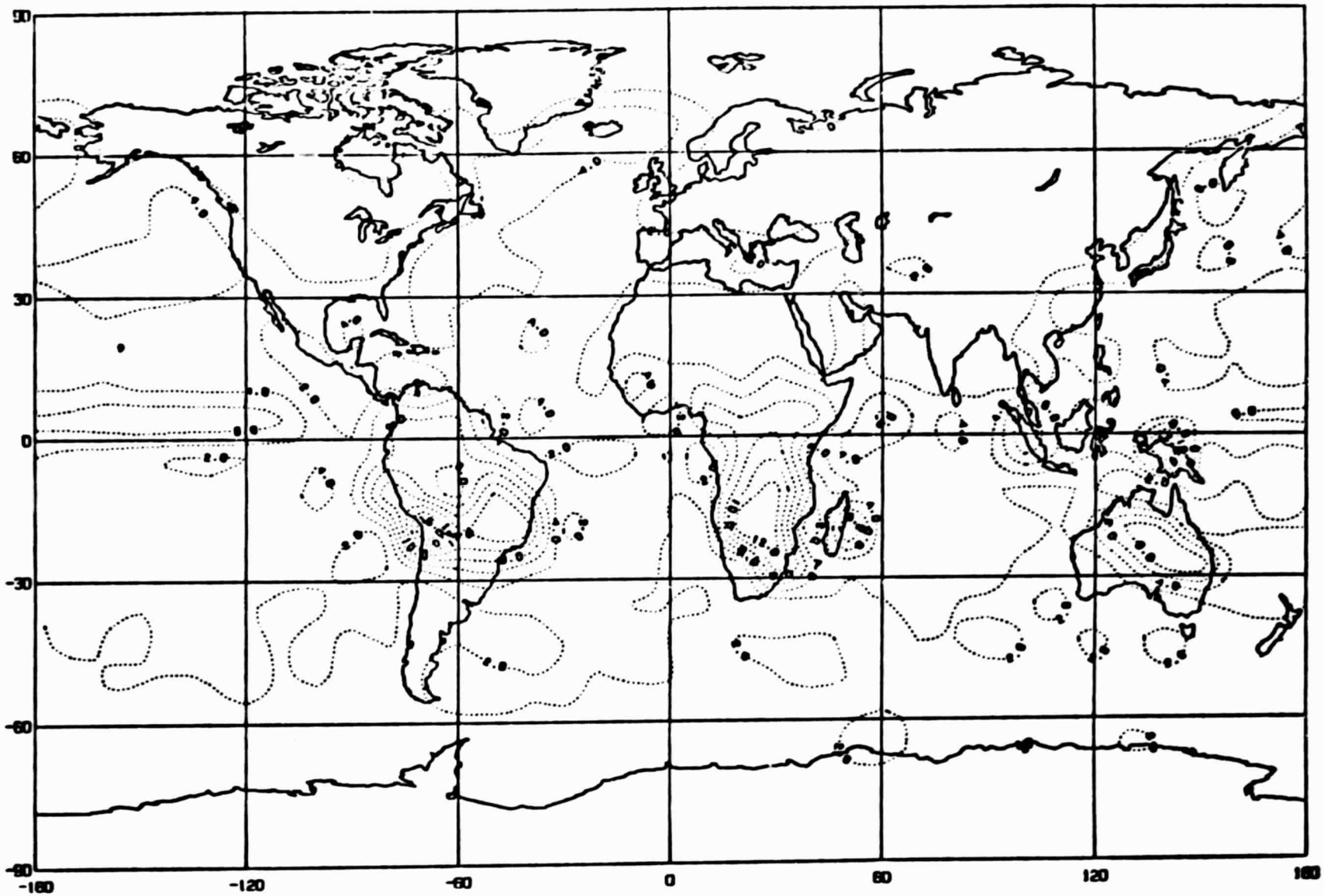

MEAN PRECIPITATION OF RUN004 (LAST 20 MONTHS IN (MM/DAY)

Fig. 4d

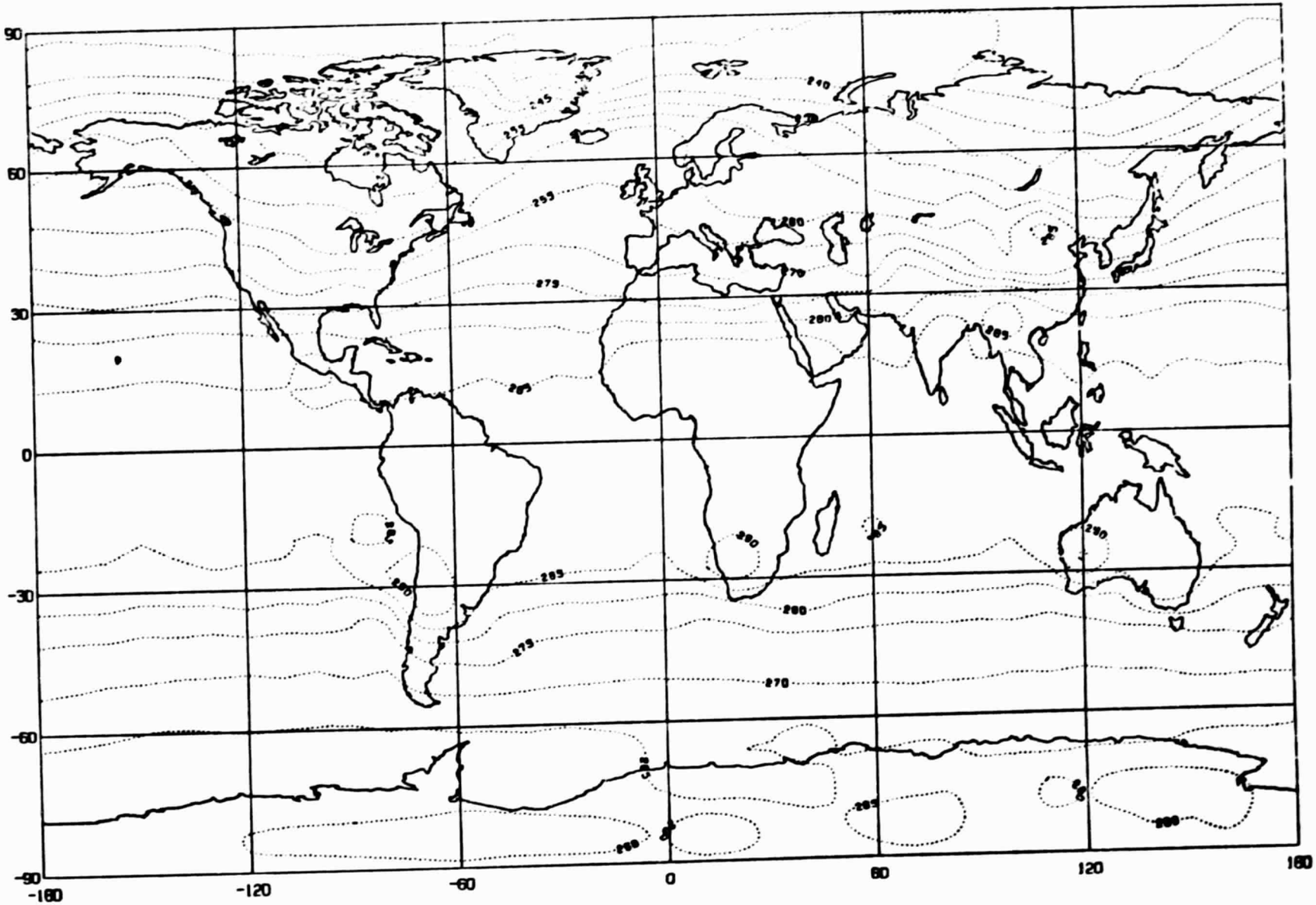

THICKNESS TEMP. OF 850-700 MB. 20 MONTHS MEAN OF RUN004 (K)

Fig. 4e

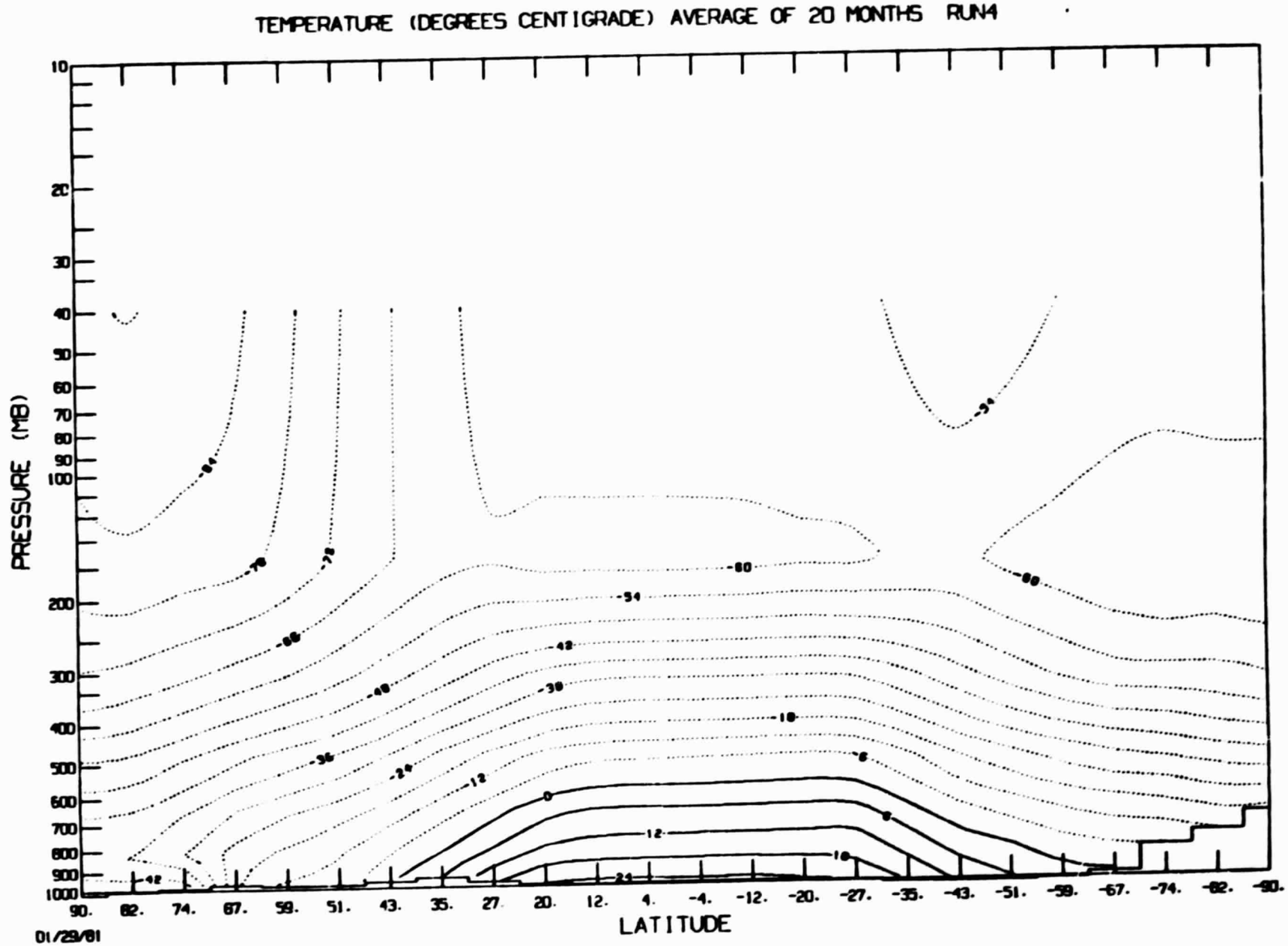
TEMPERATURE (DEGREES CENTIGRADE) AVERAGE OF 20 MONTHS RUN4
PRESSURE (MB)
10
20
30
40
50
60
70
80
100
200
300
400
500
600
700
800
900
1000
90. 82. 74. 67. 59. 51. 43. 35. 27. 20. 12. 4. -4. -12. -20. -27. -35. -43. -51. -59. -67. -74. -82. -90.
LATITUDE
01/29/81

Fig. 4f

*RUN#4*SPIN-UP FROM ISOTHERMAL ATMOSPHERE*WITH MOUNTAINS AND SURFACE PHYSICS *SPAR.COHEN.WU #4

ZONAL WIND (TENTHS OF M/SEC) RUN4 AVERAGE OF 20MONTHS

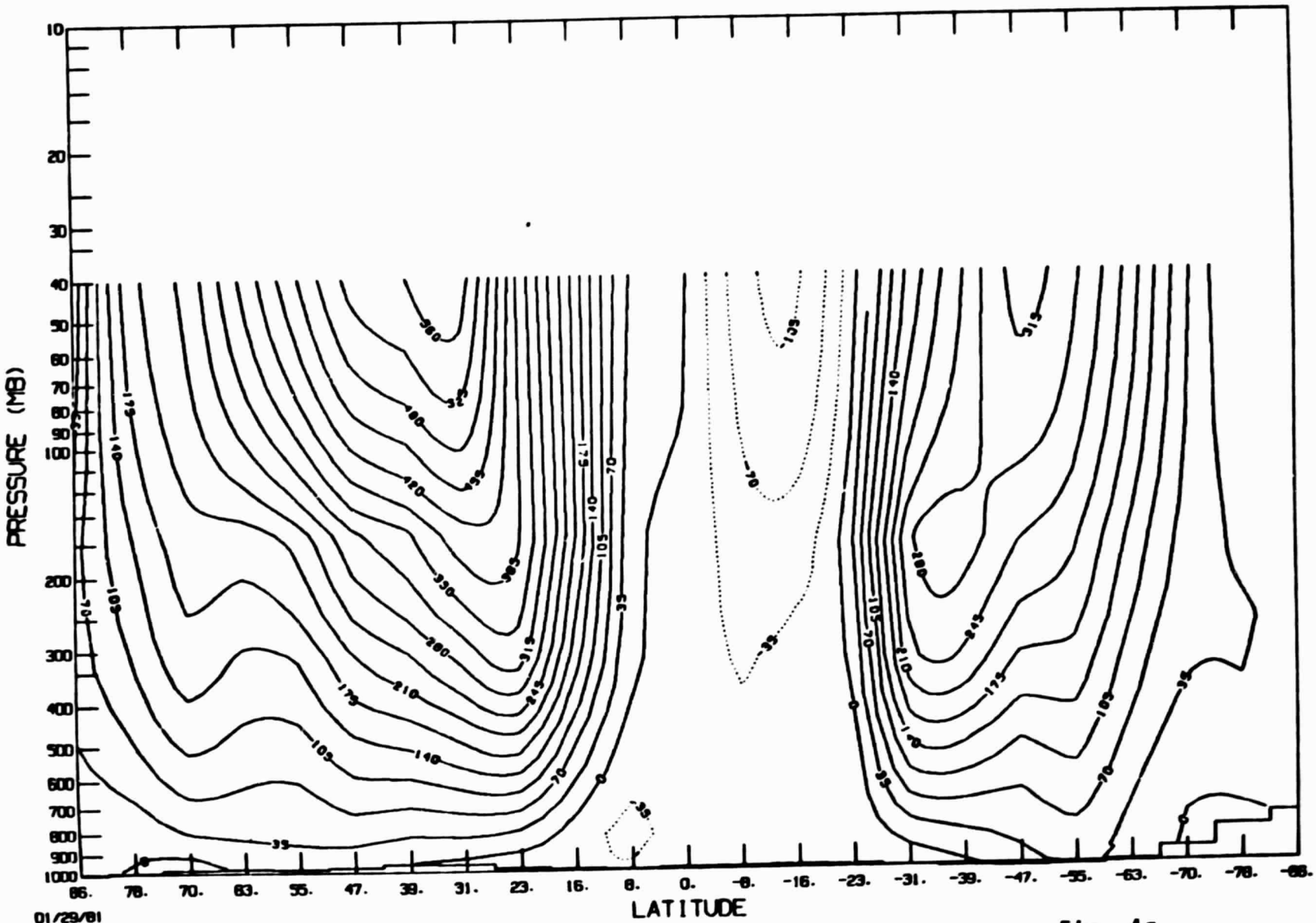

Fig. 4g

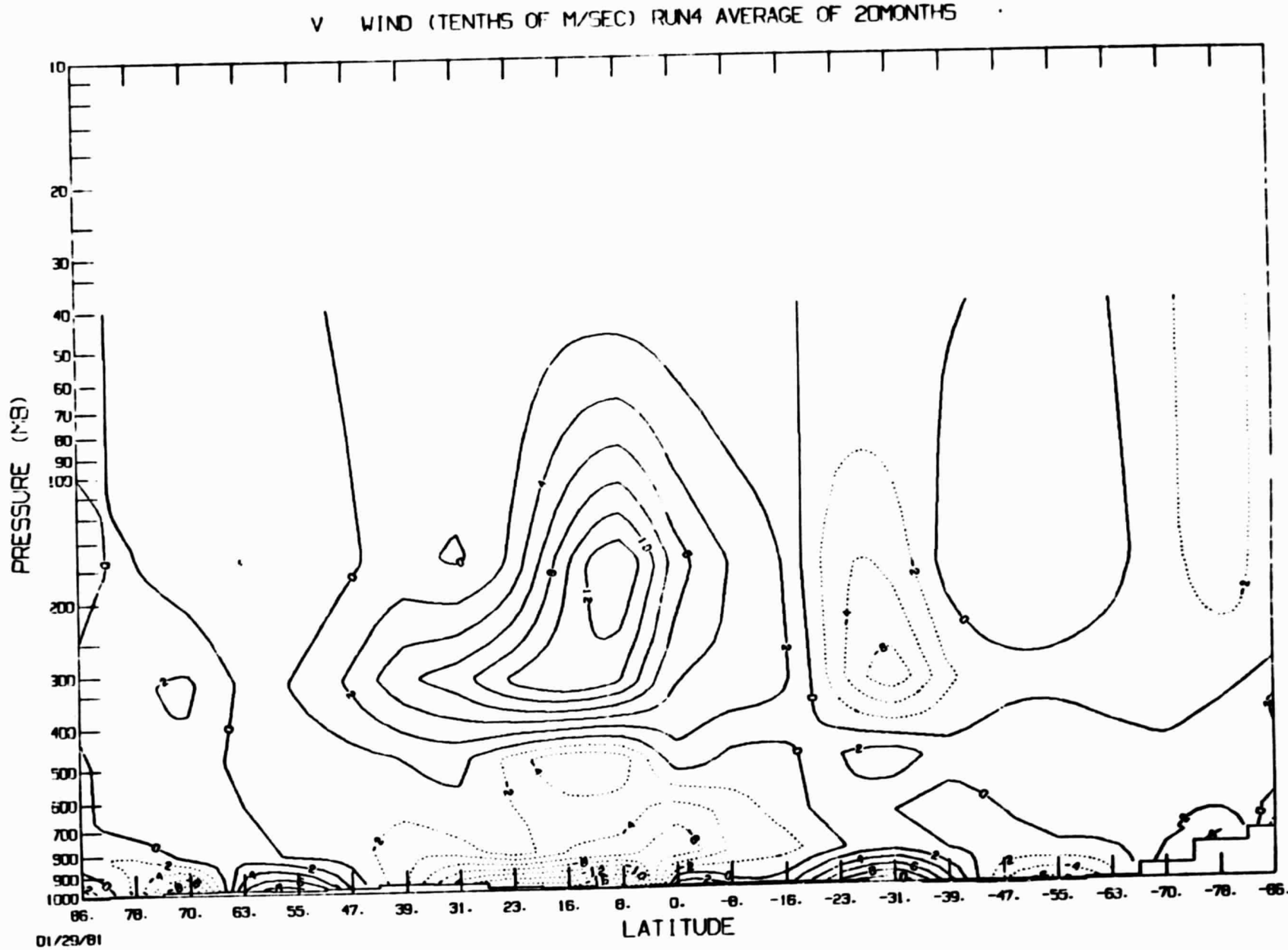

Fig. 4h

*RUN*4*SPIN-UP FROM ISOTHERMAL ATMOSPHERE*WITH MOUNTAINS AND SURFACE PHYSICS *SPAR.COHEN.WU *4

VERTICAL VELOCITY (10**-5 M/SEC) AVERAGE OF 20 MONTHS RUN4

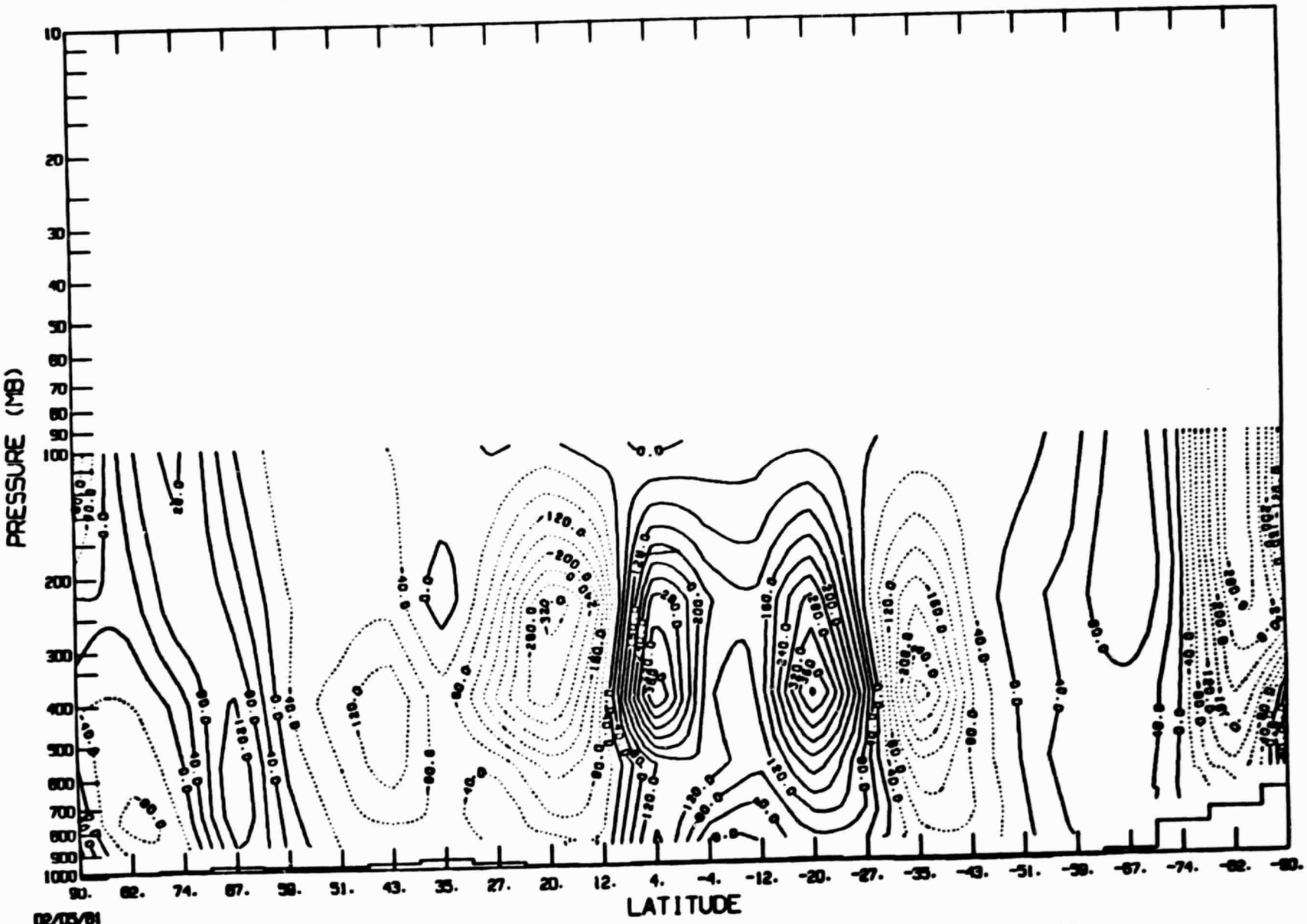

Fig. 41

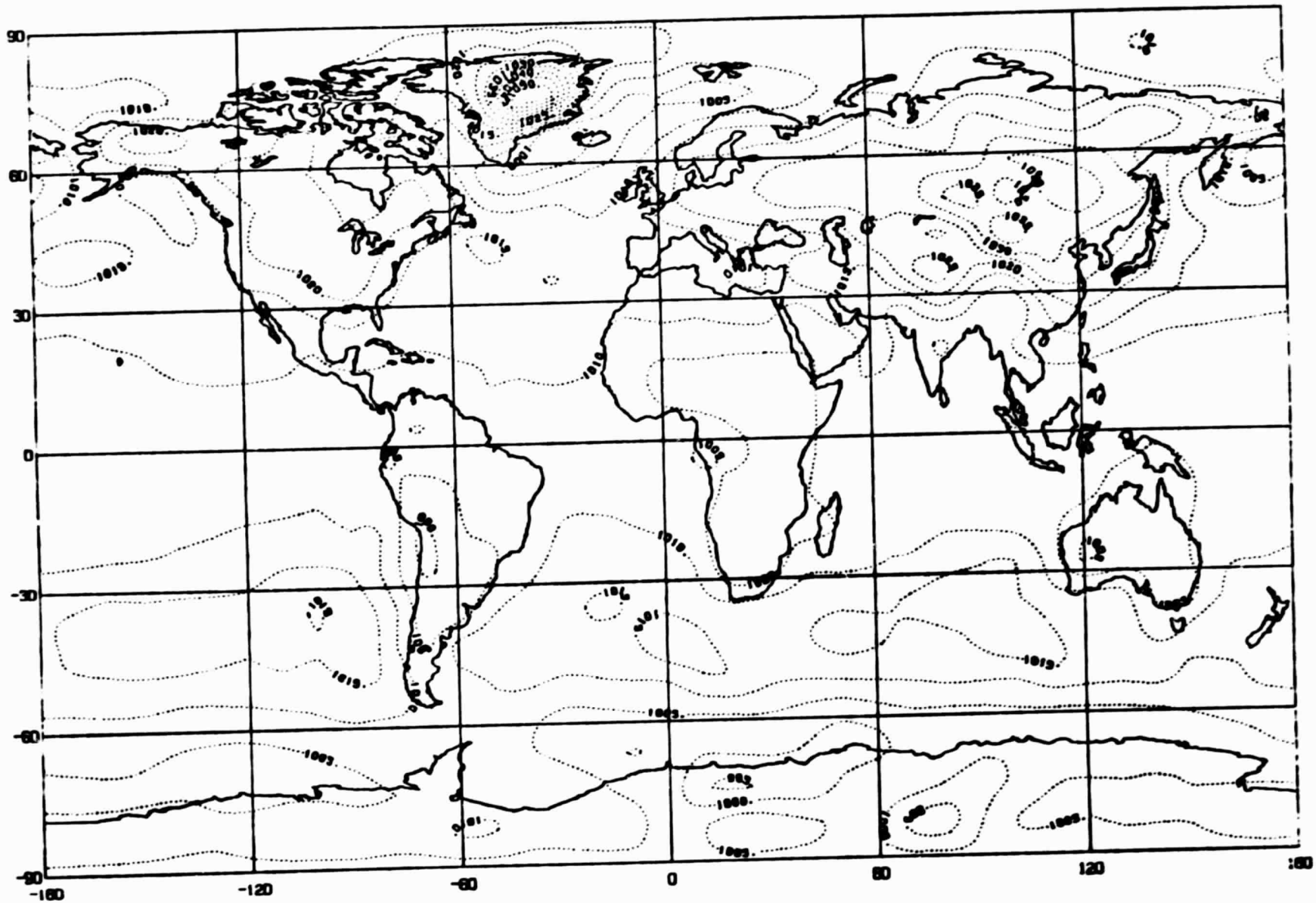

SEA LEVEL PRESSURE (IN MILLIBARS)

THE AVERAGE OF THE LAST 20 MONTHS OF RUN 005

Fig. 5a

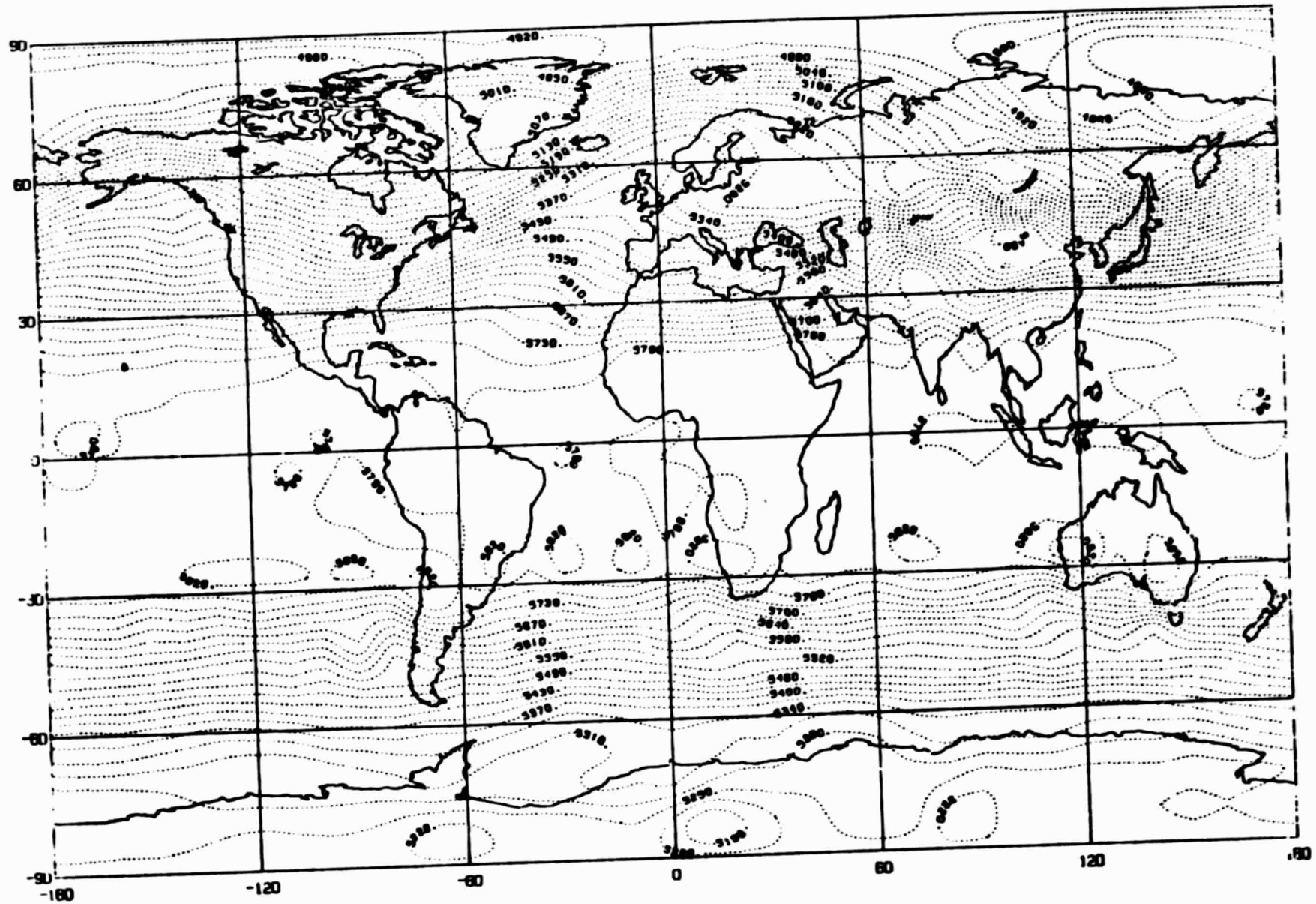

500 MB GEOPOTENTIAL HEIGHT (IN METERS)

THE AVERAGE OF THE LAST 20 MONTHS OF RUN 005

Fig. 5b

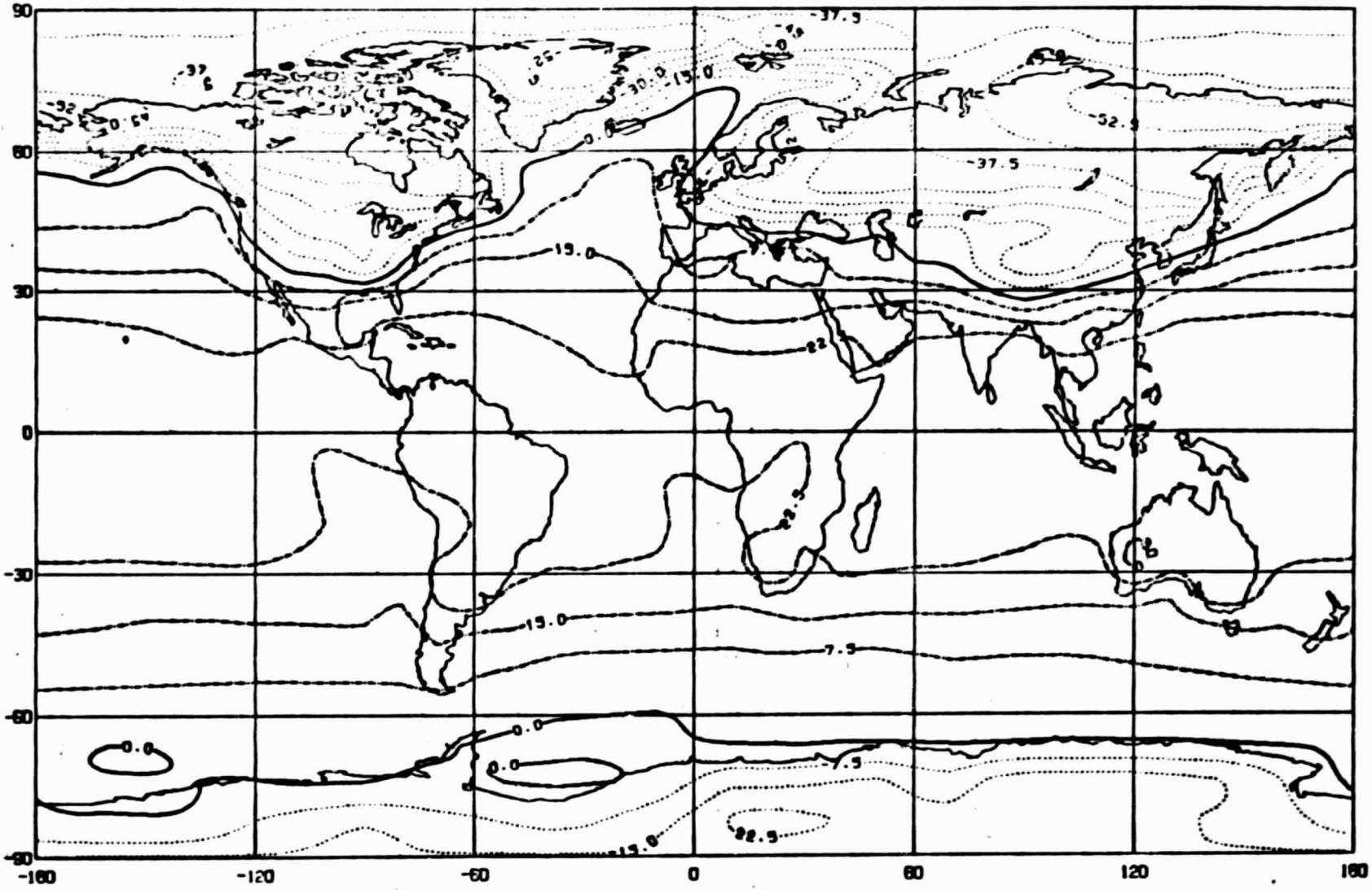

MEAN SURFACE AIR TEMPERATURE *(IN DEGREES CENTIGRADE)*

THE MEAN OF RUN5

Fig. 5c

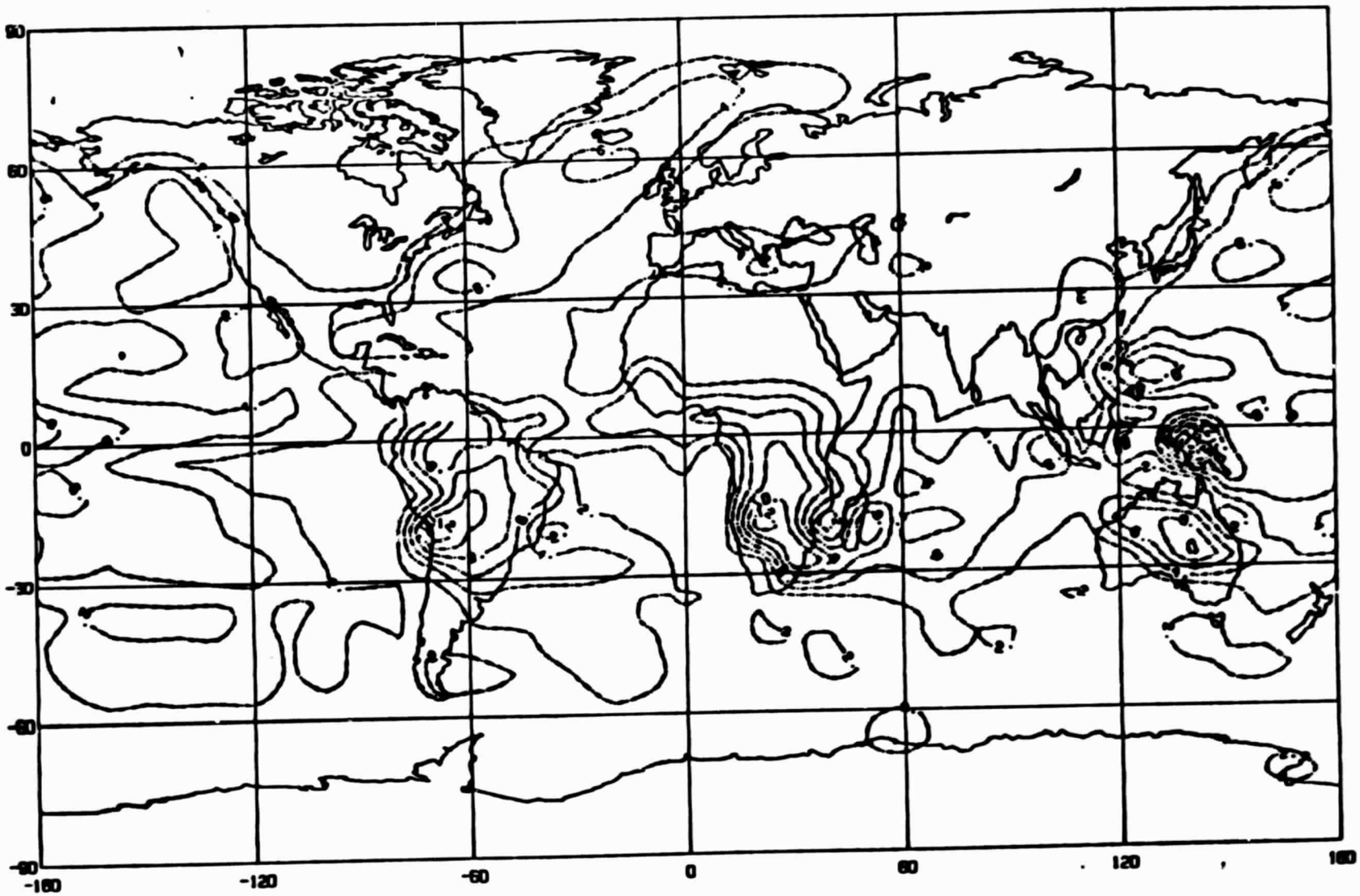

PRECIPITATION IN (MM/DAY)

The mean of RUN5

Fig. 5d

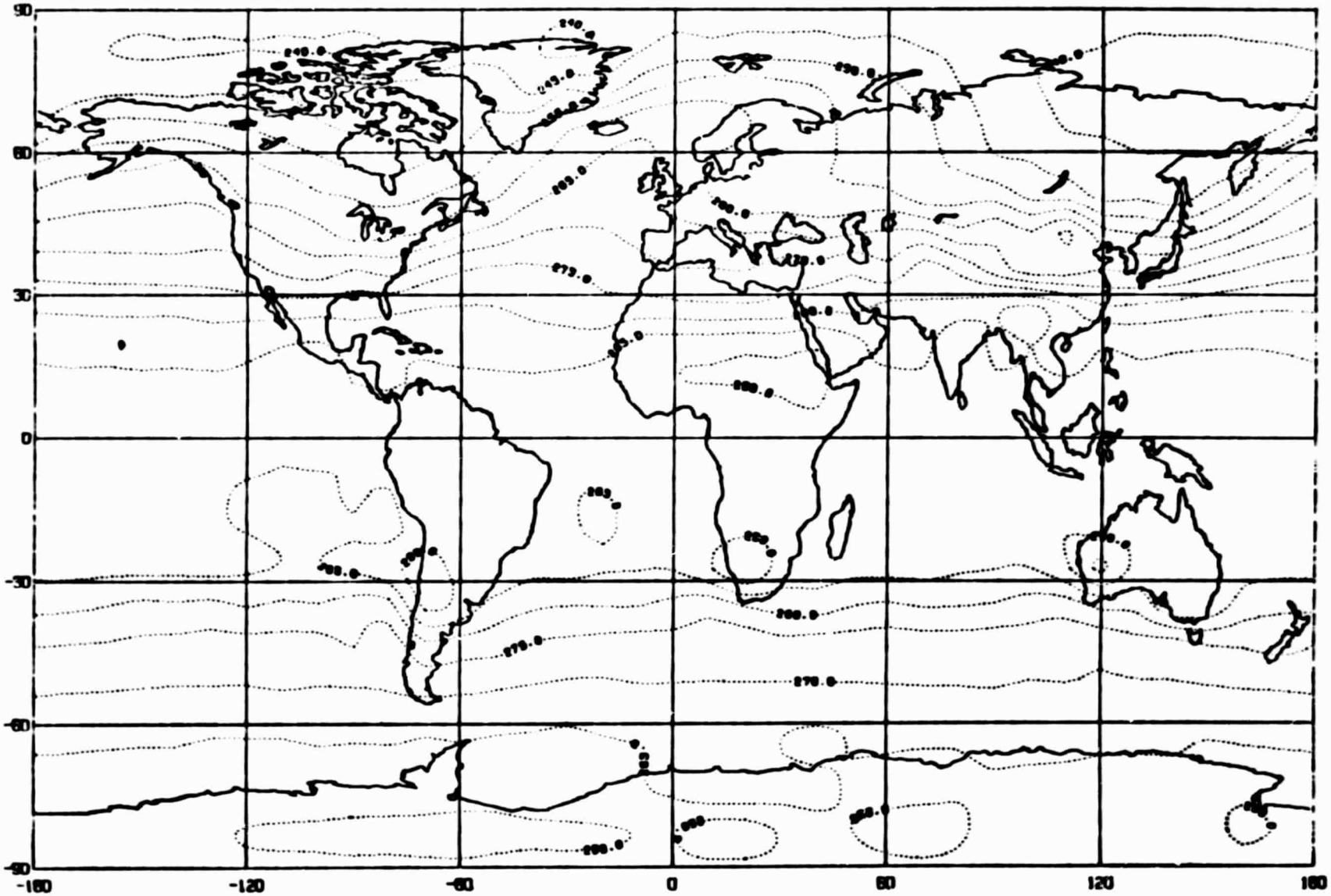

THE MEAN THICKNESS TEMPERATURES FROM 850 MB TO 700 MB IN (K)

THE AVERAGE OF THE LAST 20 MONTHS OF RUN 005

Fig. 5e

TEMPERATURE (DEGREES CENTIGRADE) AVERAGE OF 20 MONTHS RUNS

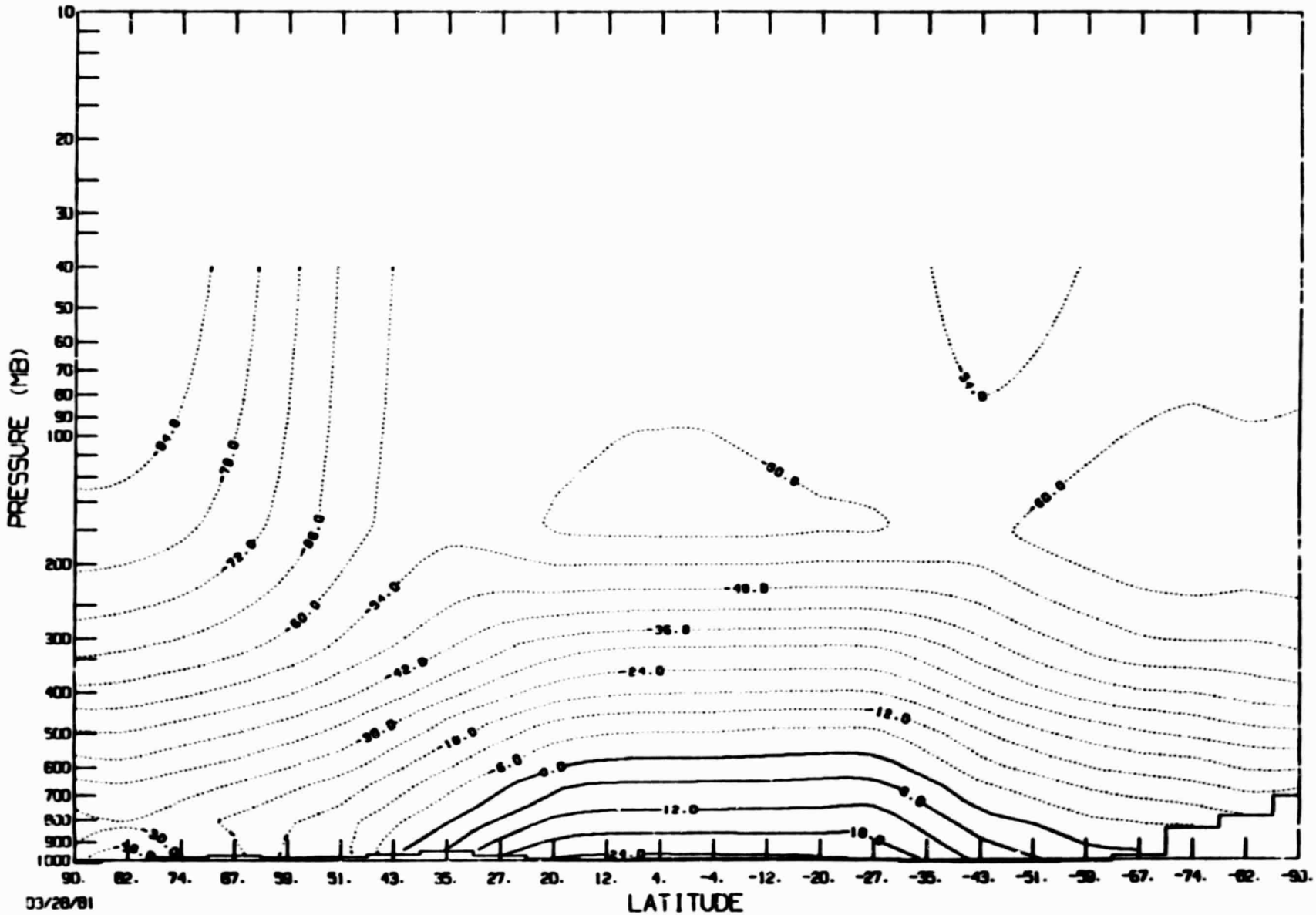

Fig. 5f

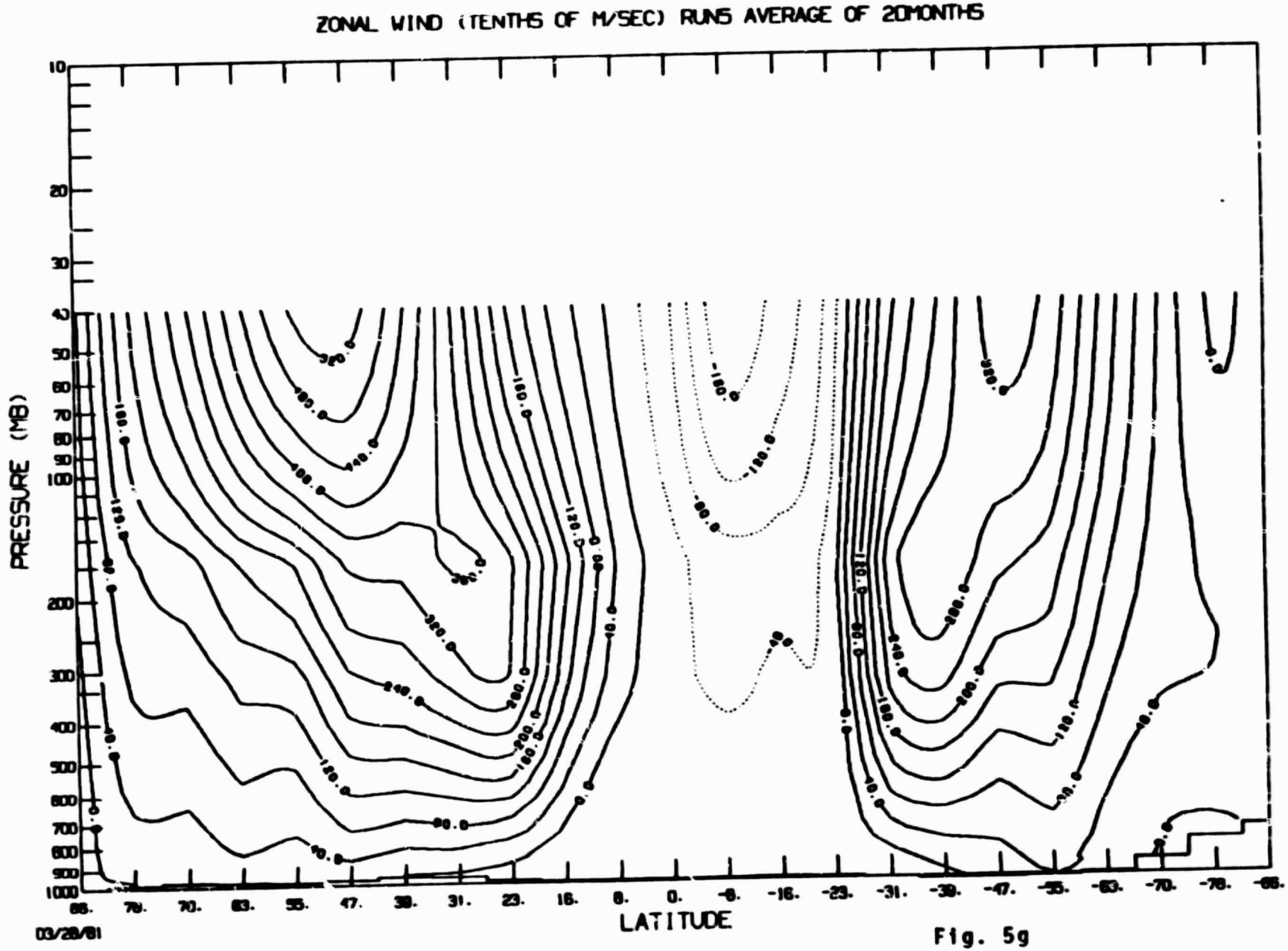
ZONAL WIND (TENTHS OF M/SEC) RUNS AVERAGE OF 20MONTHS
PRESSURE (MB)
10
20
30
40
50
70
100
200
300
400
500
600
700
800
900
1000
86. 78. 70. 63. 55. 47. 39. 31. 23. 16. 8. 0. -8. -16. -23. -31. -39. -47. -55. -63. -70. -78. -86.
LATITUDE
03/28/81

Fig. 5g

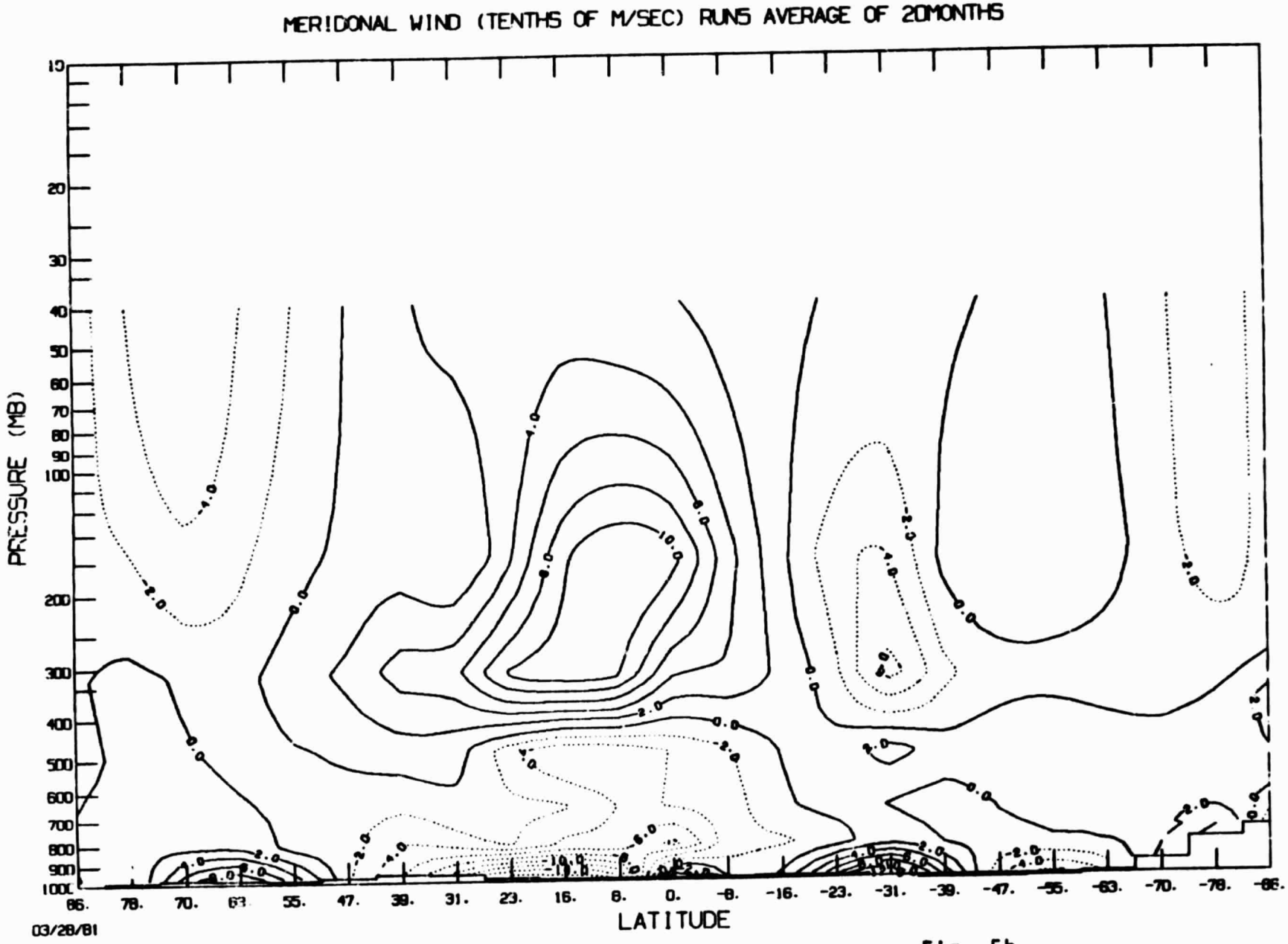
MERIDONAL WIND (TENTHS OF M/SEC) RUNS AVERAGE OF 20MONTHS
PRESSURE (MB)
10
20
30
40
50
60
70
80
90
100
200
300
400
500
600
700
800
900
1000
86. 78. 70. 63. 55. 47. 39. 31. 23. 16. 8. 0. -8. -16. -23. -31. -39. -47. -55. -63. -70. -78. -86.
LATITUDE
03/28/81

Fig. 5h

RUN#5 SPIN-UP WITH MOUNTAINS AND SURFACE PHYSICS AND REAL OCEAN TEMPERATURES SPAR.WU.COHEN RUN#5

VERTICAL VELOCITY (10**-5 M/SEC) THE MEAN OF RUN5

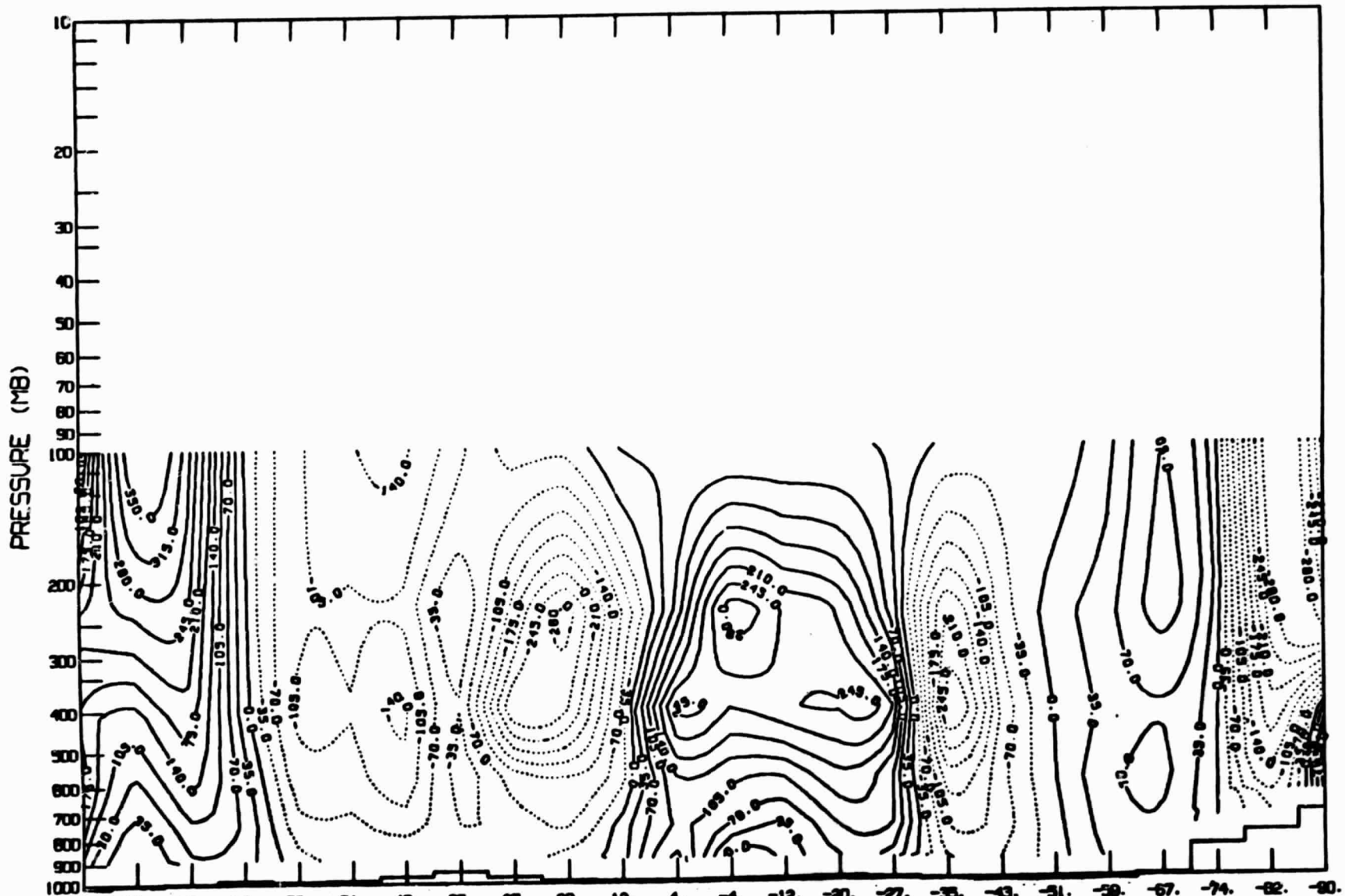

Fig. 5i

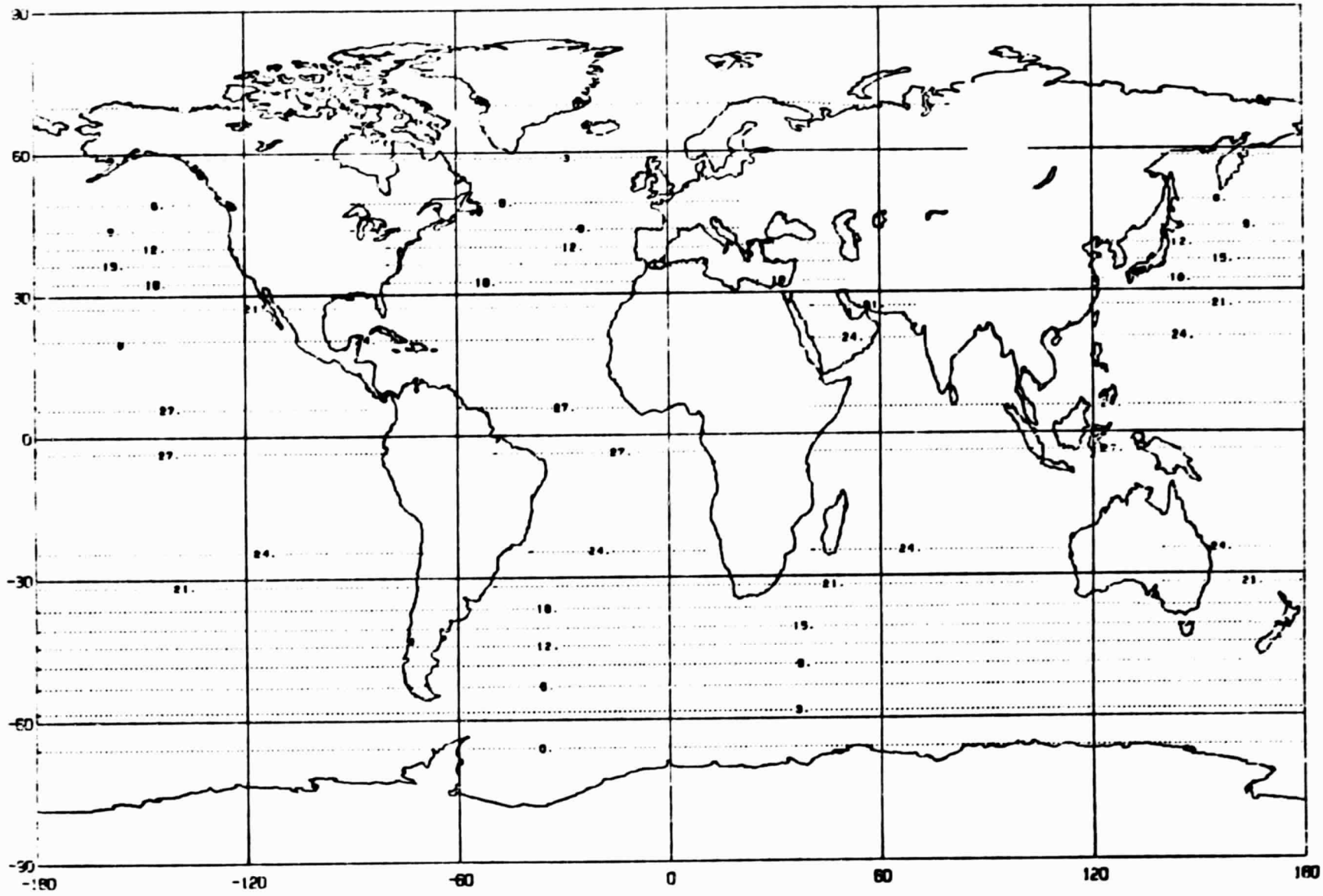

SEA SURFACE TEMPERATURE FOR RUNS 0 THROUGH 4 (DEGREES CELSIUS)

Fig. 6a

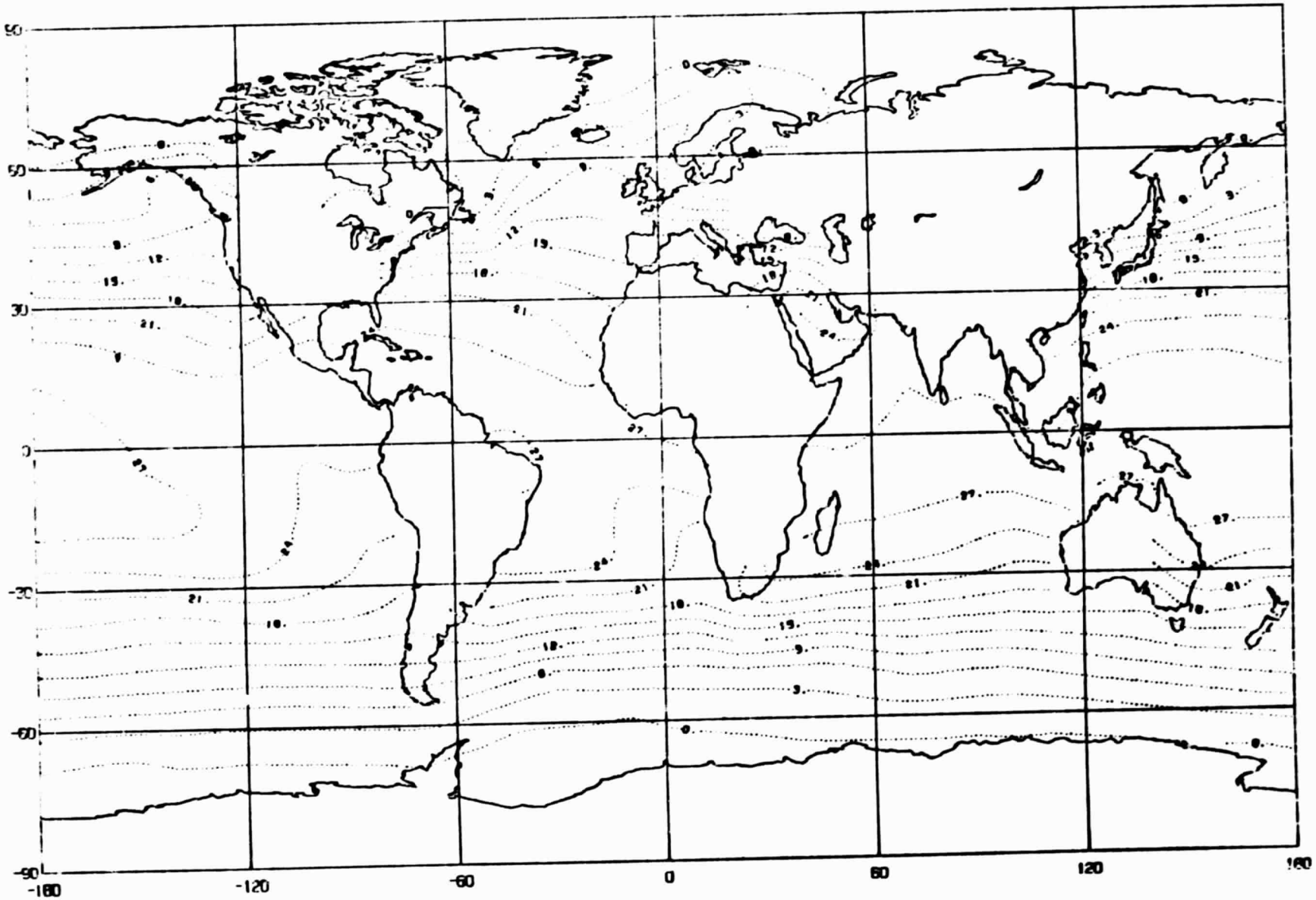

SEA SURFACE TEMPERATURE FOR RUN #5 (DEGREES CELSIUS)

Fig. 6b

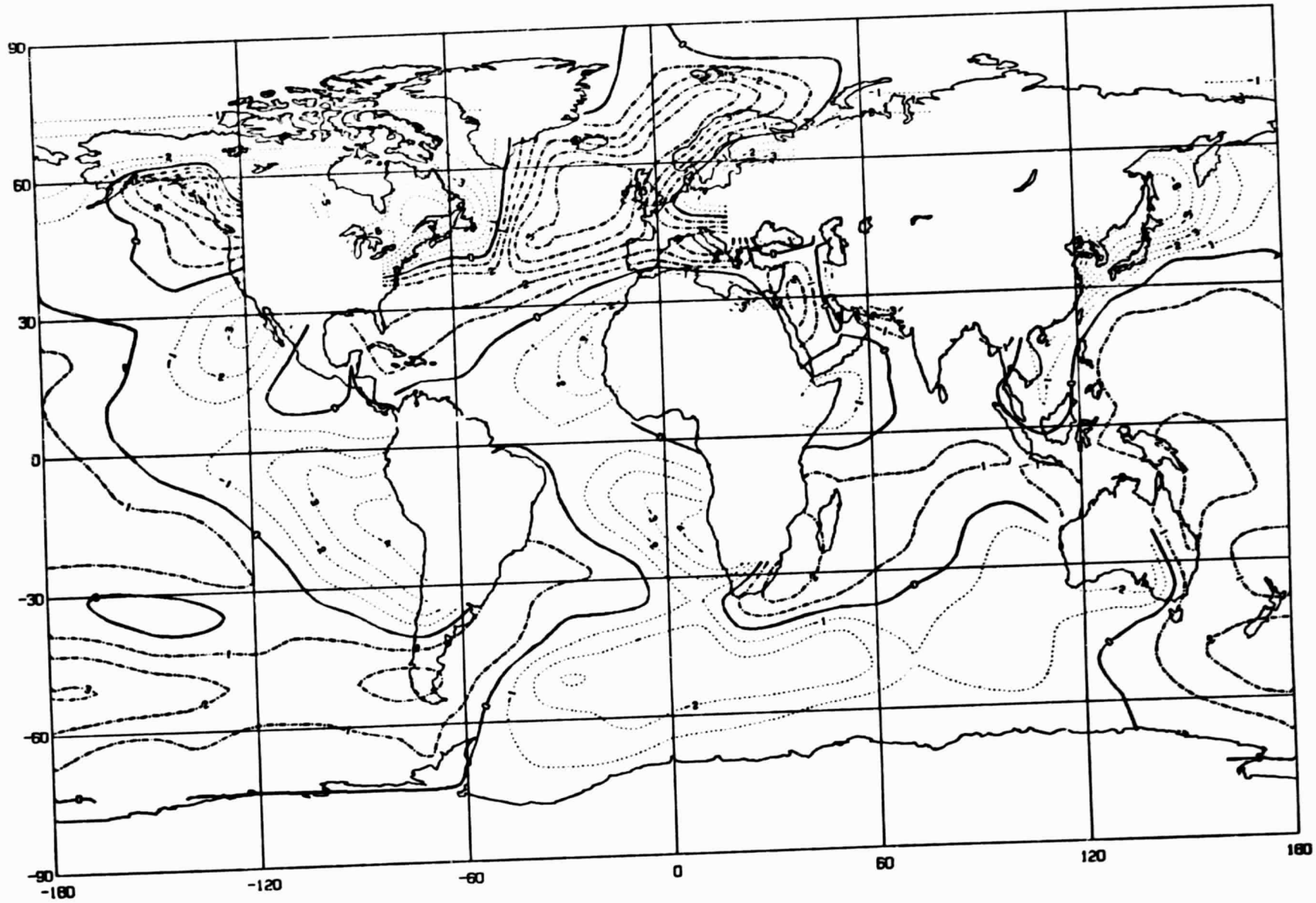

SEA SURFACE TEMPERATURE (DEGREES CELSIUS) RUN 5 MINUS RUN 4

Fig. 6c

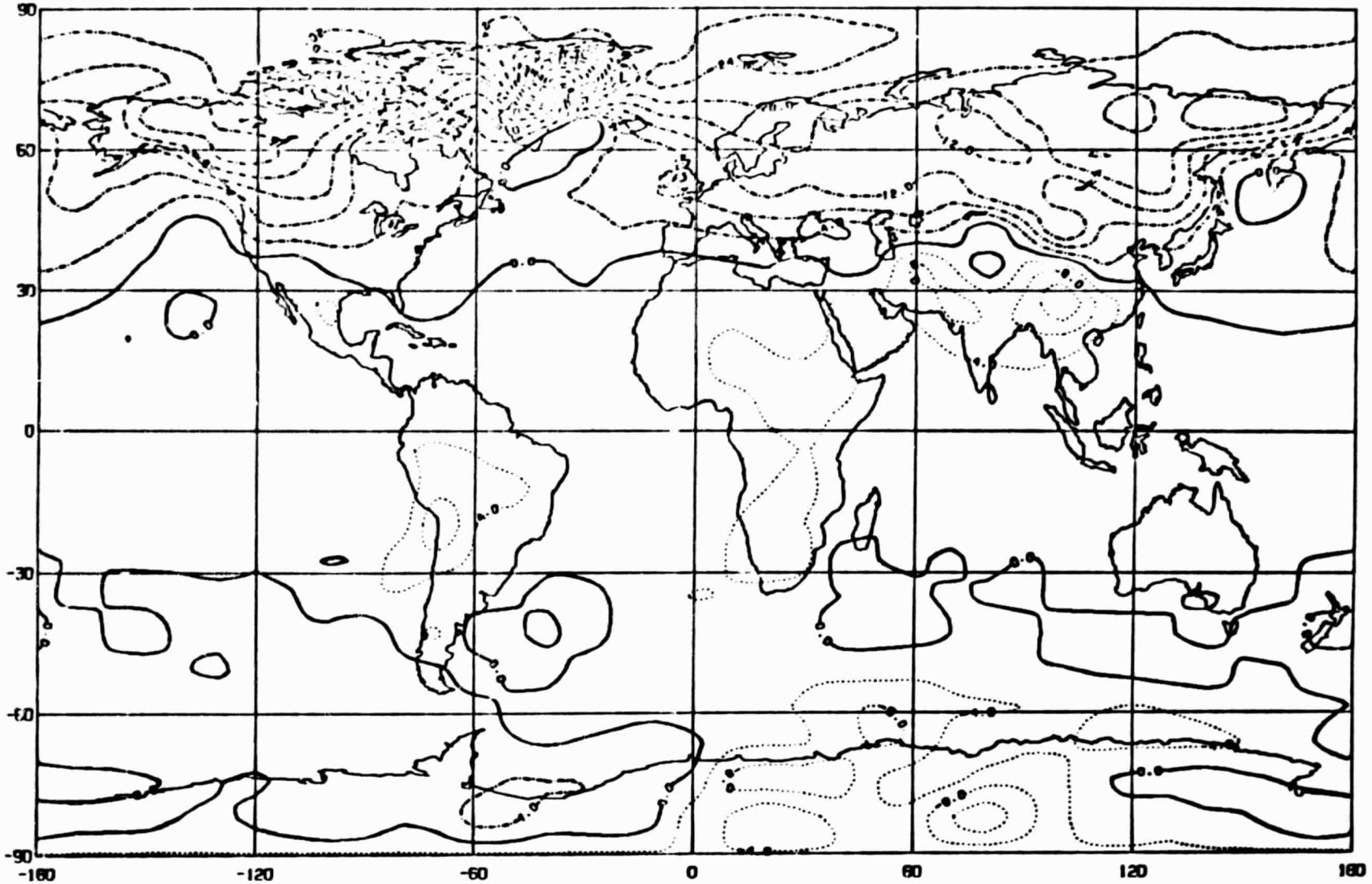

The mean Difference for RUN003-RUN002

Fig. 7a

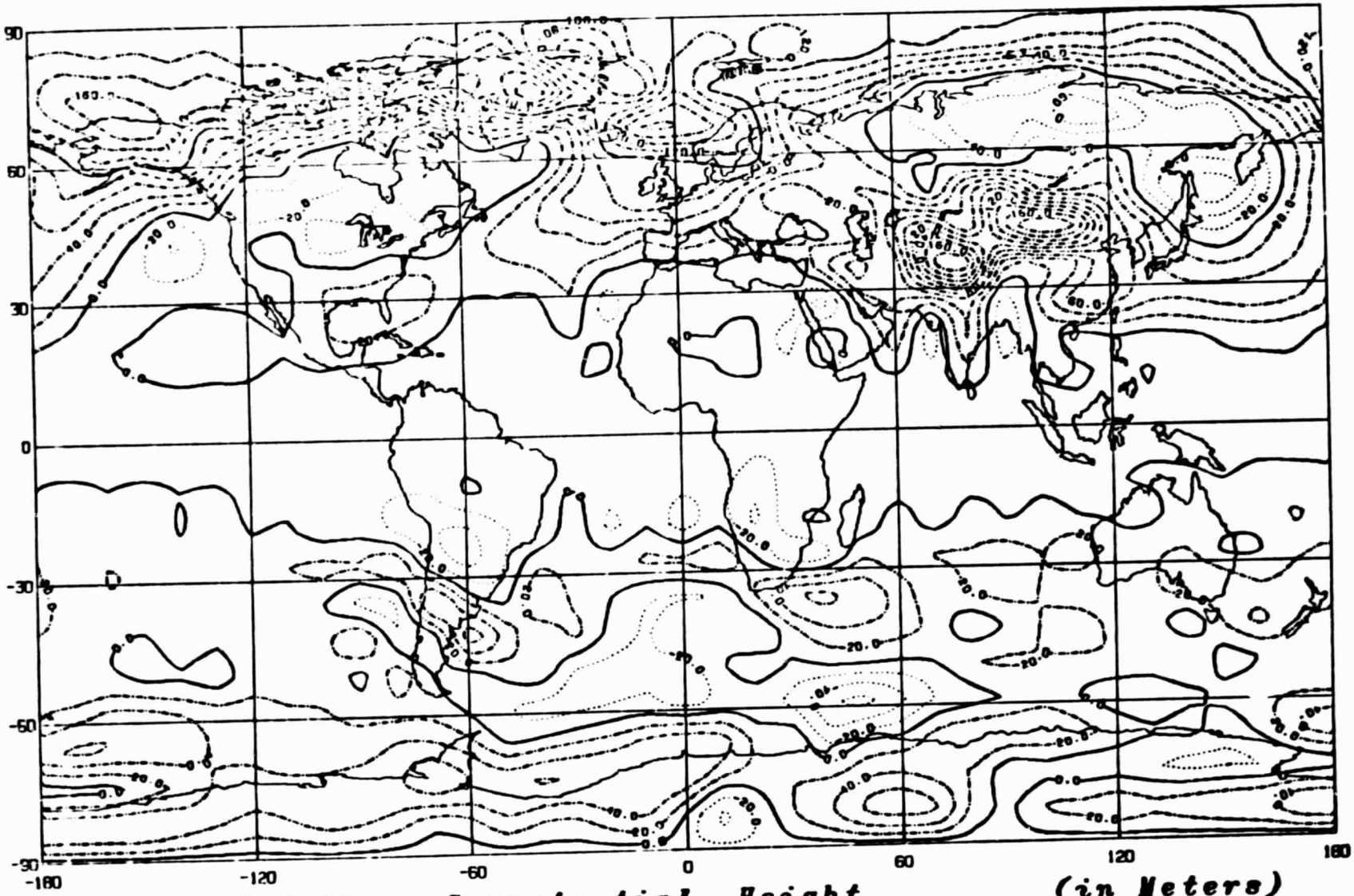

500 Millibar Geopotential Height (in Meters)

The mean Difference for RUN003-RUN002

Fig. 7b

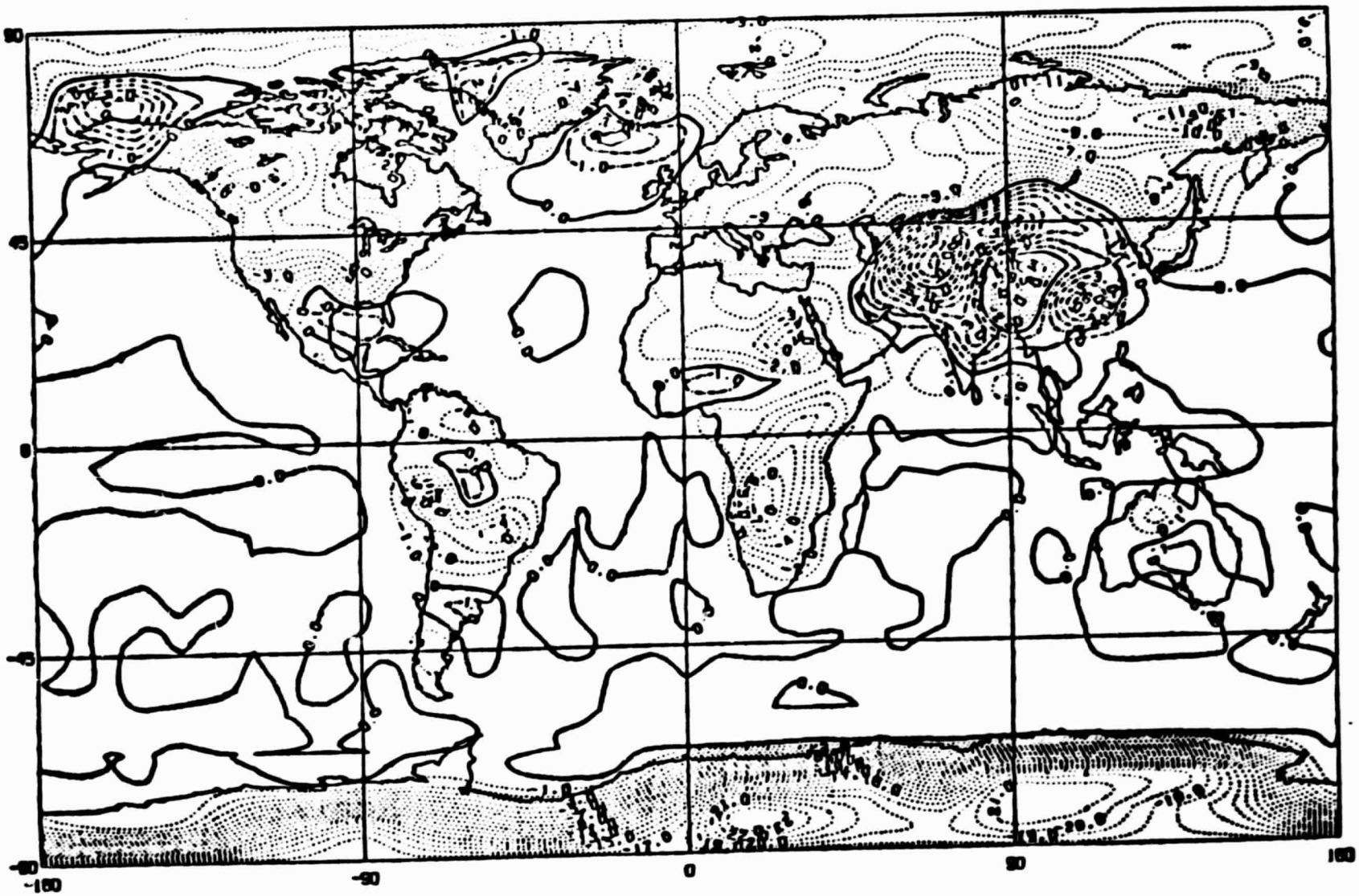

MEAN SURFACE AIR TEMPERATURE (IN DEGREES CENTIGRADE)

The mean Difference for RUN003-RUN002

Fig. 7c

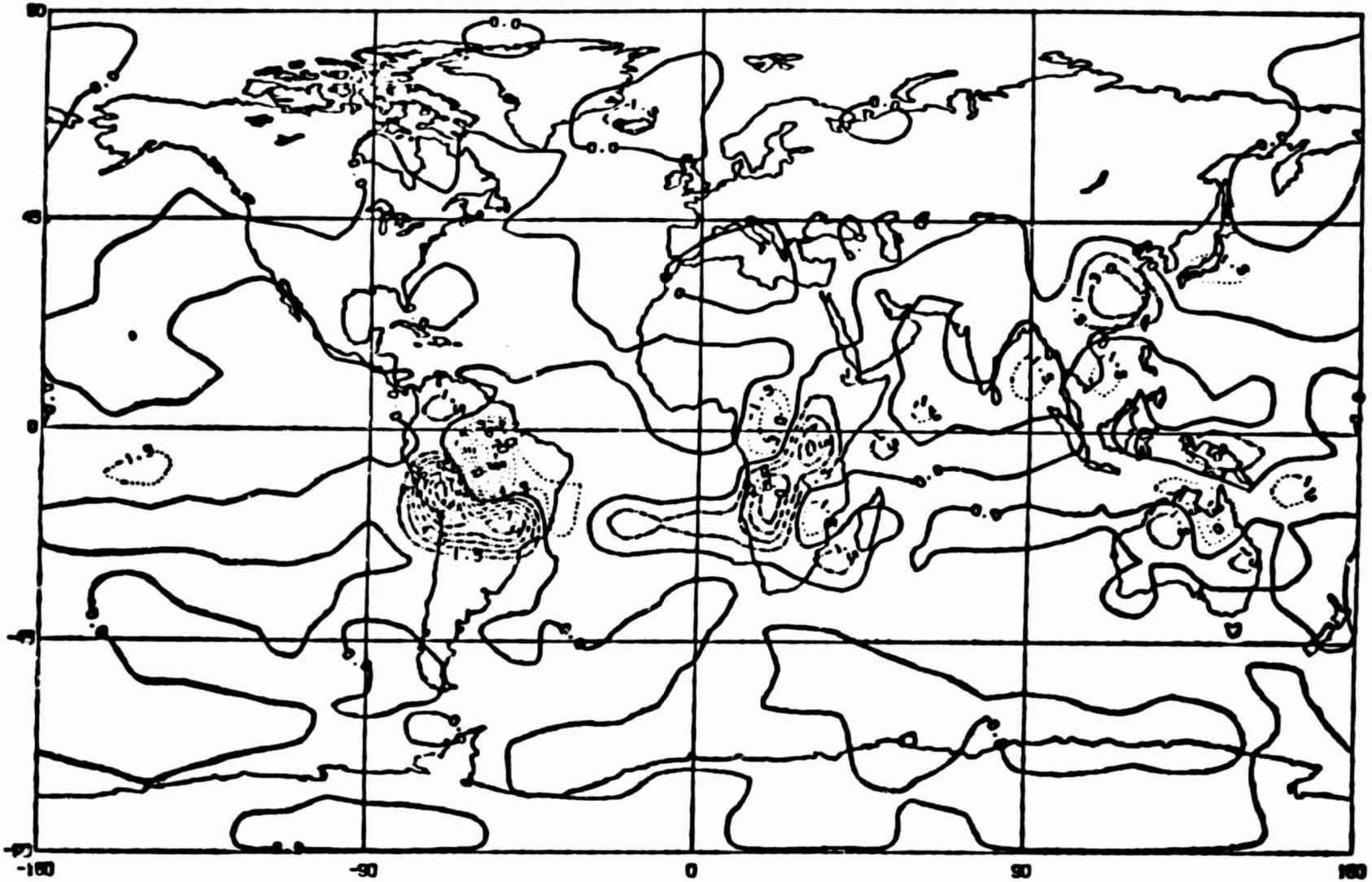

PRECIPITATION IN (MM/DAY)

The mean Difference for RUN003-RUN002

Fig. 7d

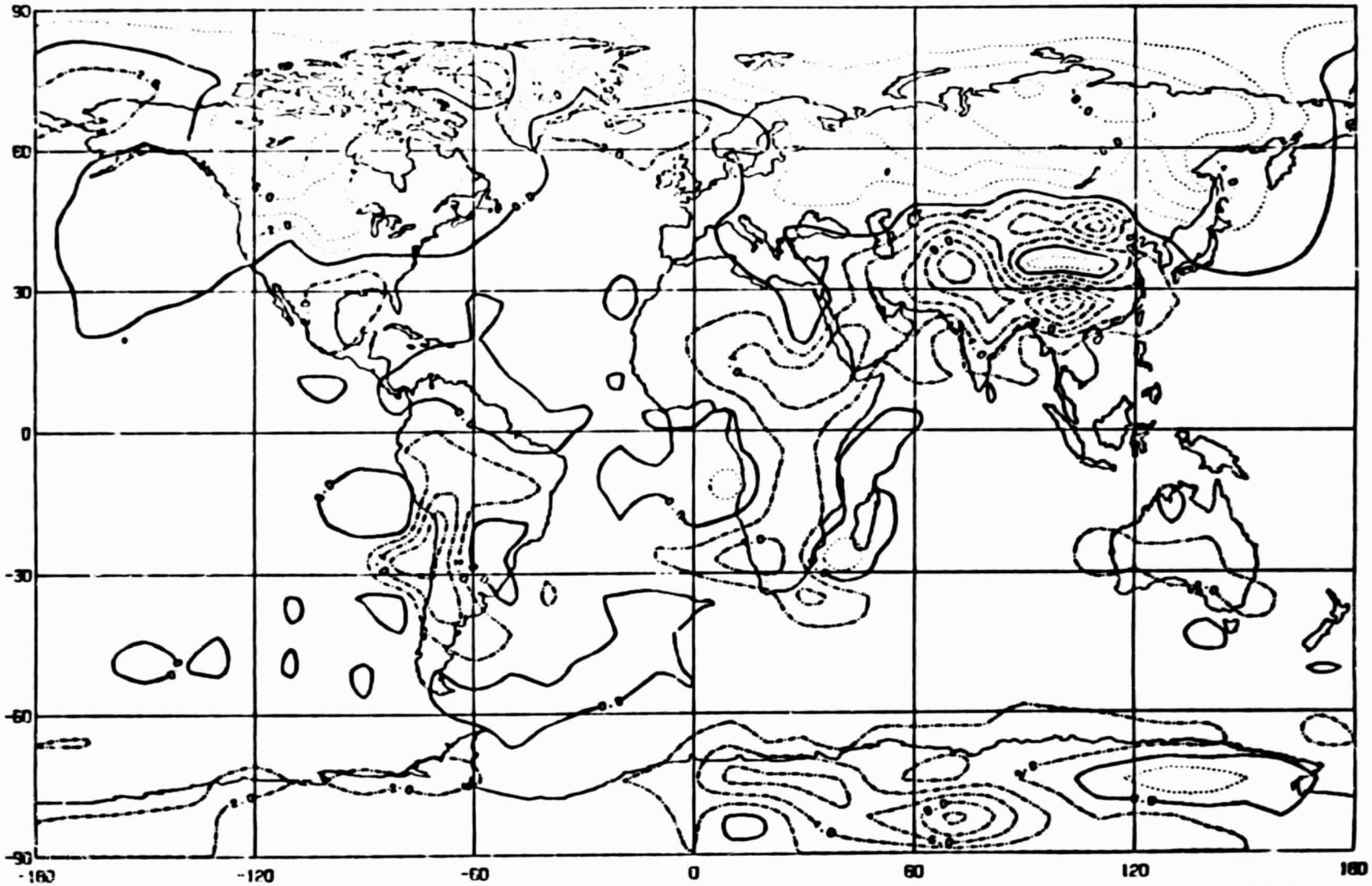

Mean Thickness Temperature from 850mb to 700mb degrees (K)

The mean Difference for RUN003-RUN002

Fig. 7e

*****RUN003*SPIN UP WITH ISOTHERMAL ATMOSPHERE INCLUDING MOUNTIAN*ZERO GROUND WETNESS SPAR.COHEN.W

TEMPERATURE (0.1°C) DIFFERENCE BETWEEN RUN3 AND RUN2

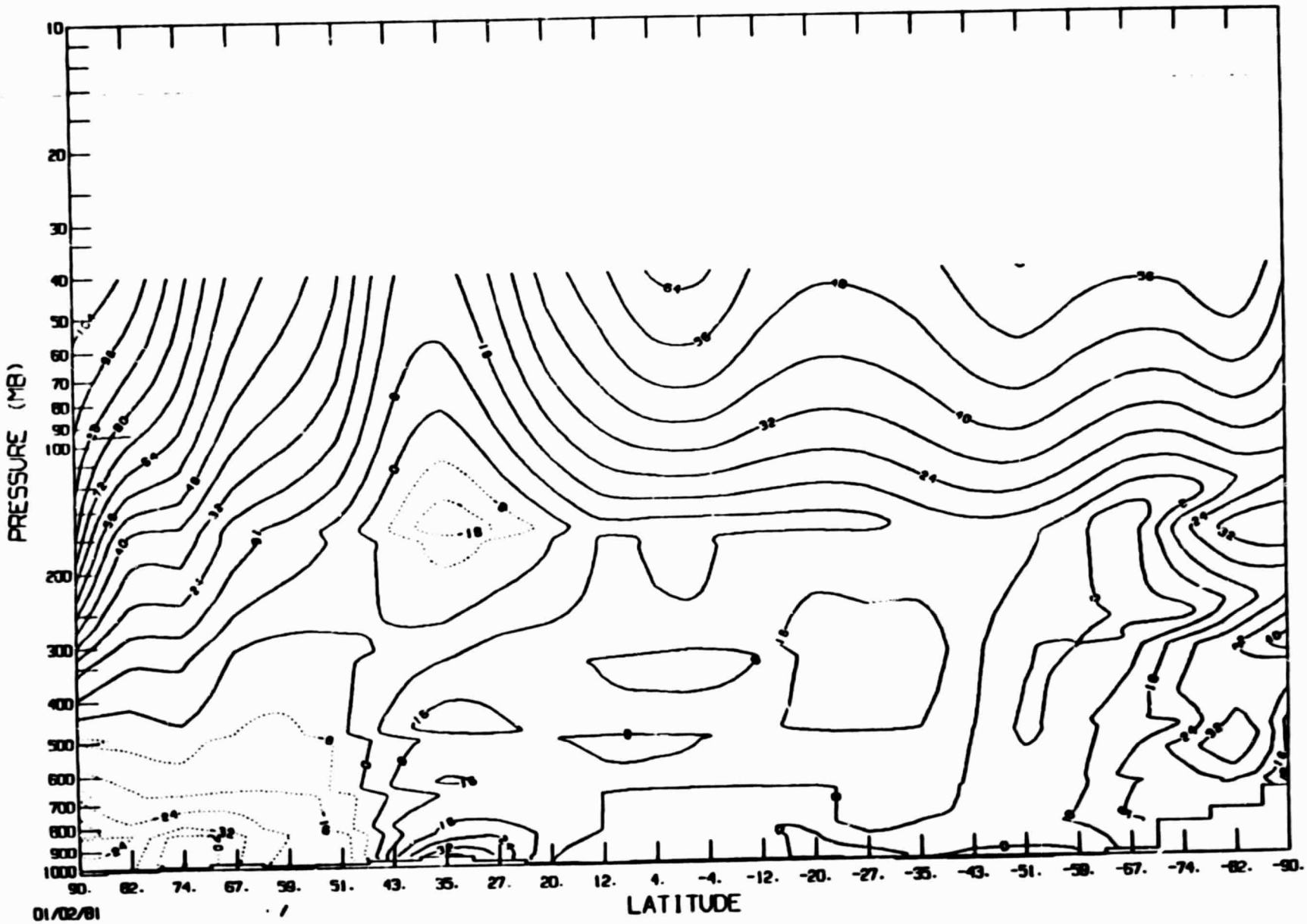

Fig. 7f

*****RUN003*SPIN UP WITH ISOTHERMAL ATMOSPHERE INCLUDING MOUNTIAN*ZERO GROUND WETNESS SPAR.COHEN.W

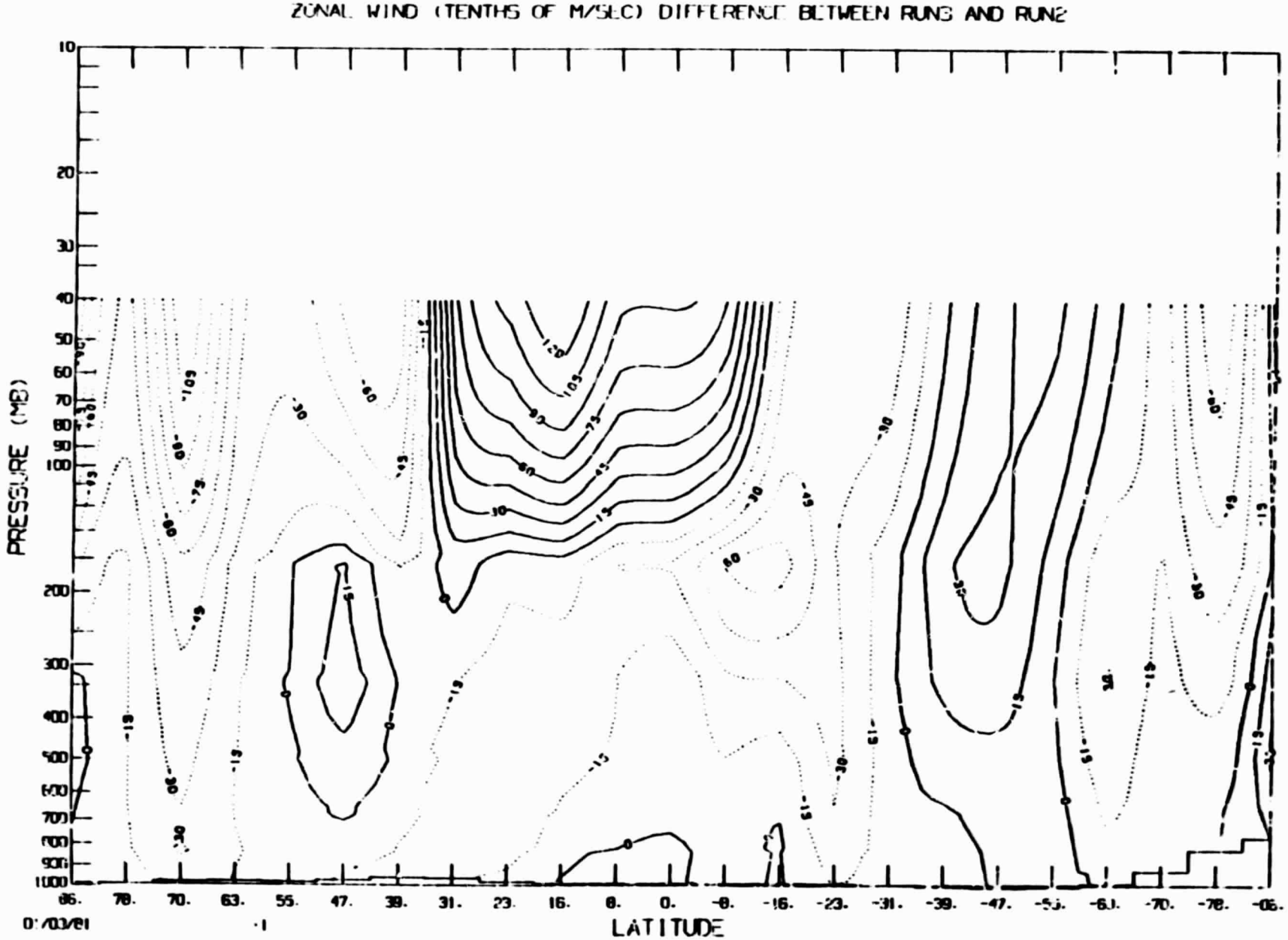

Fig. 7a

*****RUN003*SPIN UP WITH ISOTHERMAL ATMOSPHERE INCLUDING MOUNTIAN*ZERO GROUND WETNESS SPAR.COHEN.W

V WIND (TENTHS OF M/SEC) DIFFERENCE BETWEEN RUN3 AND RUN2

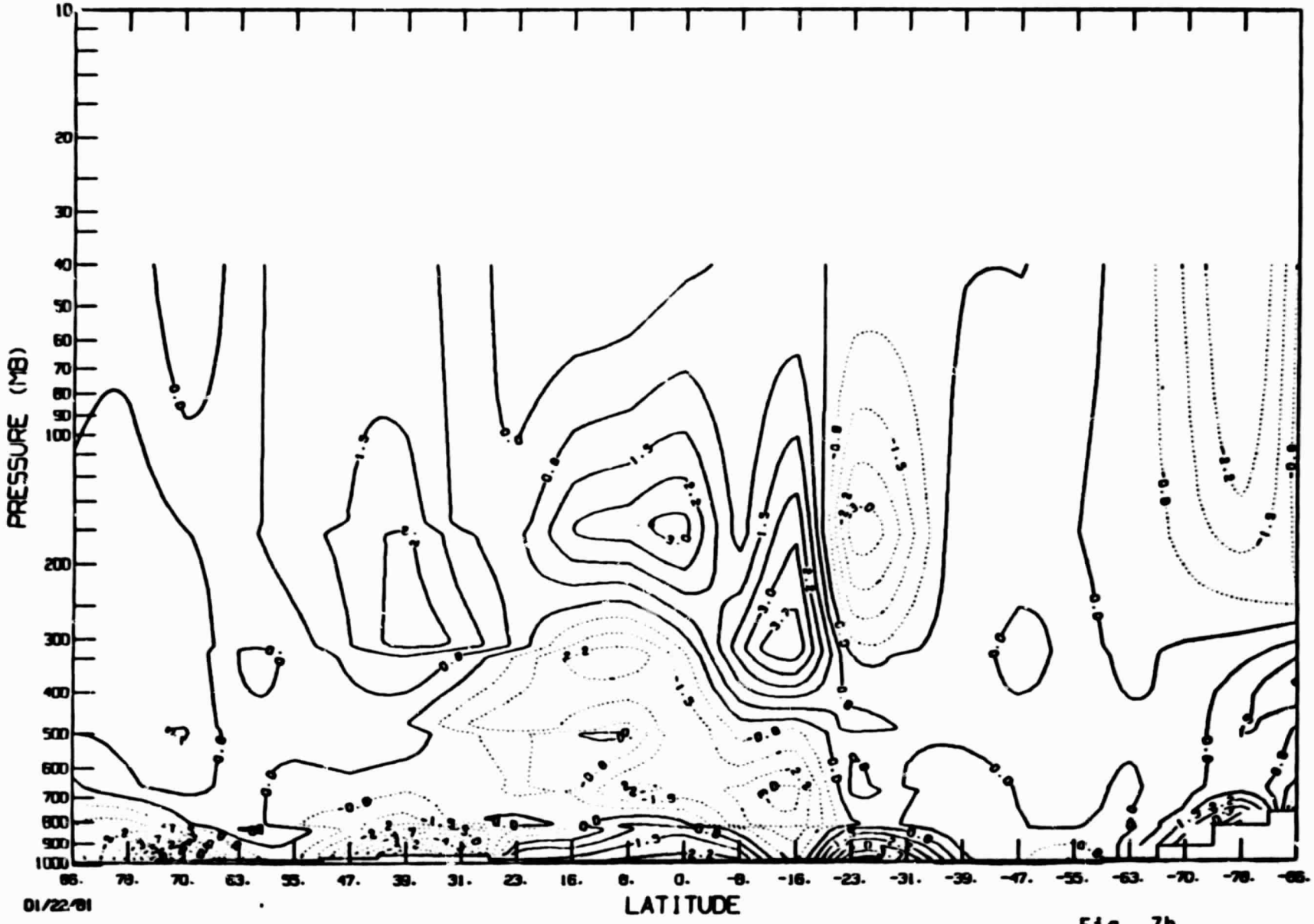

Fig. 7h

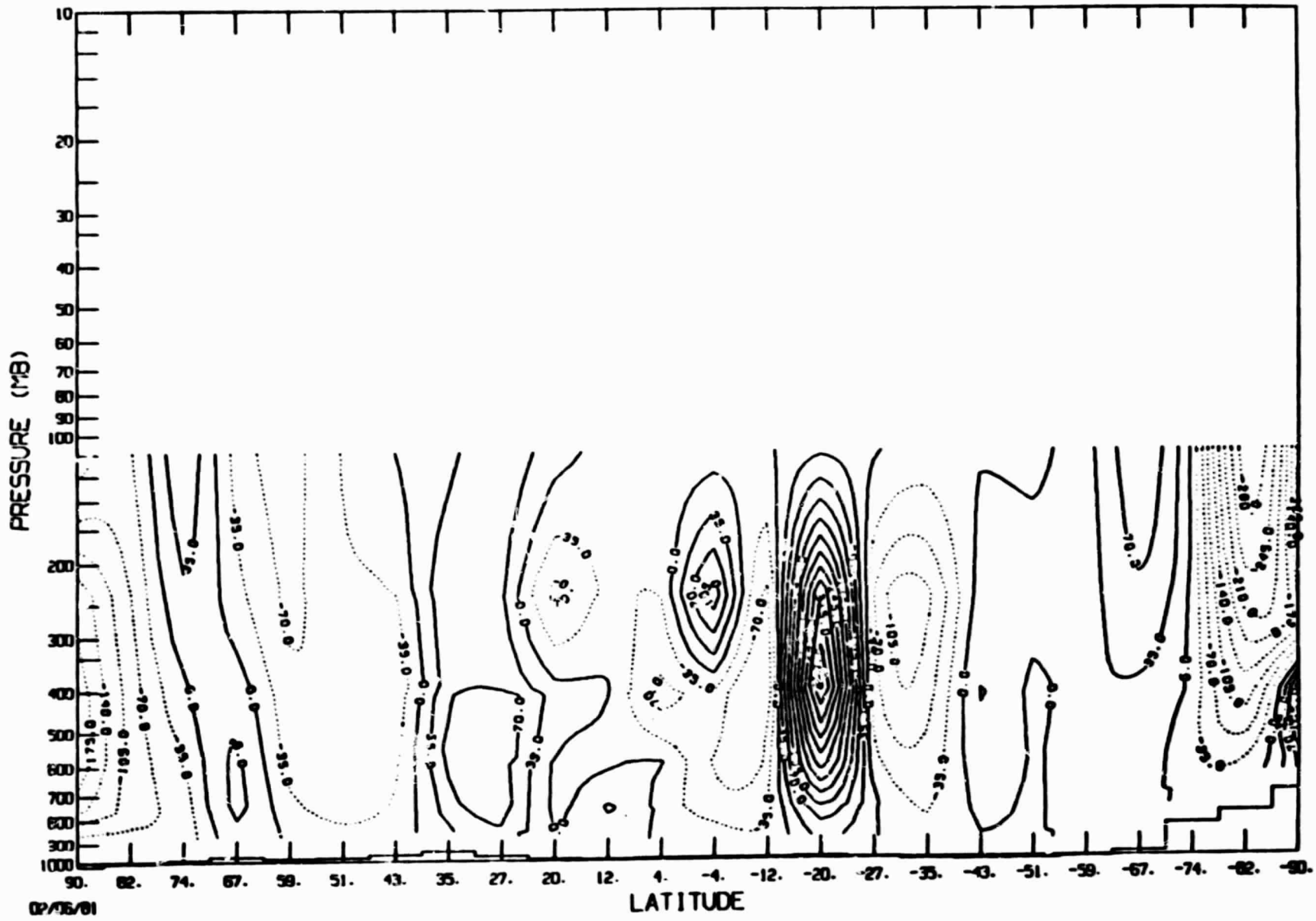

Fig. 7i

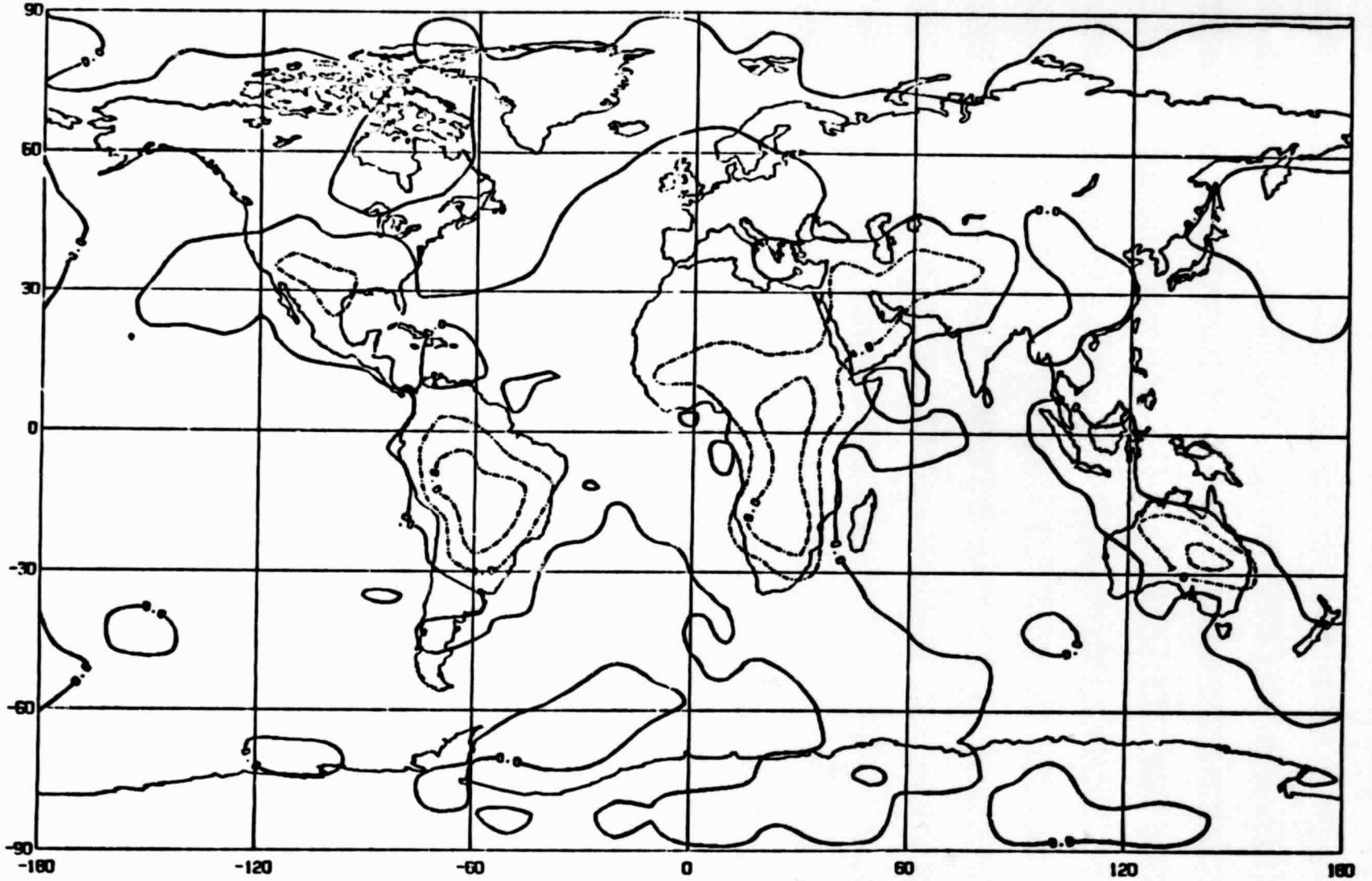

The mean Difference for RUN004-RUN003 Fig. 8a

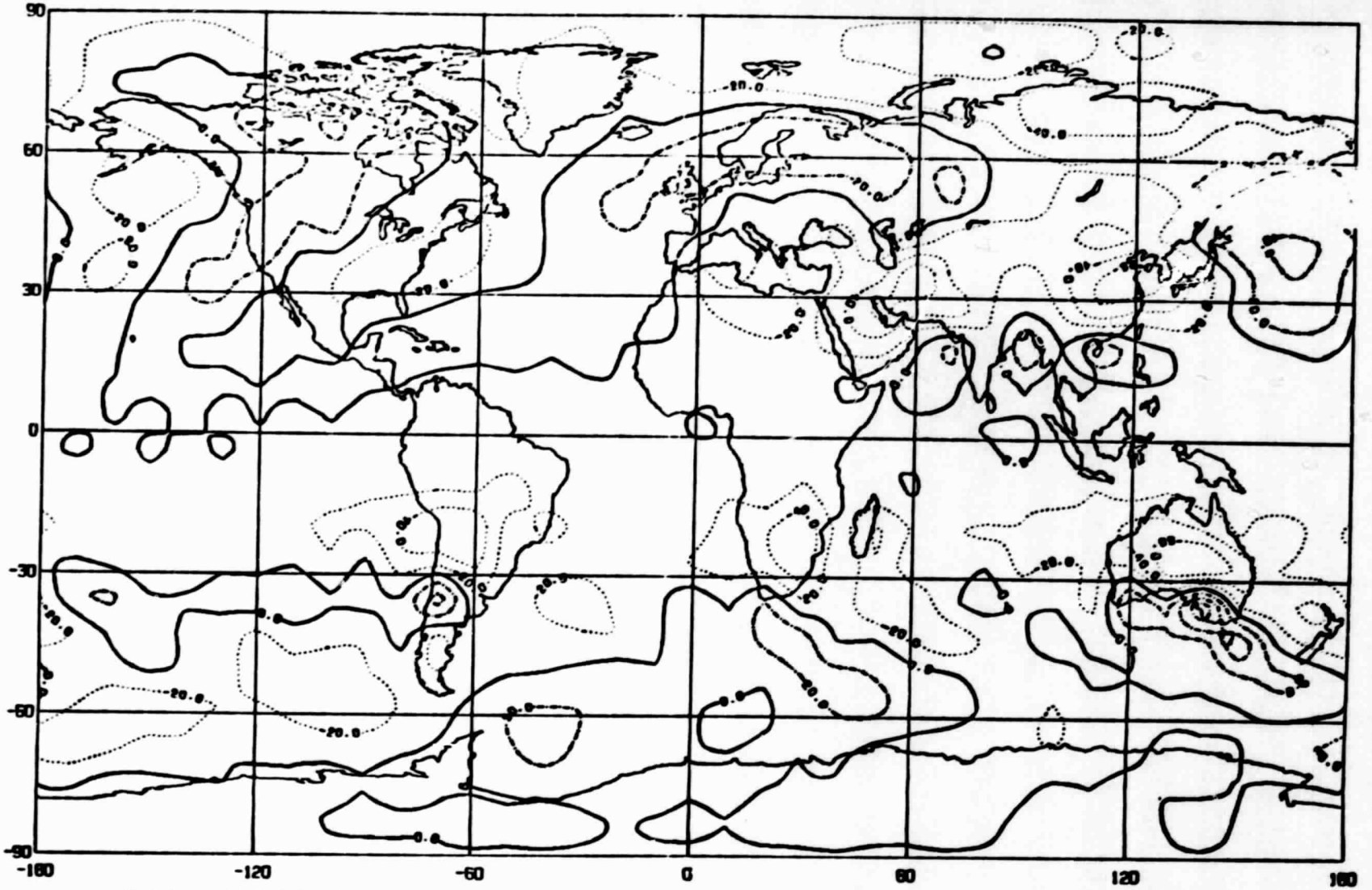

500 Millibar Geopotential Height (in Meters)

The mean Difference for RUN004-RUN003

Fig. 8b

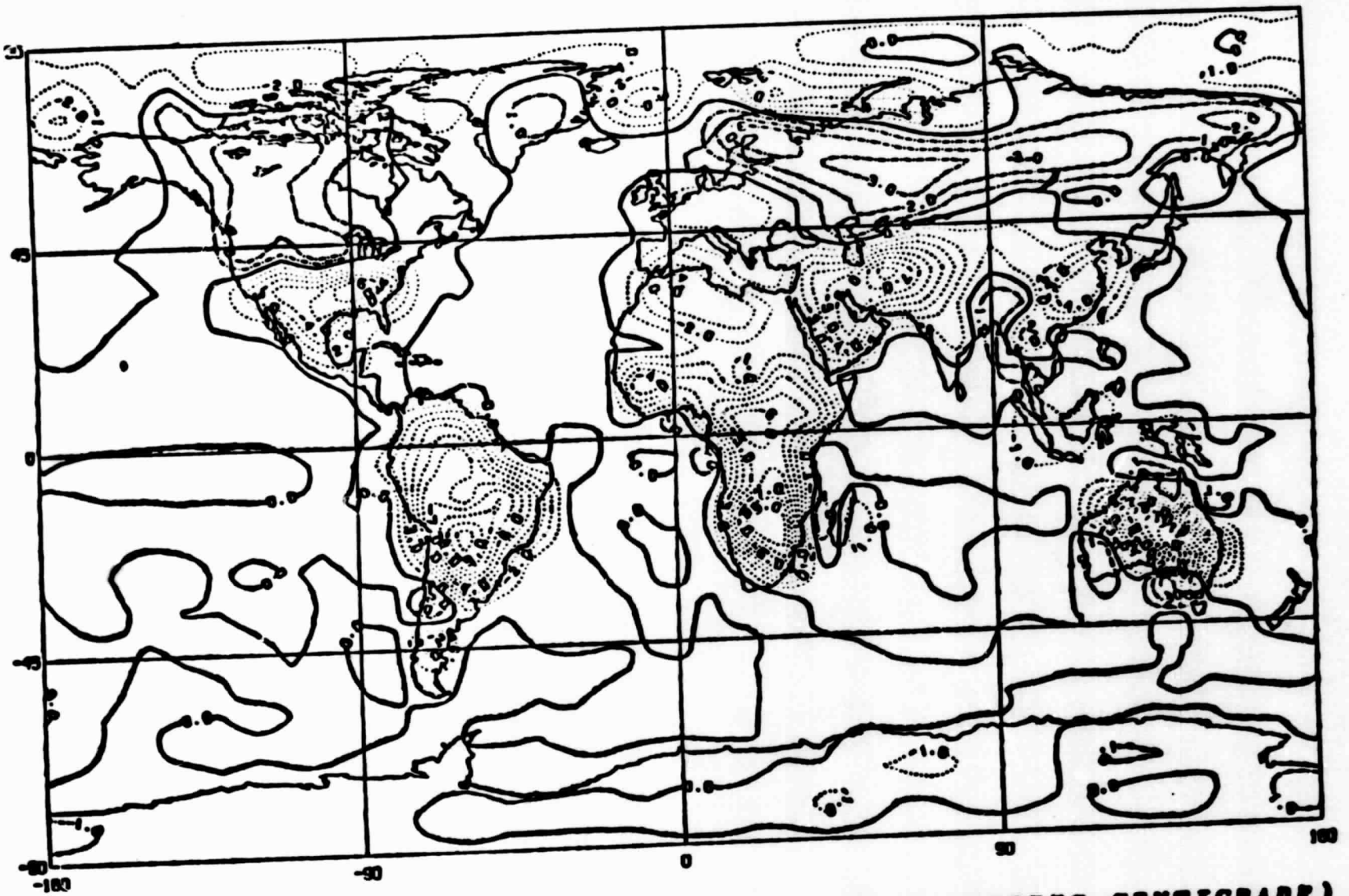

MEAN SURFACE AIR TEMPERATURE (IN DEGREES CENTIGRADE)

The mean Difference for RUN004-RUN003

Fig. 8c

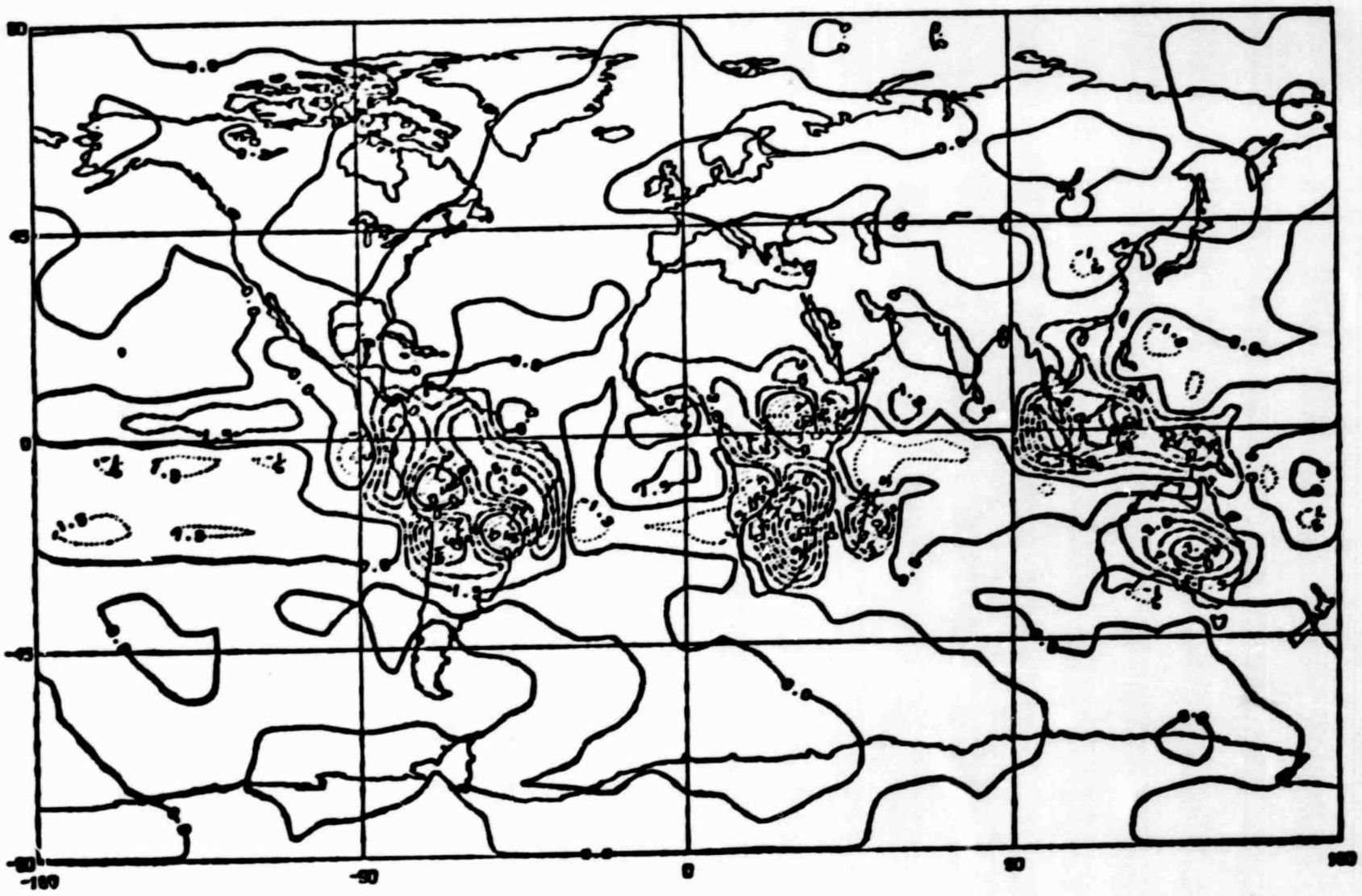

PRECIPITATION IN (MM/DAY)

The mean Difference for RUN004-RUN003

Fig. 8d

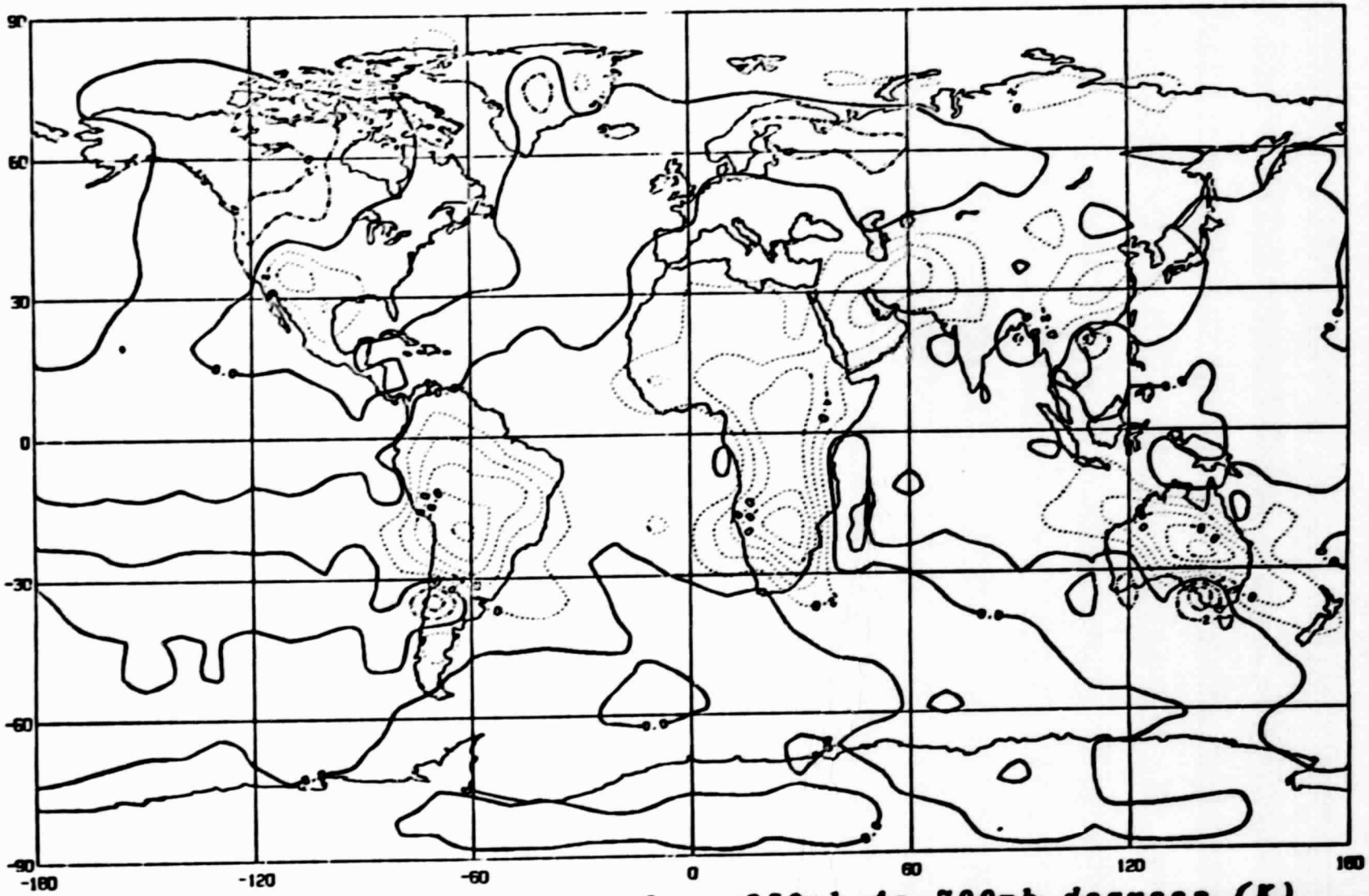

Mean Thickness Temperature from 850mb to 700mb degrees (K)

The mean Difference for RUN004-RUN003

Fig. 8e

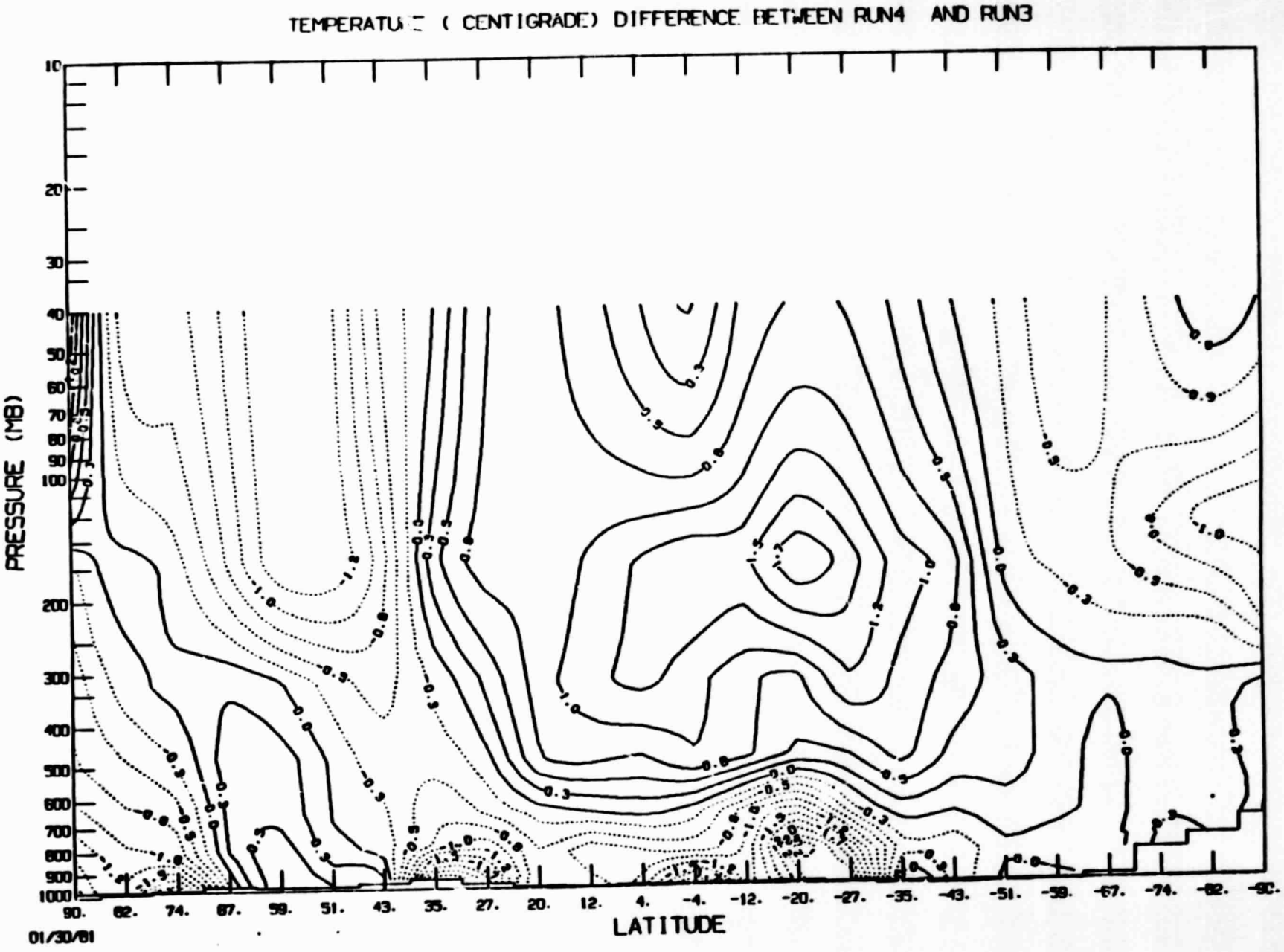

Fig. 8f

ZONAL WIND (TENTHS OF M/SEC) DIFFERENCE BETWEEN RUN4 - RUN3

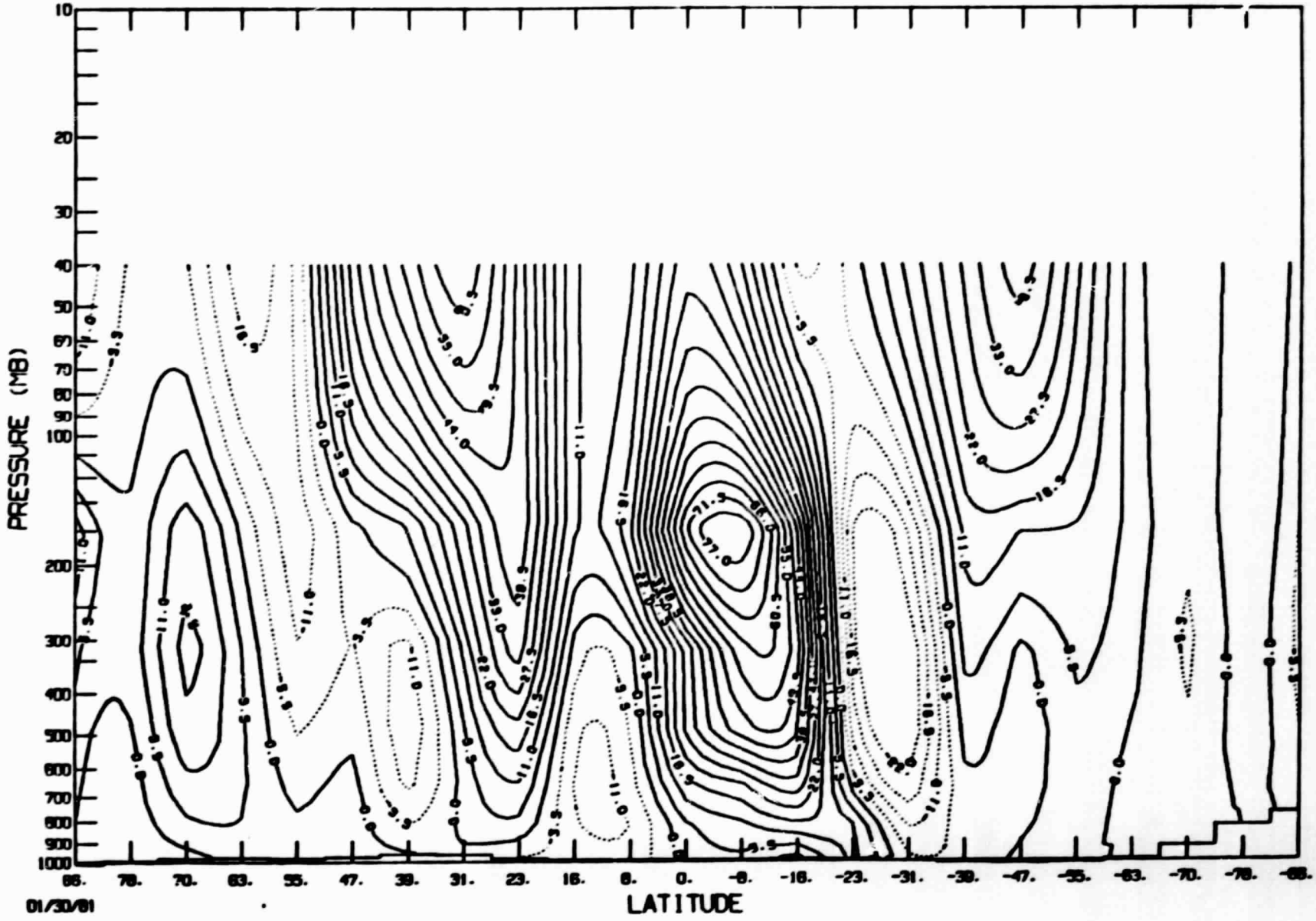

Fig. 8g

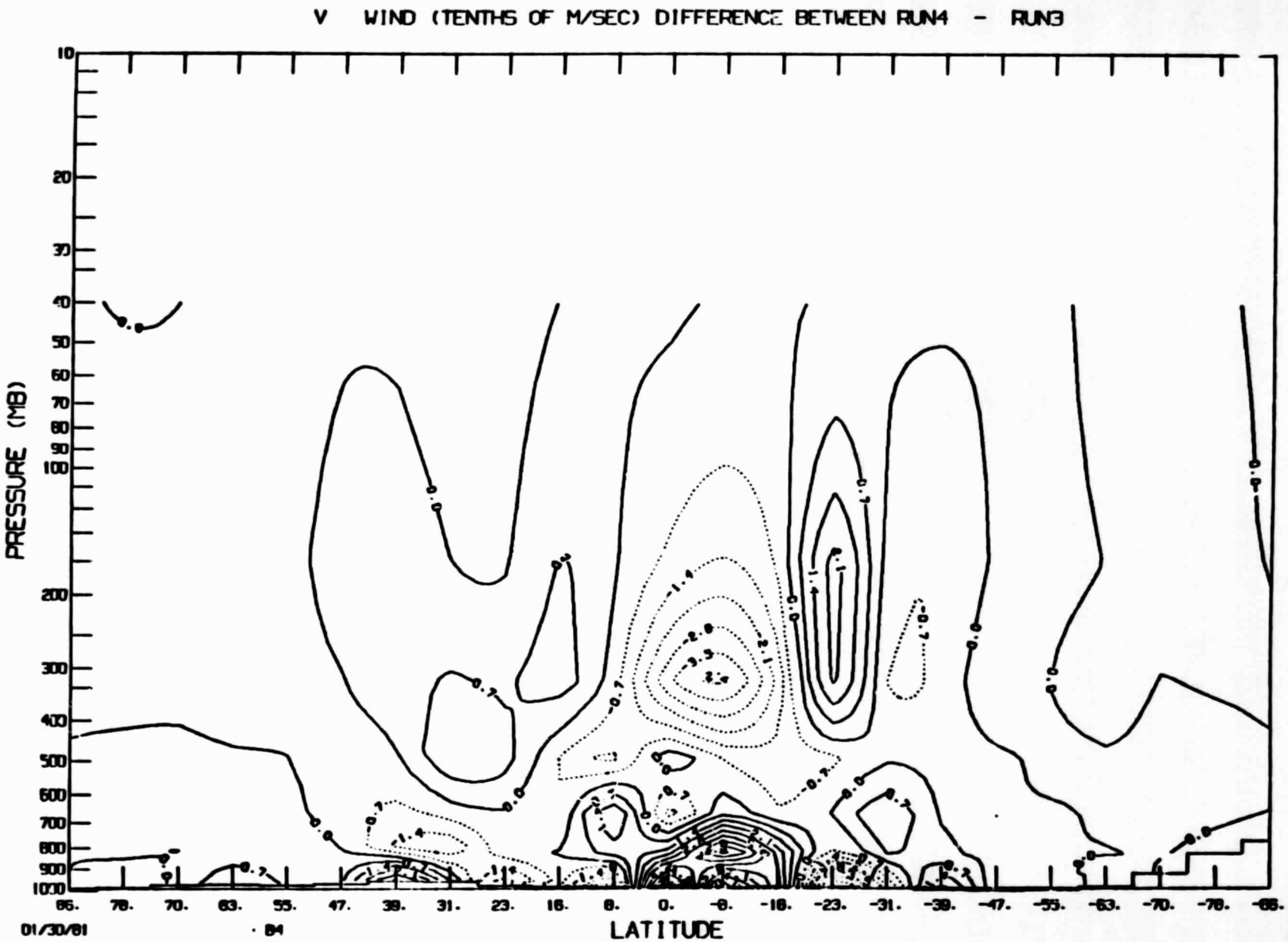

Fig. 8h

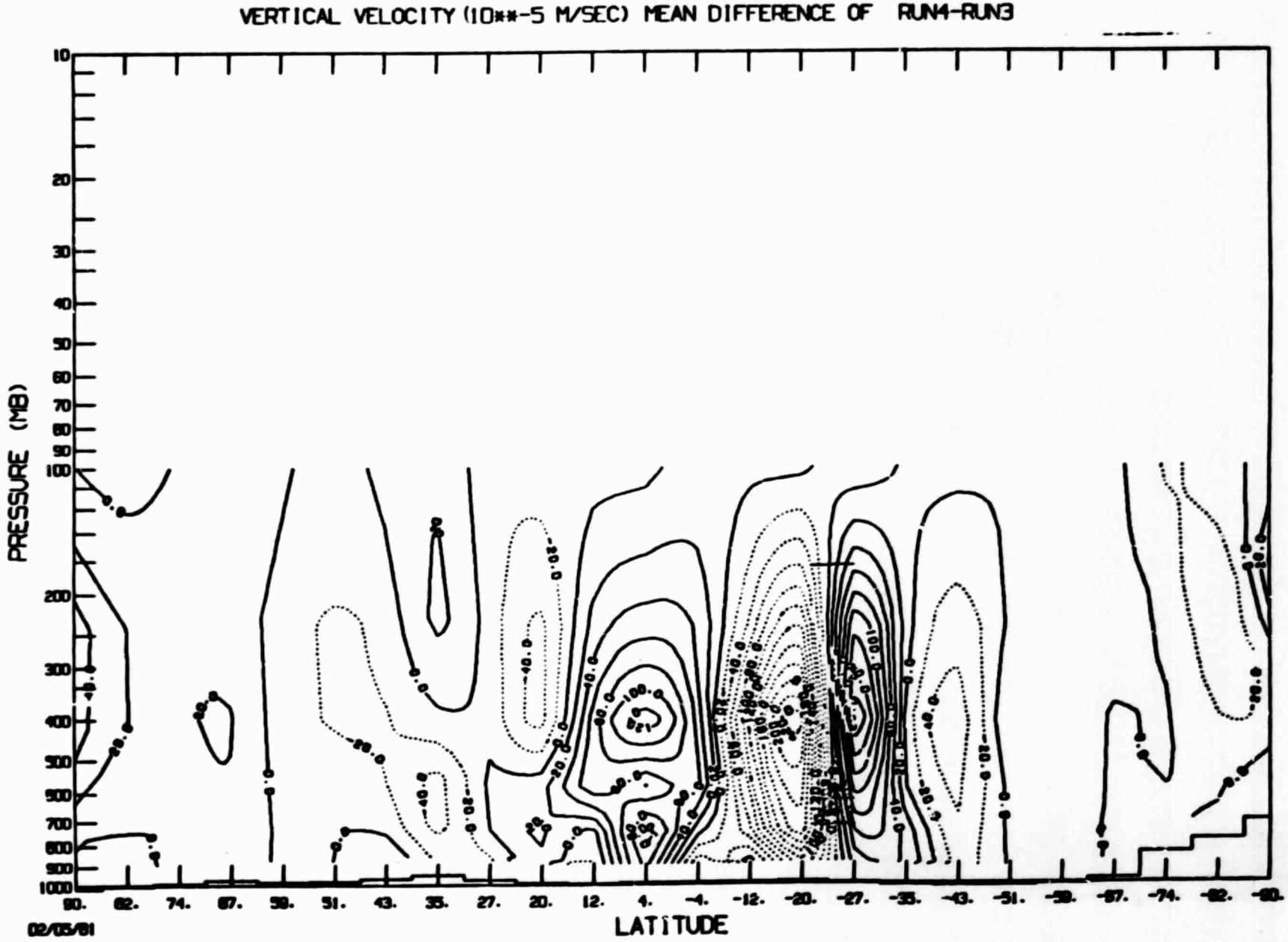
VERTICAL VELOCITY (10**-5 M/SEC) MEAN DIFFERENCE OF RUN4-RUN3
PRESSURE (MB)
10
20
30
40
50
60
70
80
90
100
200
300
400
500
600
700
800
900
1000
90. 82. 74. 67. 59. 51. 43. 35. 27. 20. 12. 4. -4. -12. -20. -27. -35. -43. -51. -59. -67. -74. -82. -90.
LATITUDE
02/05/81

Fig. 81

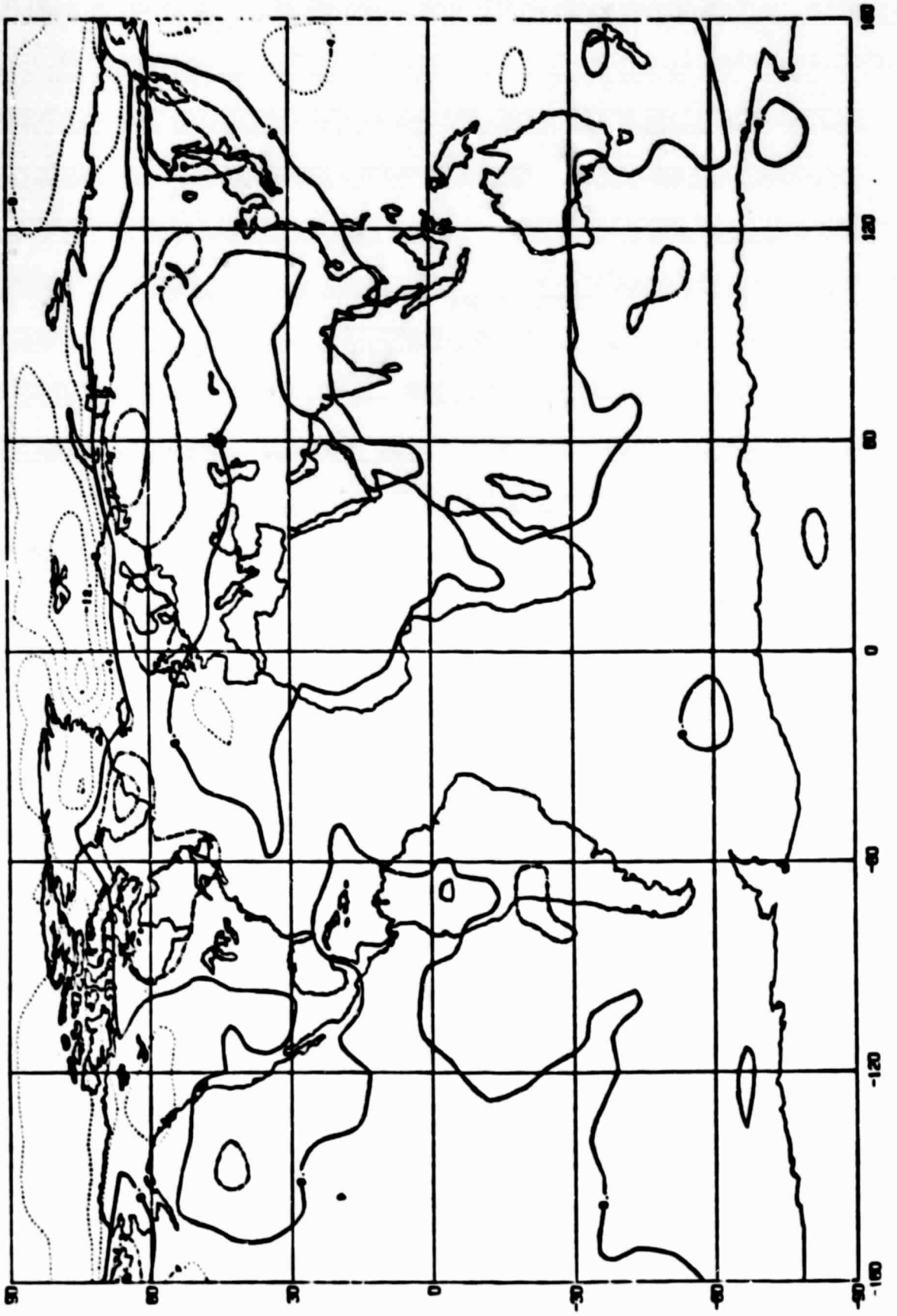

The mean Difference for RUN5 - RUN4

Sea level pressure in (millibars)

Fig. 9a

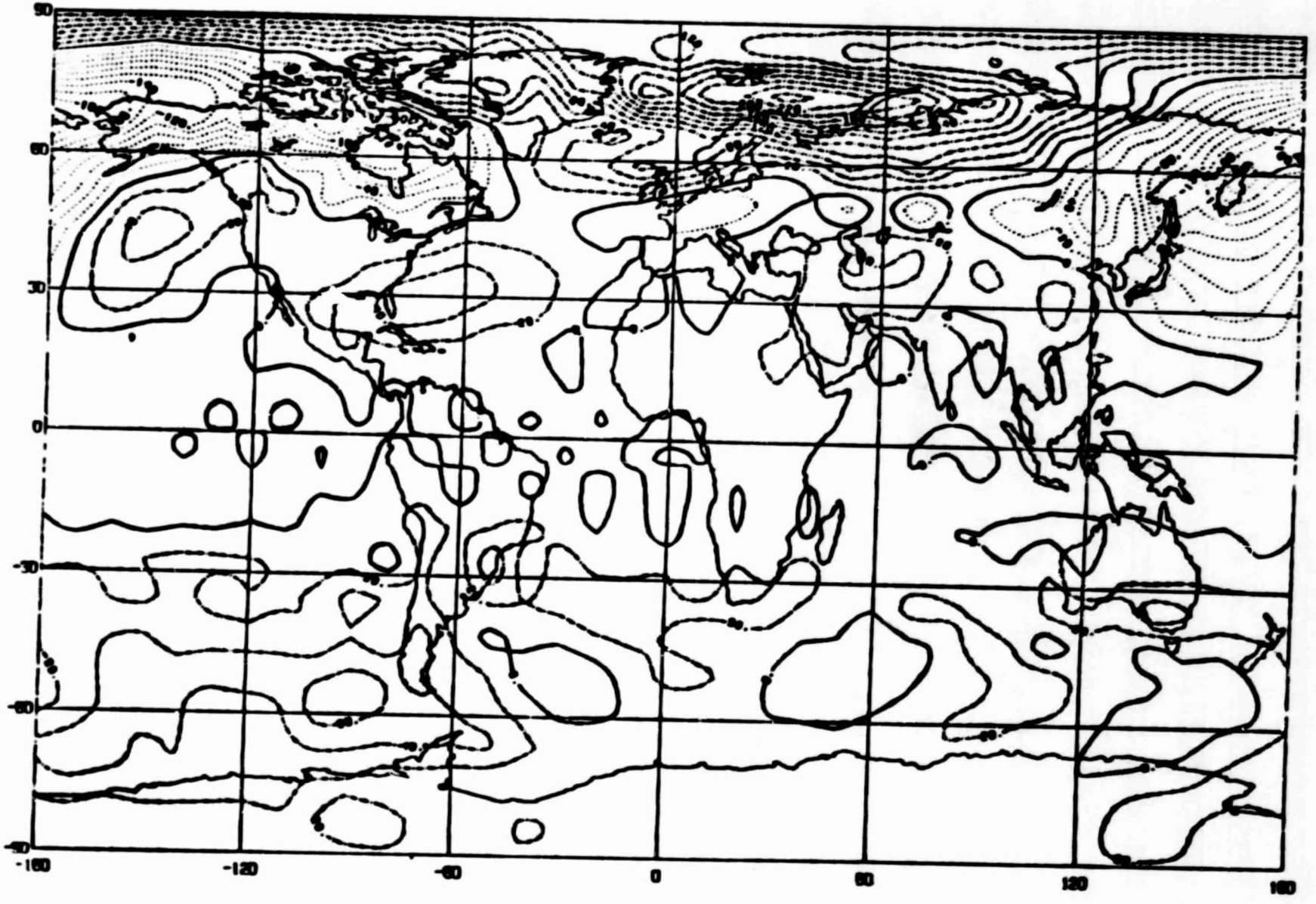

600 Millibar Geopotential Height (in Meters)

The mean Difference for RUN6 - RUN4

Fig. 9b

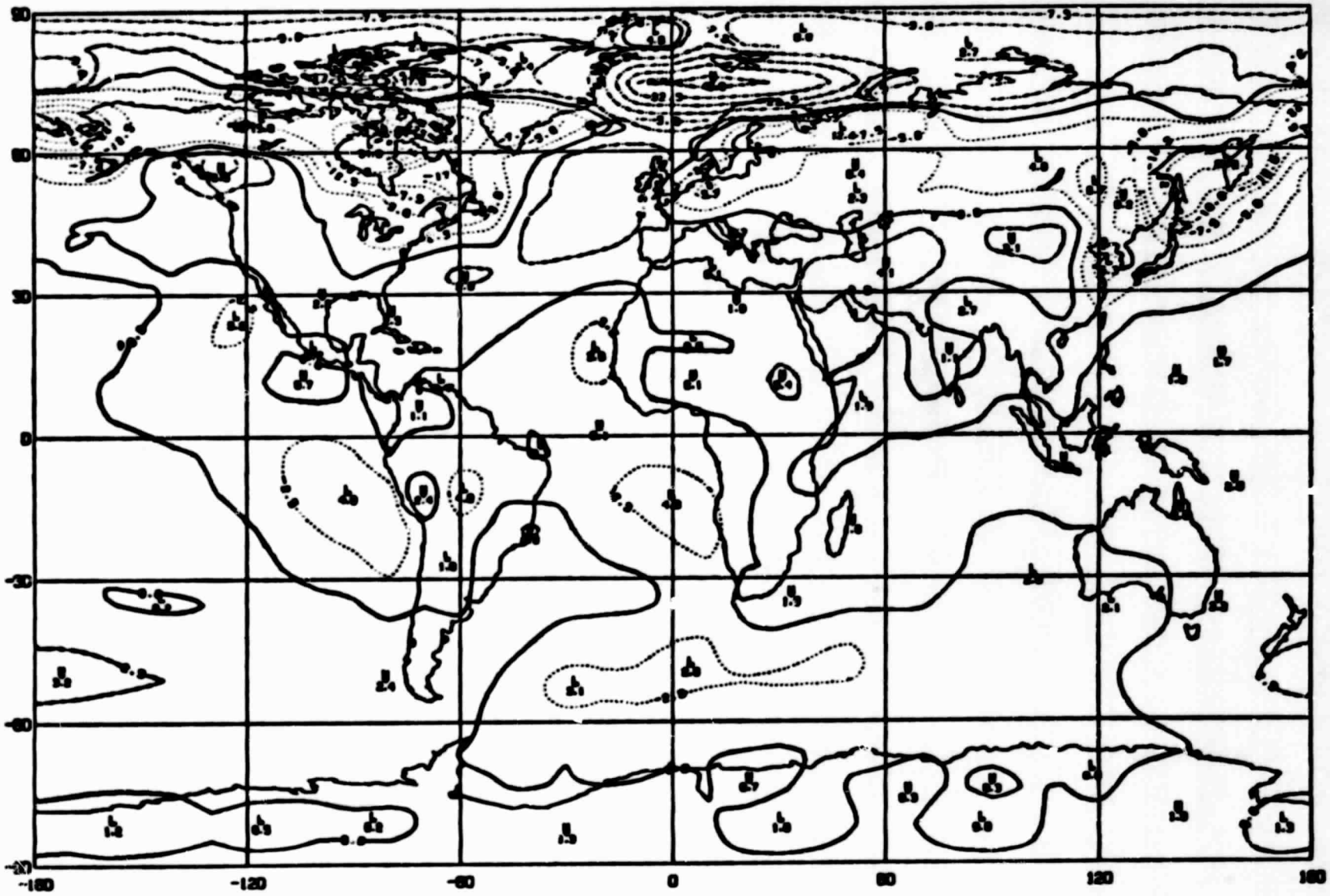

MEAN SURFACE AIR TEMPERATURE (IN DEGREES CENTIGRADE)

The mean Difference for RUN5 - RUN4

Fig. 9c

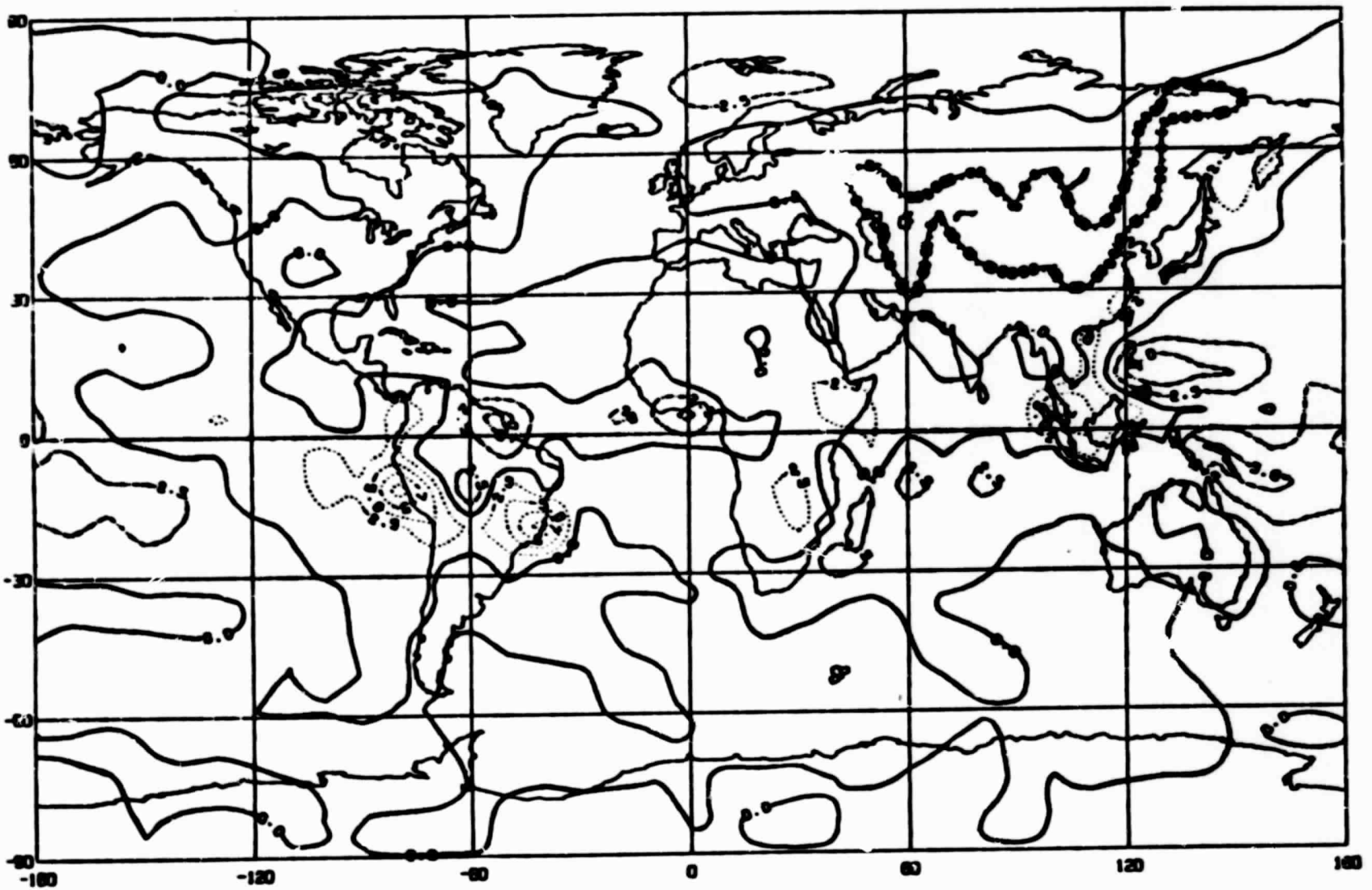

PRECIPITATION IN (MM/DAY)

The mean Difference for RUN005-RUN004

Fig. 9d

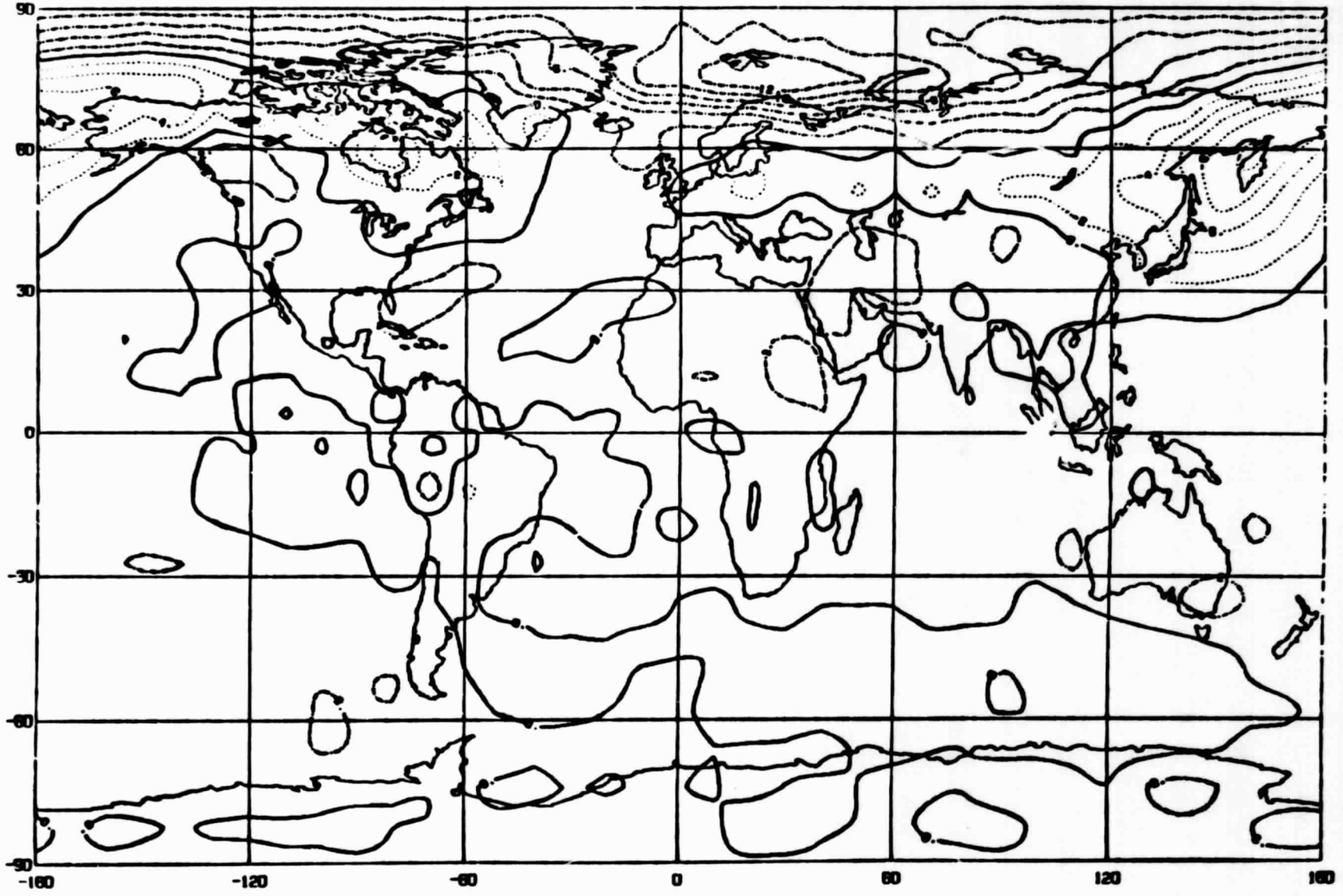

Mean Thickness Temperature from 850mb to 700mb degrees (K)

The mean Difference for RUN5 - RUN4

Fig. 9e

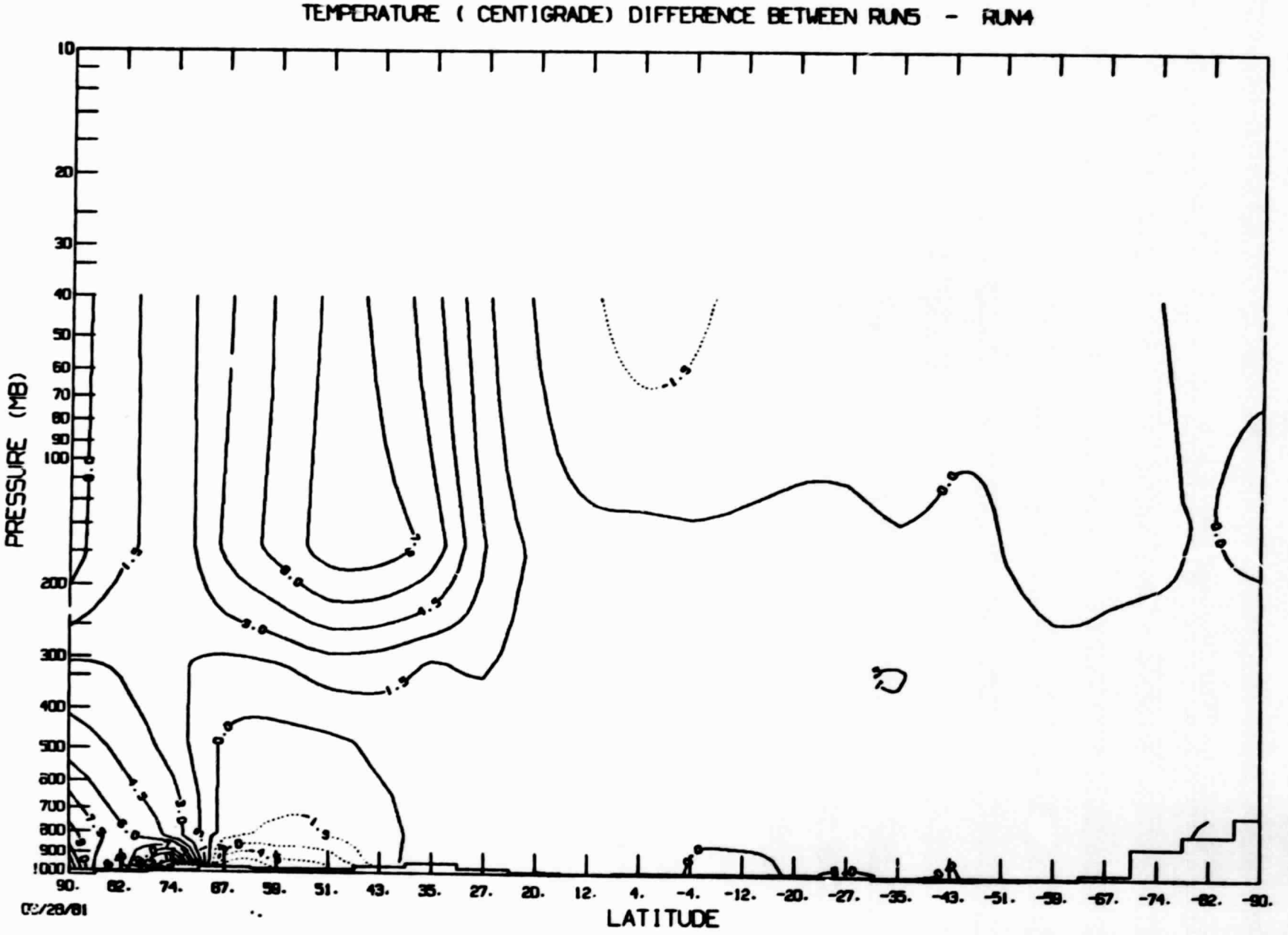
TEMPERATURE (CENTIGRADE) DIFFERENCE BETWEEN RUN5 - RUN4
PRESSURE (MB)
10
20
30
40
50
60
70
80
90
100
200
300
400
500
600
700
800
900
1000
90. 82. 74. 67. 59. 51. 43. 35. 27. 20. 12. 4. -4. -12. -20. -27. -35. -43. -51. -59. -67. -74. -82. -90.
LATITUDE
02/28/81

Fig. 9f

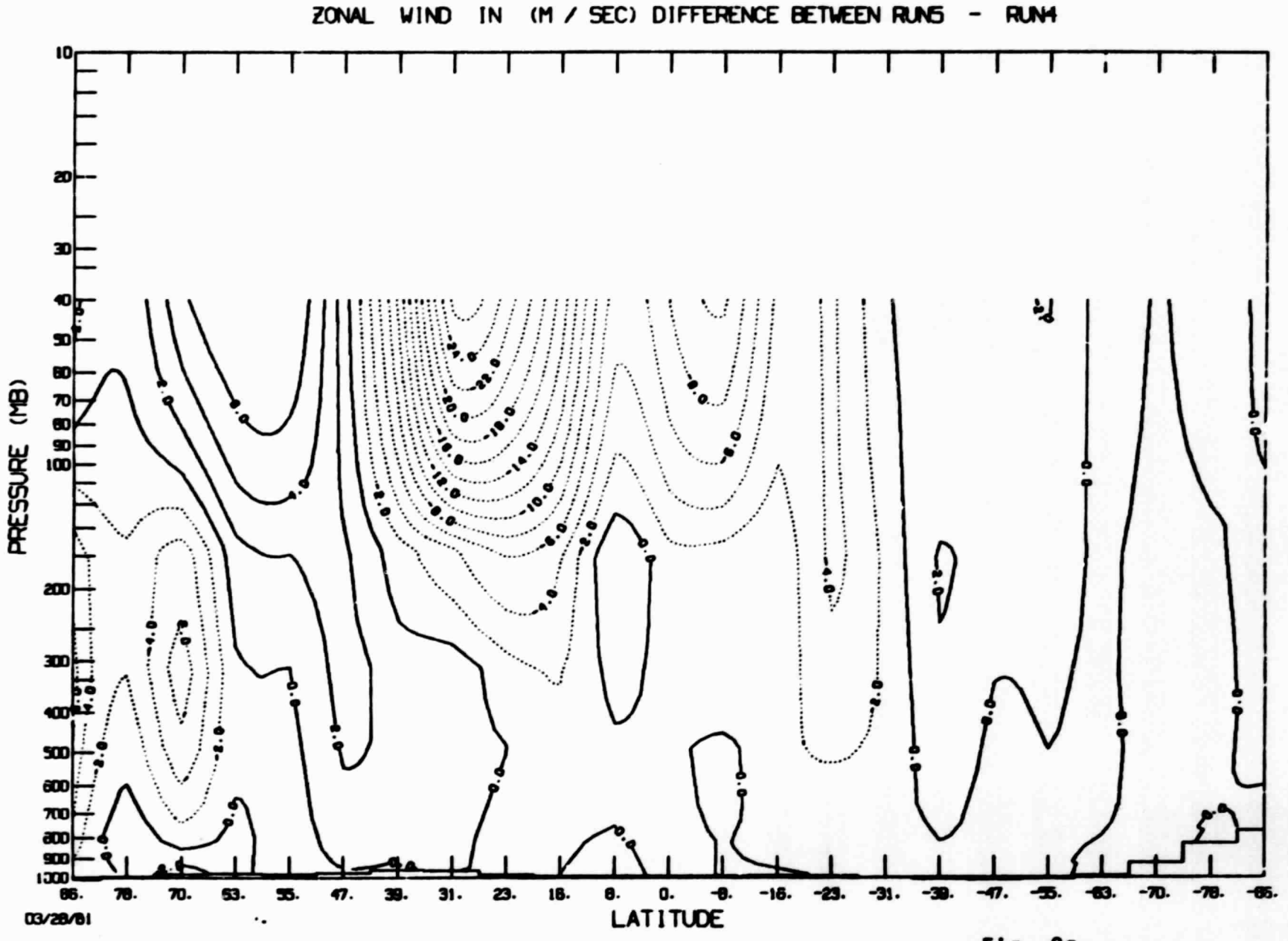
ZONAL WIND IN (M / SEC) DIFFERENCE BETWEEN RUN5 - RUN4
PRESSURE (MB)
10
20
30
40
50
60
70
80
100
200
300
400
500
600
700
800
900
1000
86. 78. 70. 63. 55. 47. 39. 31. 23. 16. 8. 0. -8. -16. -23. -31. -39. -47. -55. -63. -70. -78. -86.
LATITUDE
03/28/81

Fig. 9g

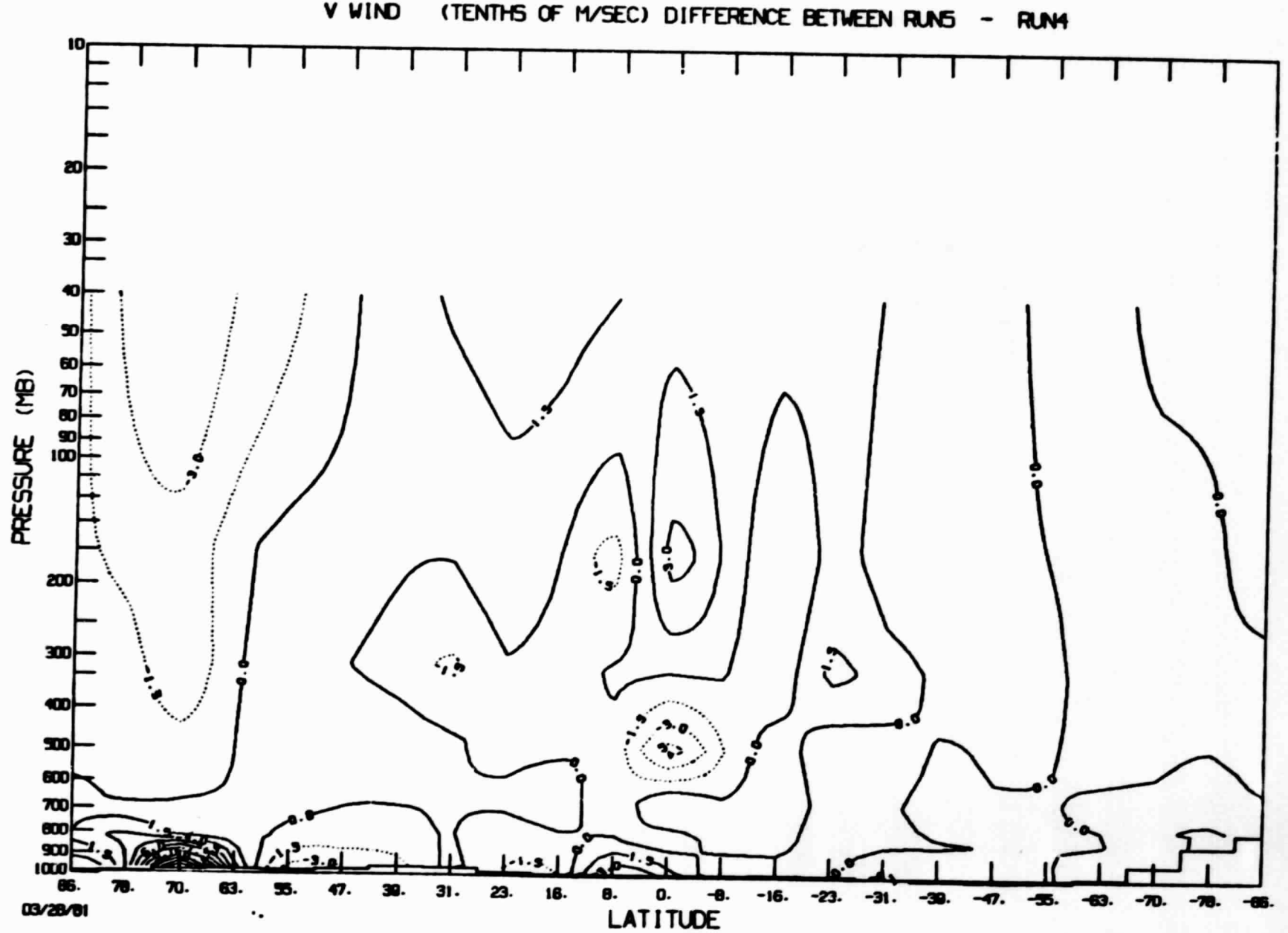
V WIND (TENTHS OF M/SEC) DIFFERENCE BETWEEN RUN5 - RUN4
PRESSURE (MB)
10
20
30
40
50
60
70
80
90
100
200
300
400
500
600
700
800
900
1000
86. 78. 70. 63. 55. 47. 39. 31. 23. 16. 8. 0. -8. -16. -23. -31. -39. -47. -55. -63. -70. -78. -86.
LATITUDE
03/28/81

Fig. 9h

RUN#5 SPIN-UP WITH MOUNTAINS AND SURFACE PHYSICS AND REAL OCEAN TEMPERATURES SPAR.WU.COHEN RUN#5

VERTICAL VELOCITY (10**-5 M/SEC) DIFFERENCE OF RUN5-RUN4

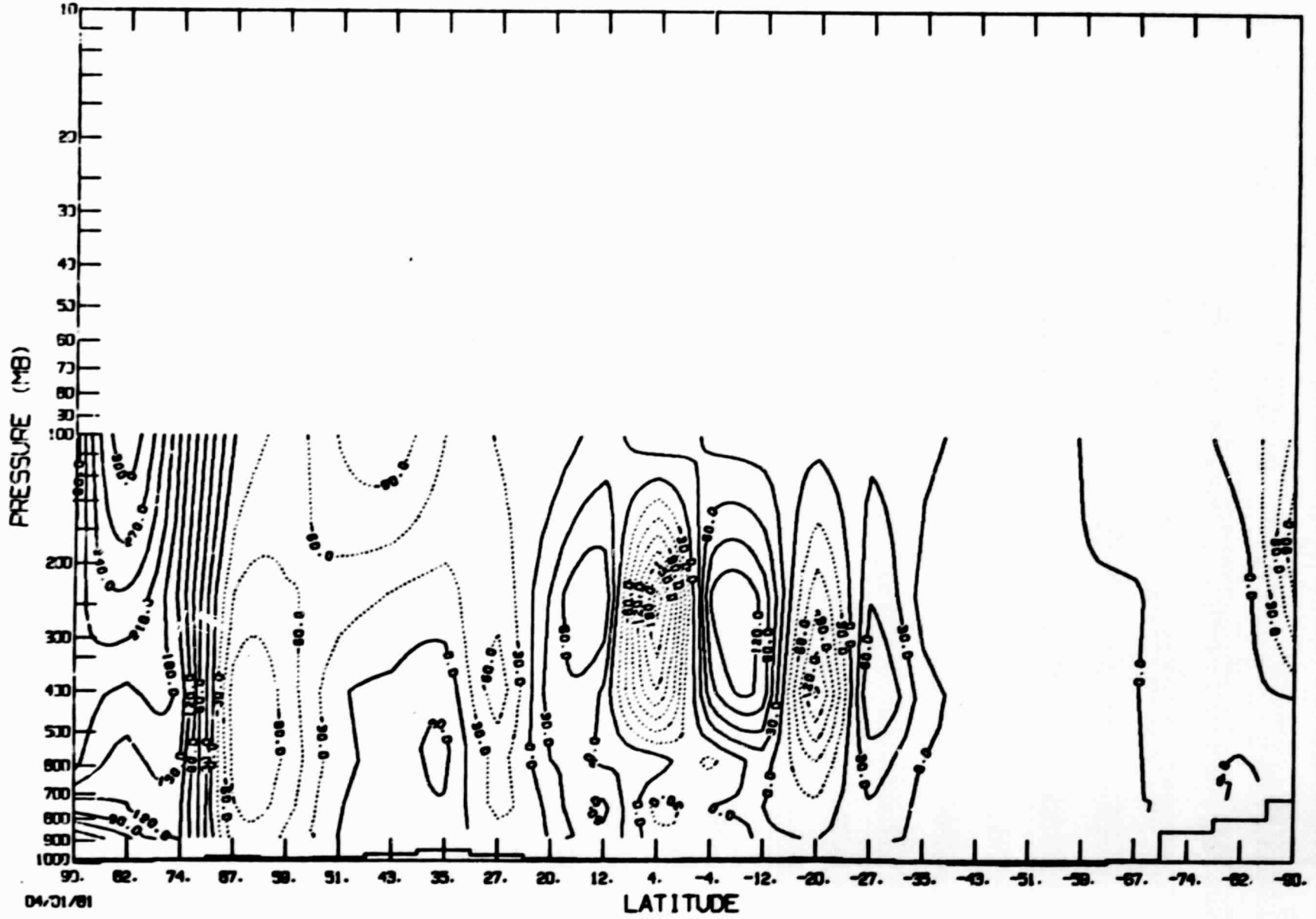

Fig. 91

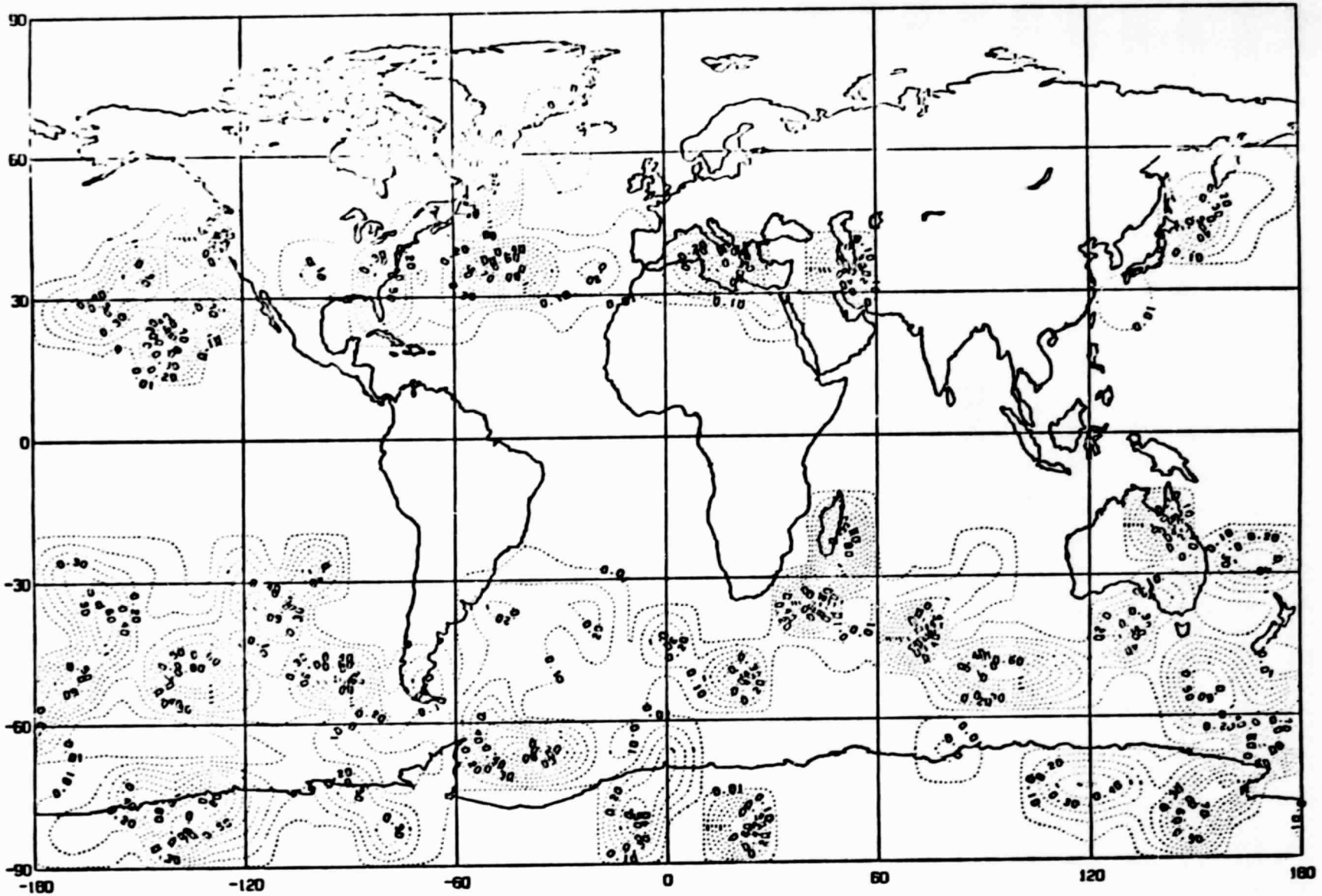

SIGNIFICANCE LEVELS OF DIFFERENCE OF MEANS: SLP. RUNS 2 & 3

Fig. 10a

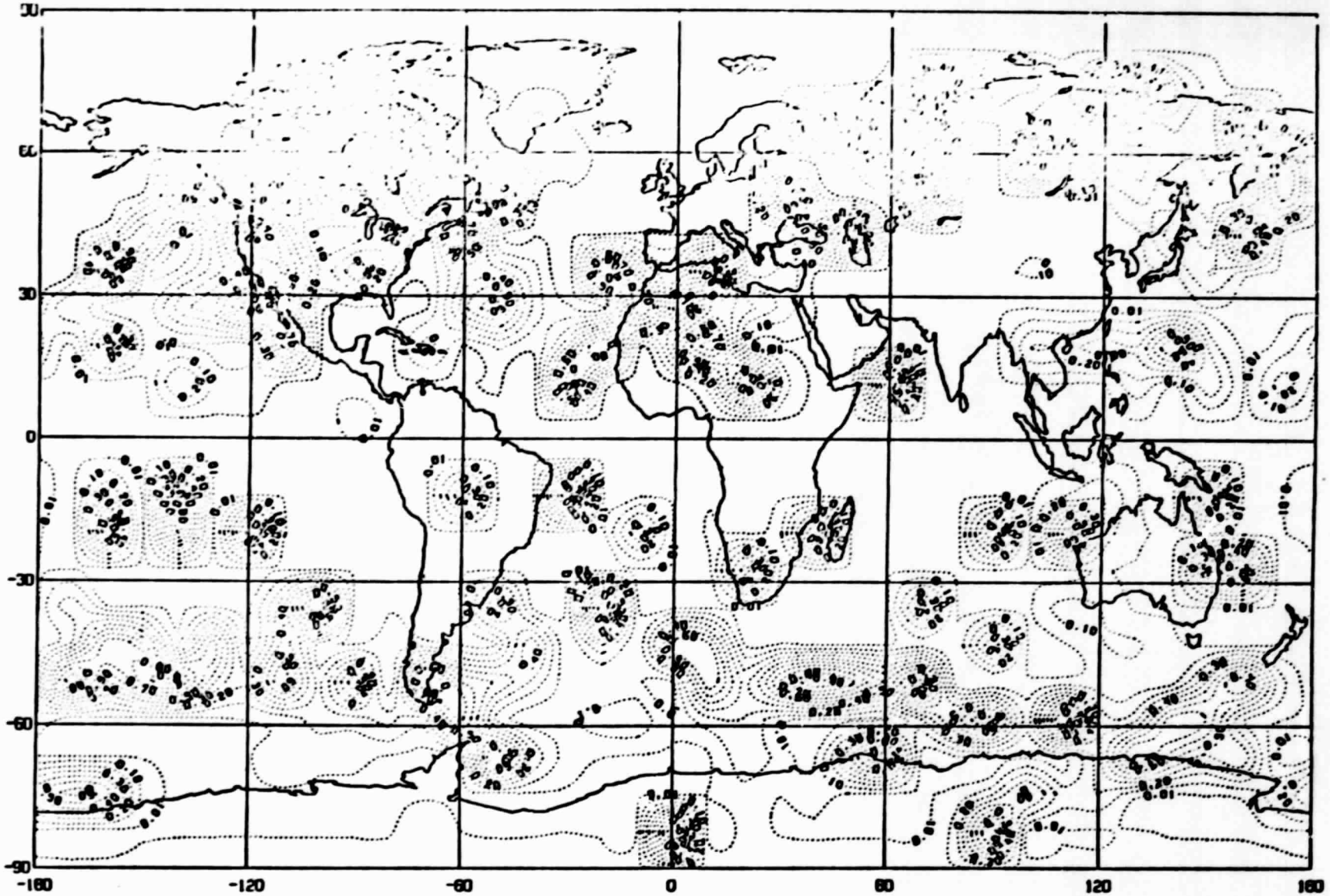

SIGNIFICANCE LEVELS OF DIFFERENCE OF MEANS: Z500, RUNS 2 & 3

Fig. 10b

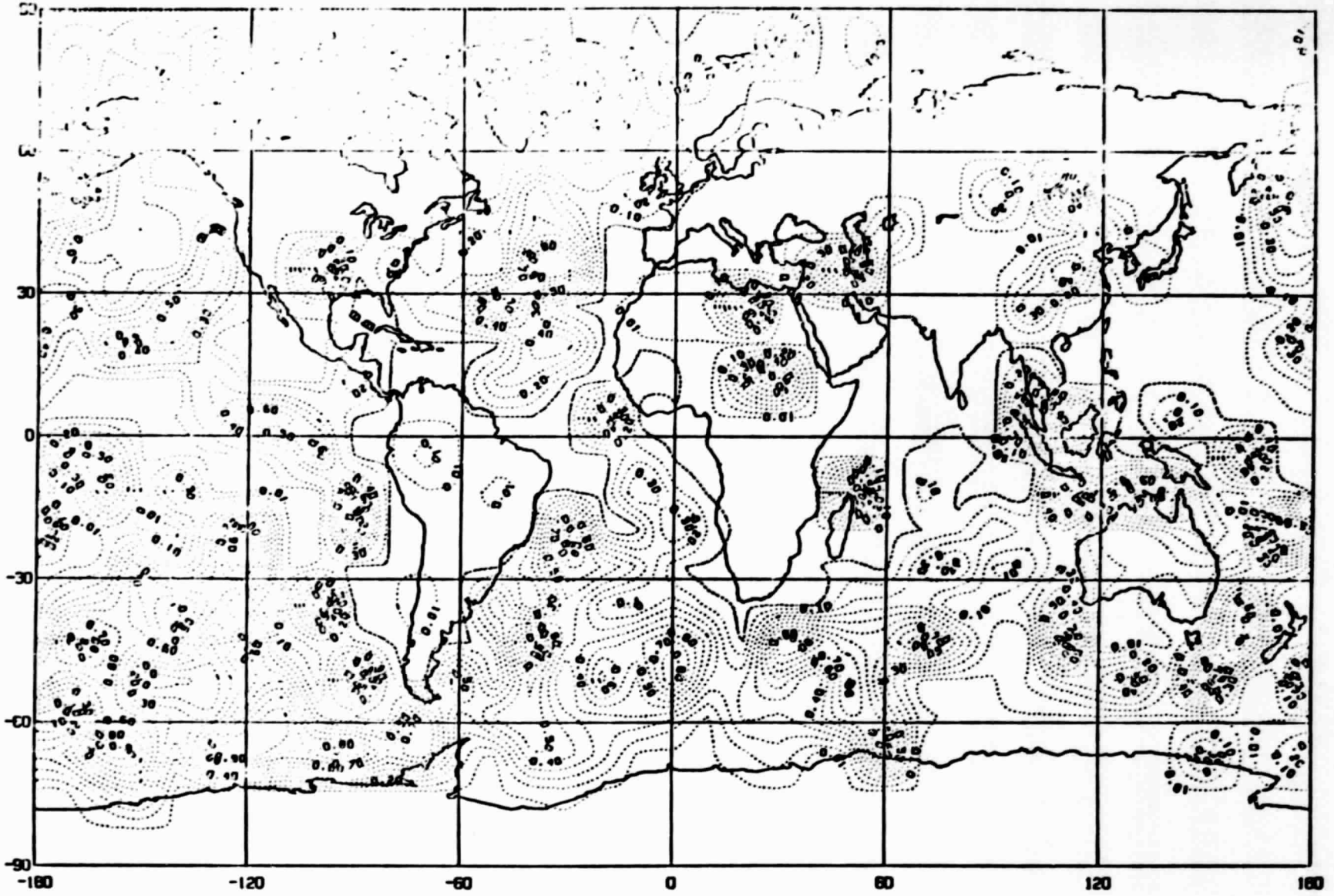

SIGNIFICANCE LEVELS OF DIFFERENCE OF MEANS: SFC. TEMP. RUNS 2 & 3

Fig. 10c

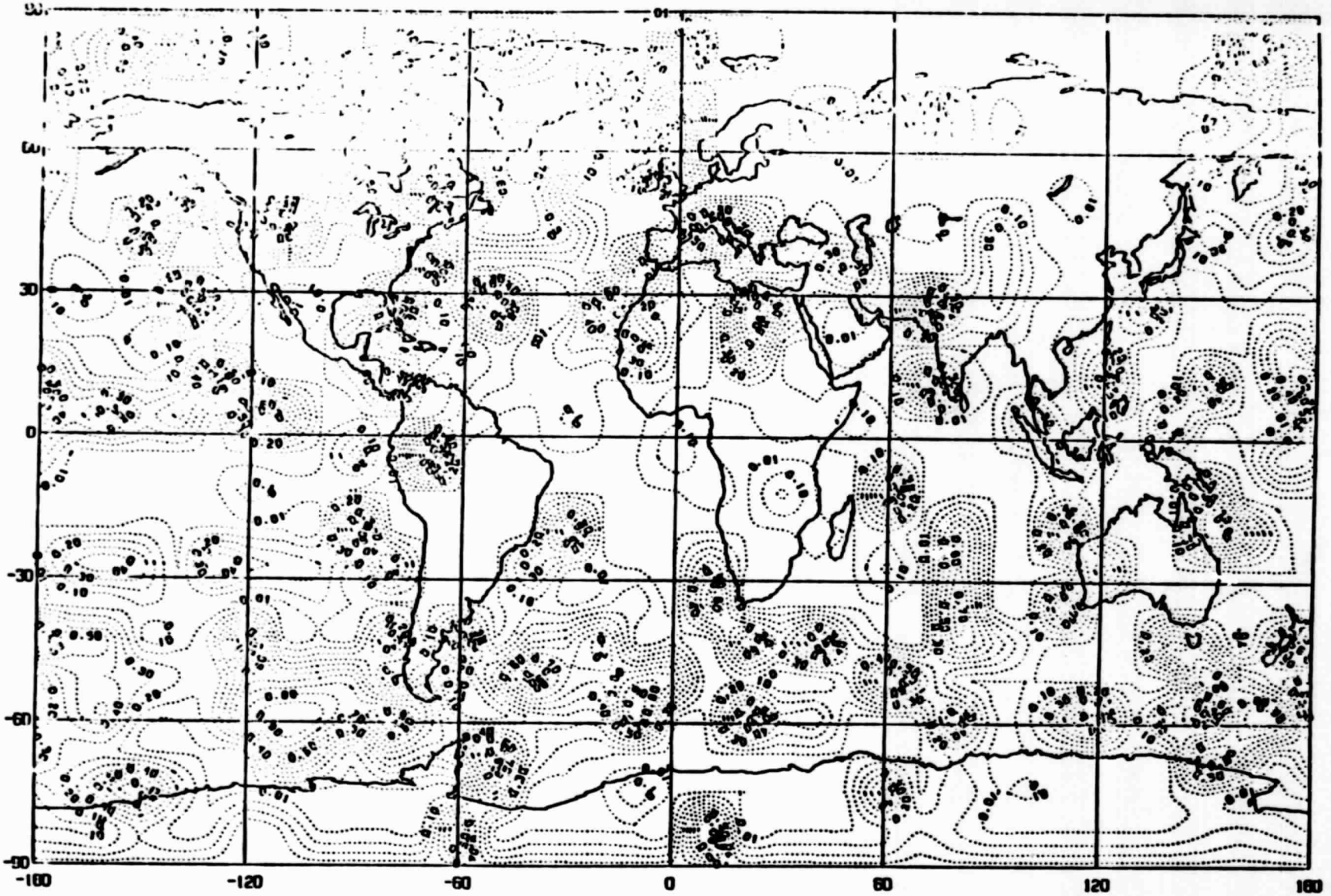

SIGNIFICANCE LEVELS OF DIFFERENCE OF MEANS: PRECIP. RUNS 2 & 3

Fig. 10d

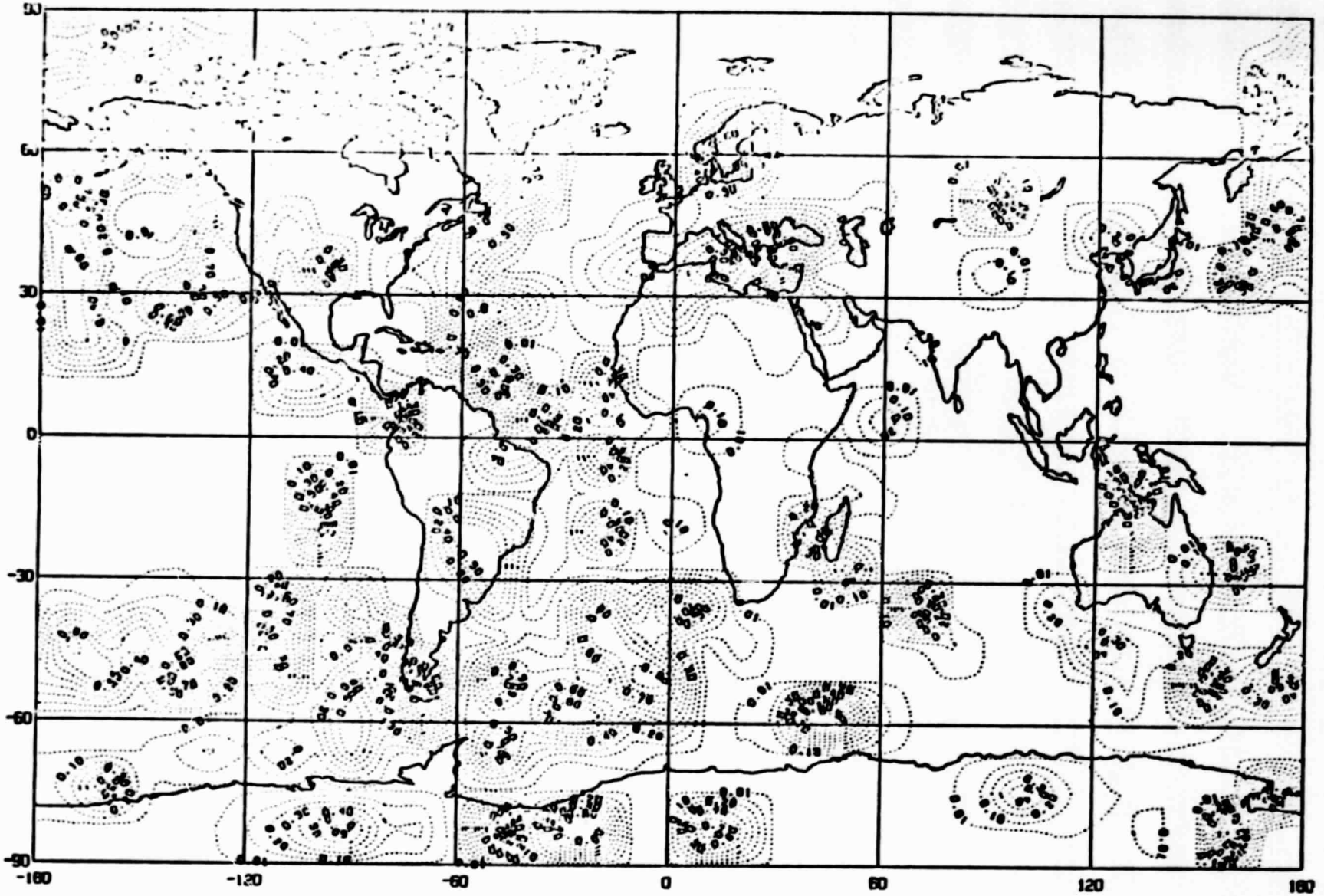

SIGNIFICANCE LEVELS OF DIFFERENCE OF MEANS: T850/700, RUNS 2 & 3

Fig. 10e

*****RUN003*SPIN UP WITH ISOTHERMAL ATMOSPHERE INCLUDING MOUNTIAN*ZERO GROUND WETNESS SPAR.COHEN.W

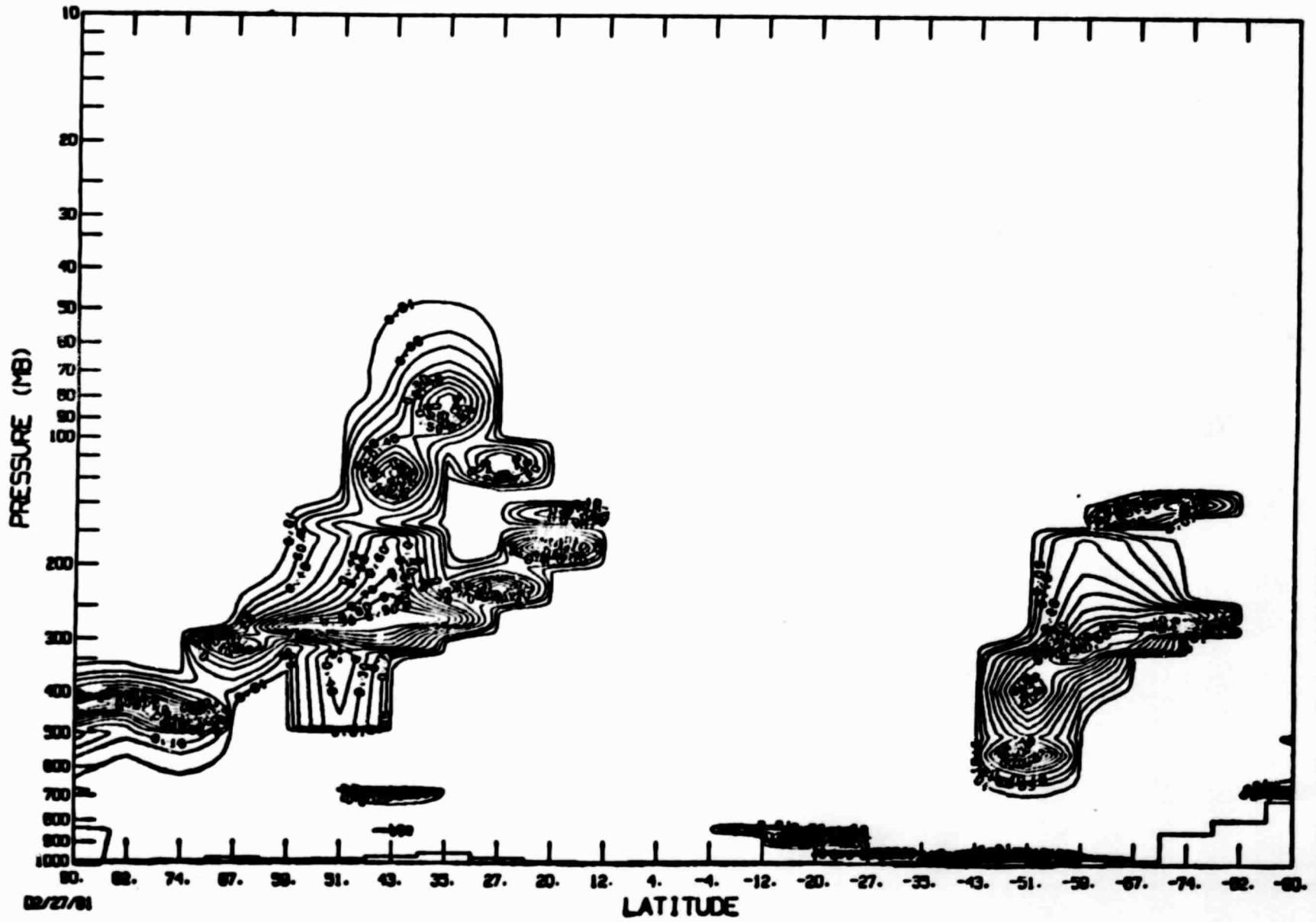

Fig. 10f

#####RUN003=SPIN UP WITH ISOTHERMAL ATMOSPHERE INCLUDING MOUNTIAN=ZERO GROUND WETNESS SPAR.COHEN.W

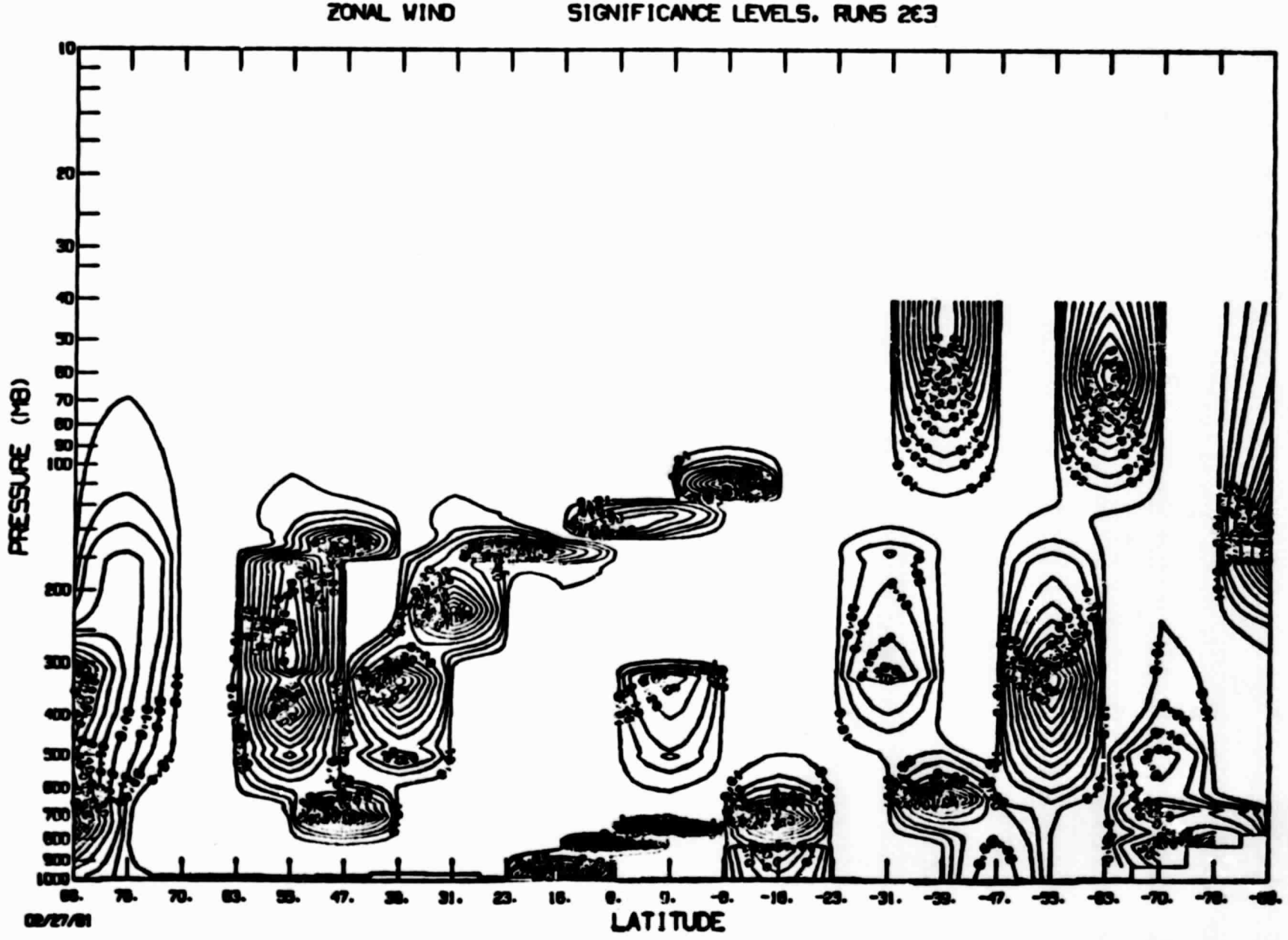

Fig. 10g

#####RUN003*SPIN UP WITH ISOTHERMAL ATMOSPHERE INCLUDING MOUNTIAN*ZERO GROUND WETNESS SPAR.COHEN.W

MERIDIONAL WIND SIGNIFICANCE LEVELS. RUNS 2&3

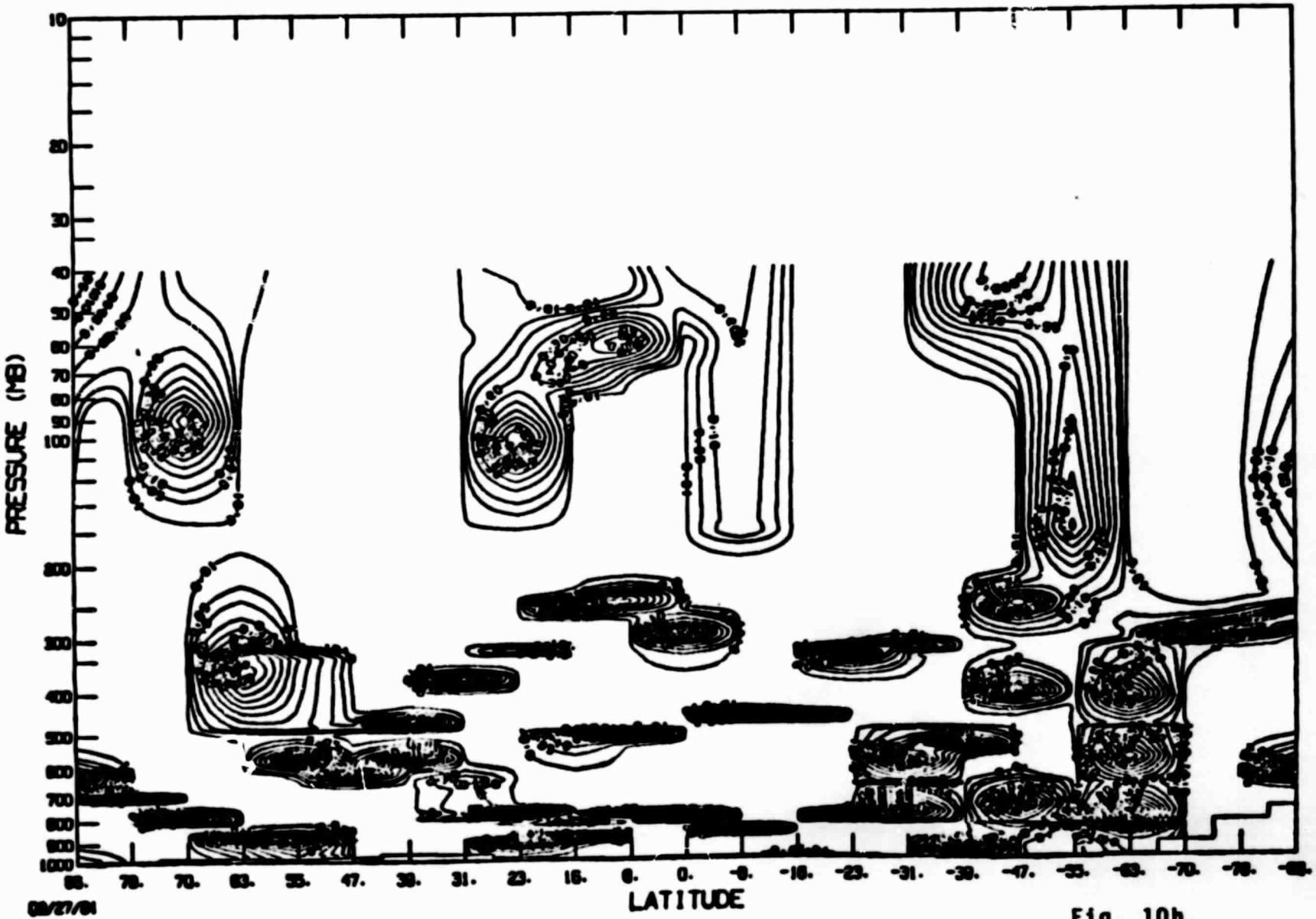

Fig. 10h

*****RUN003*SPIN UP WITH ISOTHERMAL ATMOSPHERE INCLUDING MOUNTIAN*ZERO GROUND WETNESS SPAR.COHEN.W

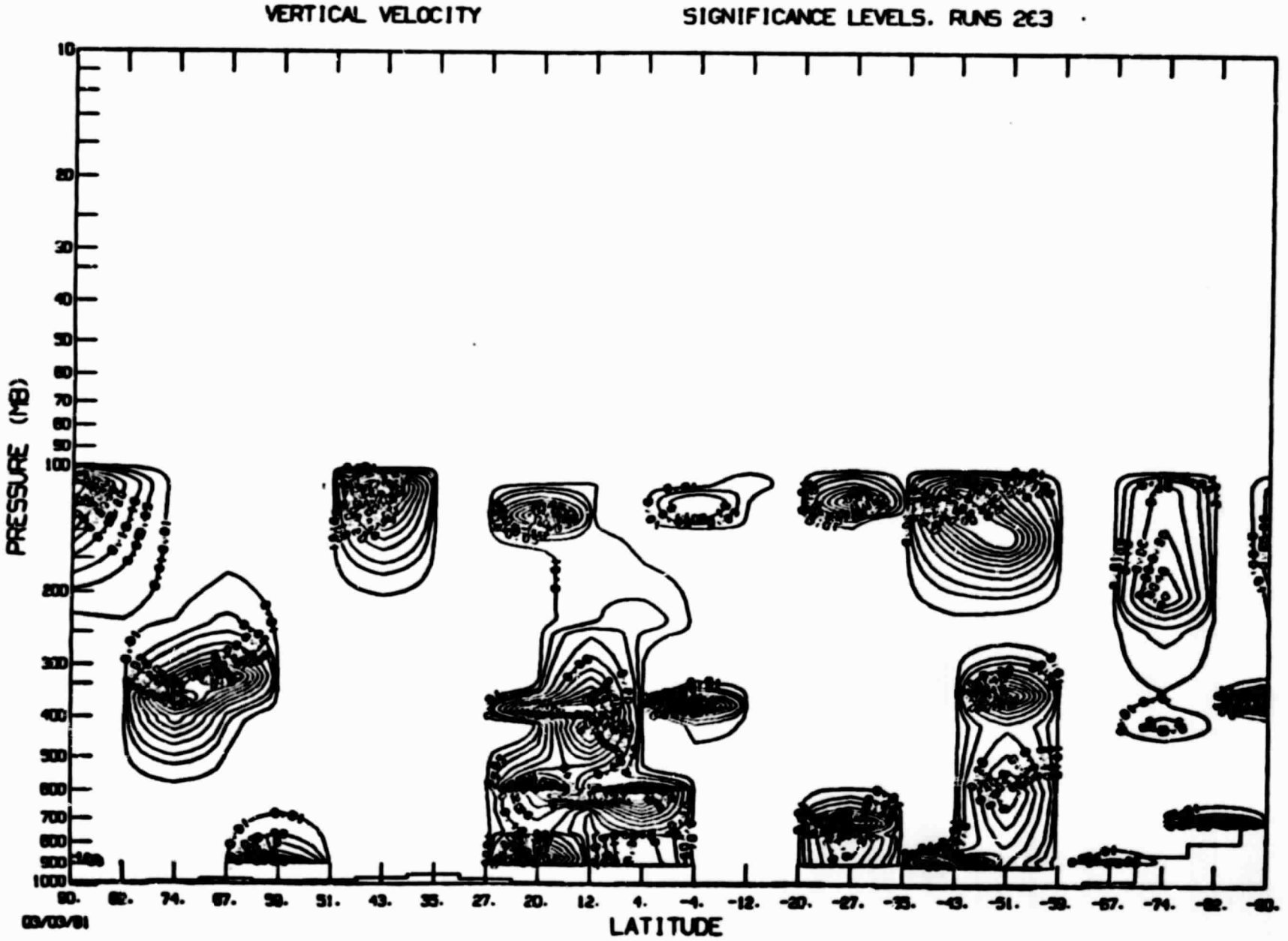

Fig. 101

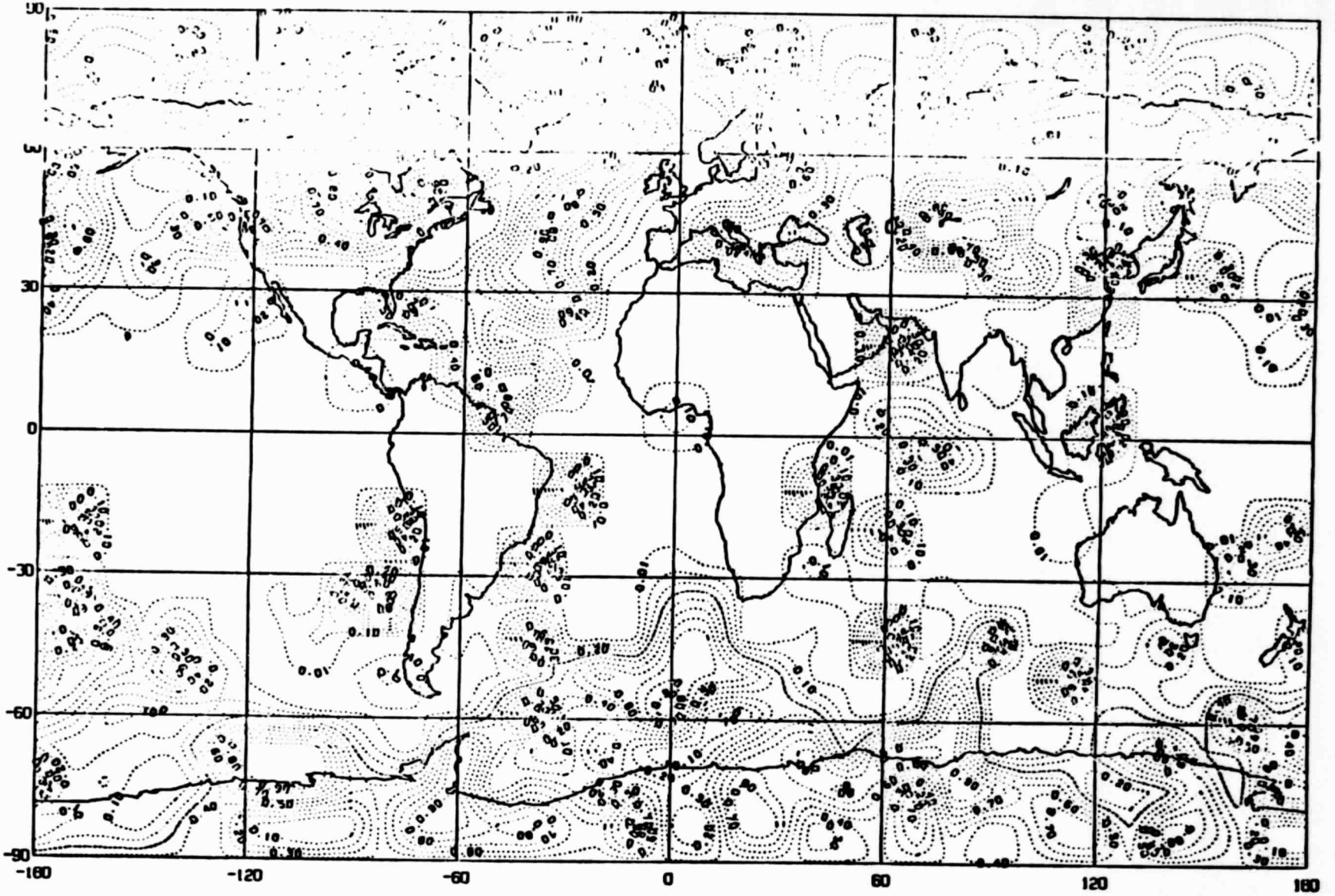

SIGNIFICANCE LEVELS OF DIFFERENCE OF MEANS: SLP. RUNS 3 & 4

Fig. 11a

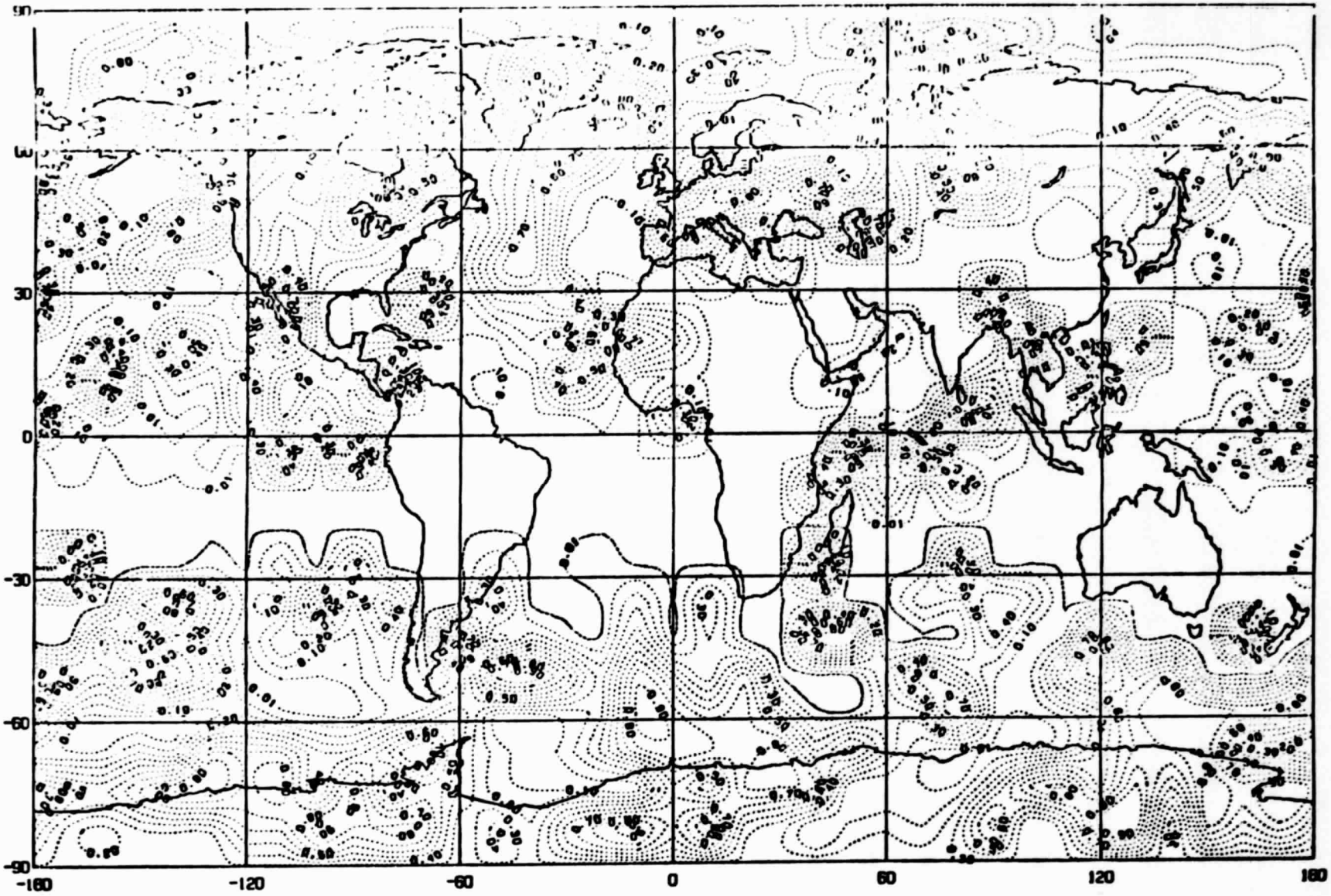

SIGNIFICANCE LEVELS OF DIFFERENCE OF MEANS: Z500. RUNS 3 & 4

Fig. 11b

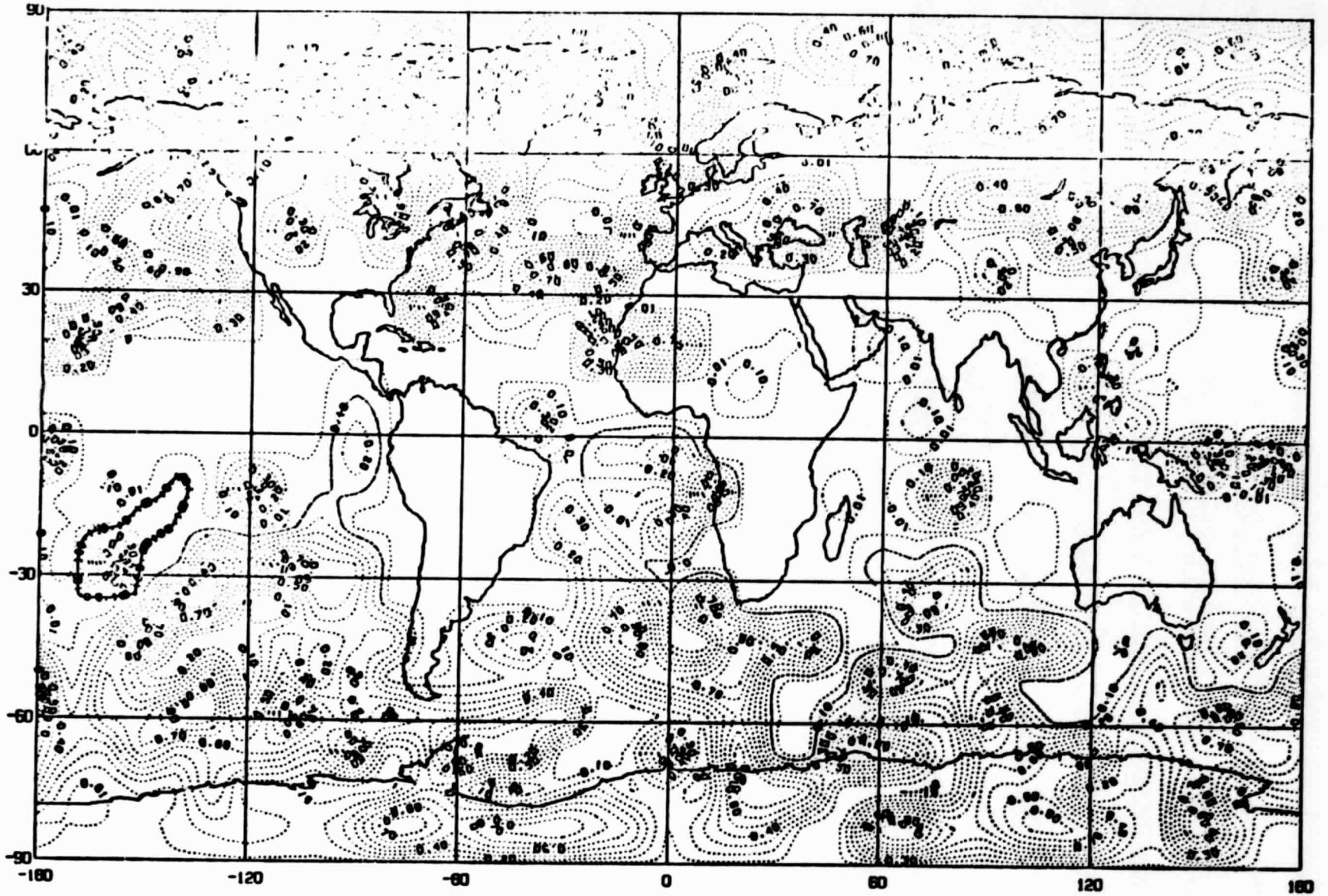

SIGNIFICANCE LEVELS OF DIFFERENCE OF MEANS: SFC. TEMP. RUNS 3 & 4

Fig. 11c

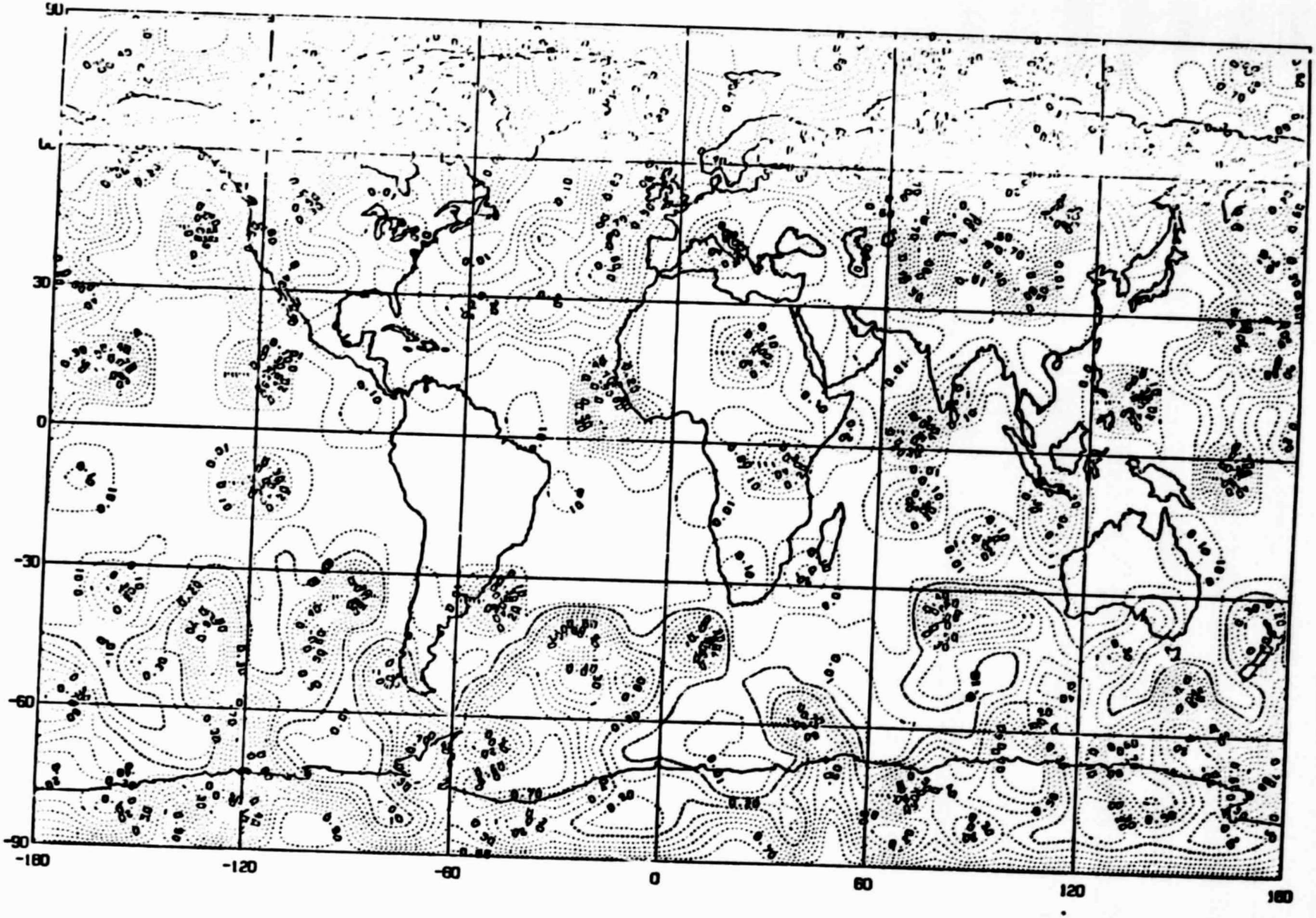

SIGNIFICANCE LEVELS OF DIFFERENCE OF MEANS: PRECIP. RUNS 3 & 4

Fig. 11d

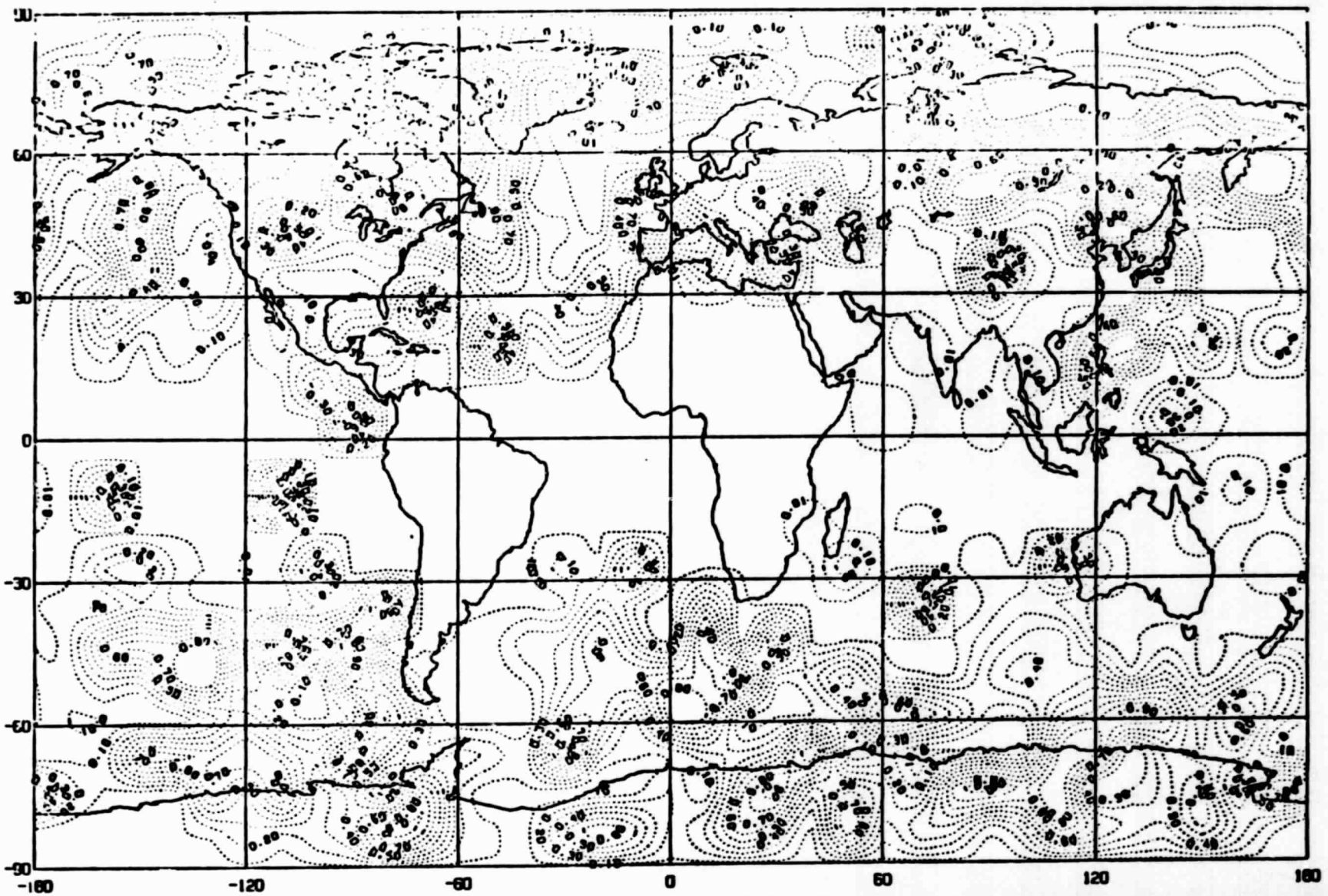

SIGNIFICANCE LEVELS OF DIFFERENCE OF MEANS: T850/700.RUNS 3 & 4

Fig. 11e

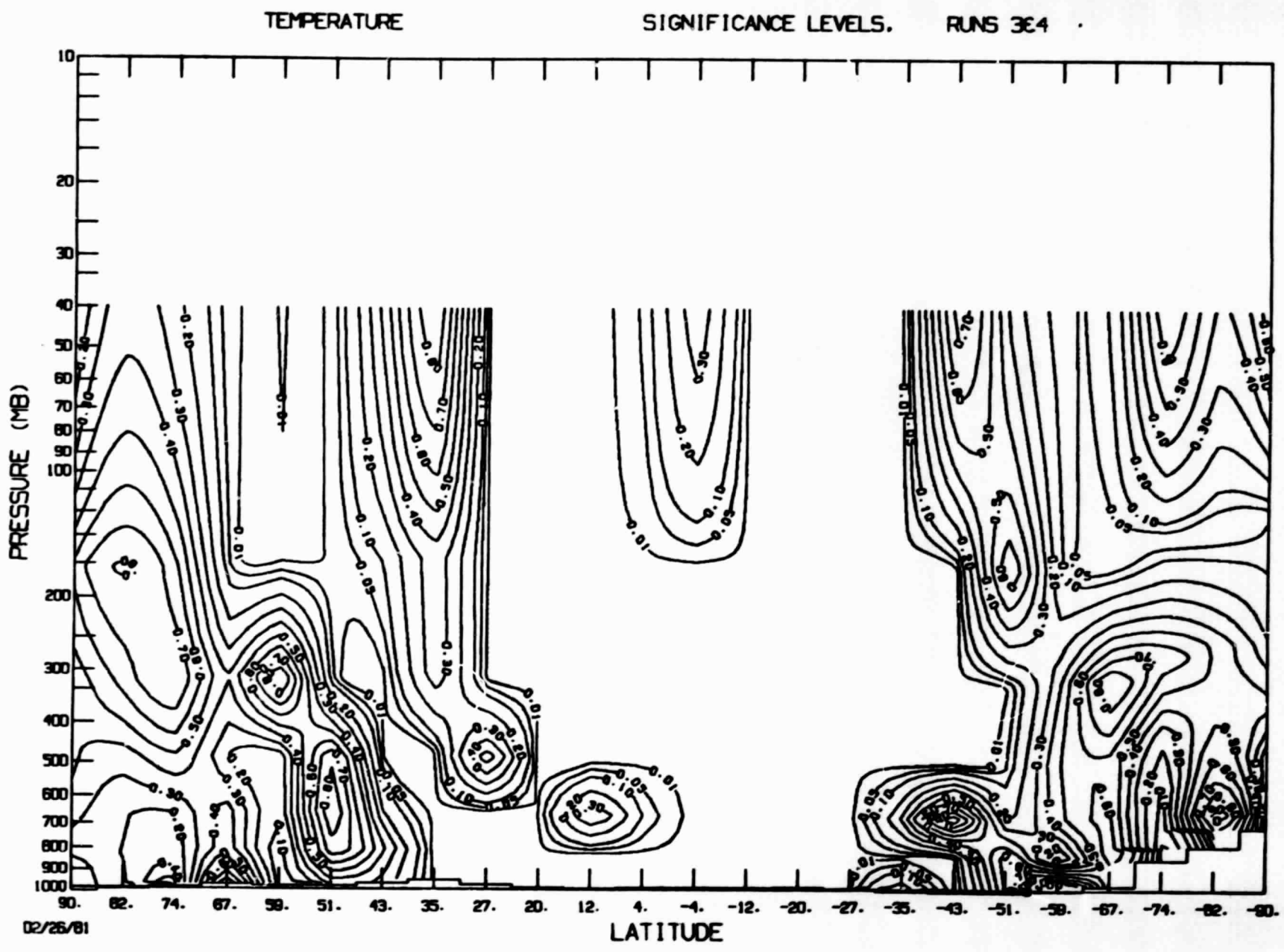
TEMPERATURE
SIGNIFICANCE LEVELS. RUNS 3&4
PRESSURE (MB)
10
20
30
40
50
60
70
80
90
100
200
300
400
500
600
700
800
900
1000
90. 82. 74. 67. 59. 51. 43. 35. 27. 20. 12. 4. -4. -12. -20. -27. -35. -43. -51. -59. -67. -74. -82. -90.
LATITUDE
02/26/81

Fig. 11f

*RUN#4*SPIN-UP FROM ISOTHERMAL ATMOSPHERE*WITH MOUNTAINS AND SURFACE PHYSICS *SPAR.COHEN.WU #4

ZONAL WIND SIGNIFICANCE LEVELS. RUNS 3&4

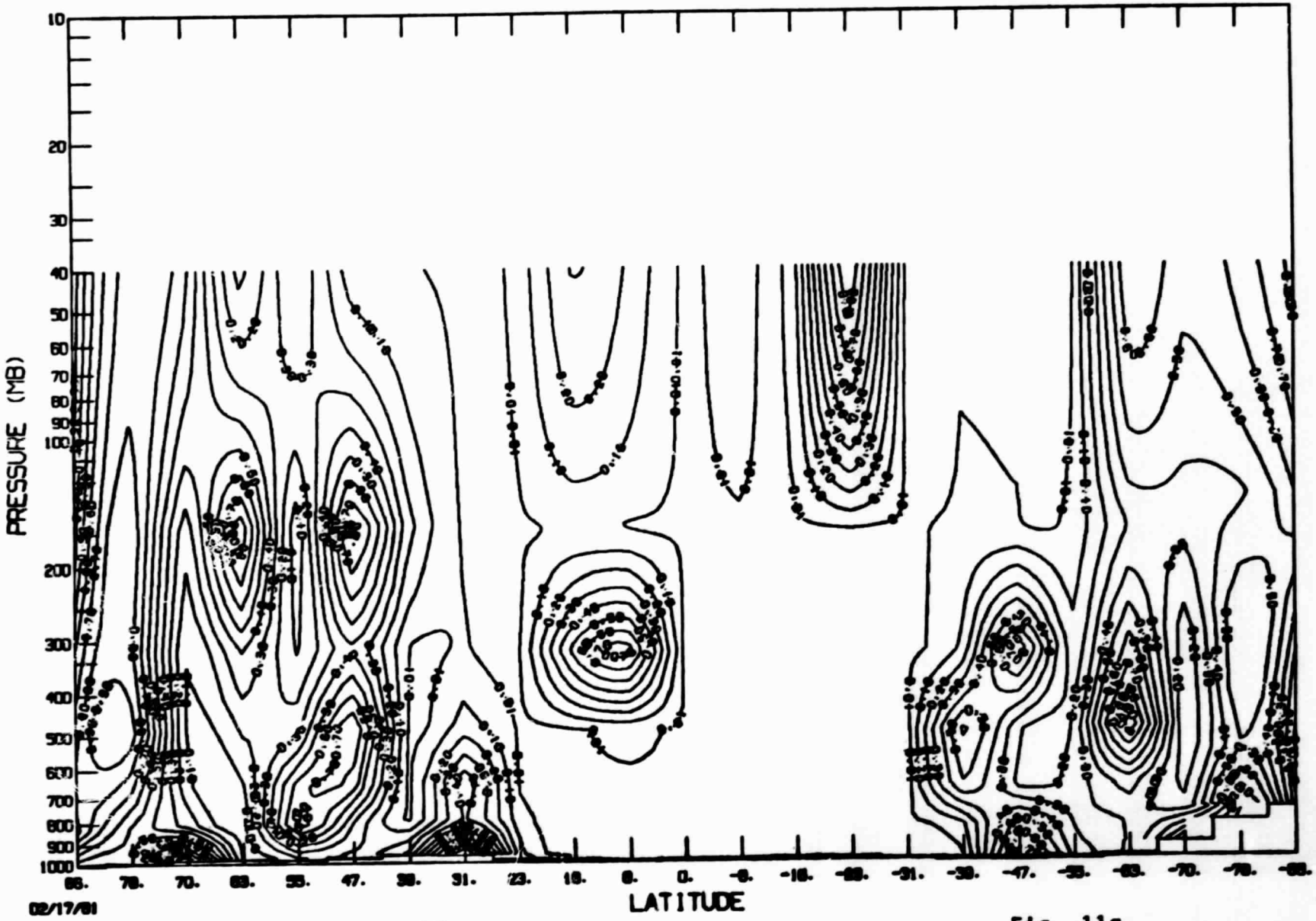

Fig. 11g

MERIDIONAL WIND SIGNIFICANCE LEVELS. RUNS 3&4

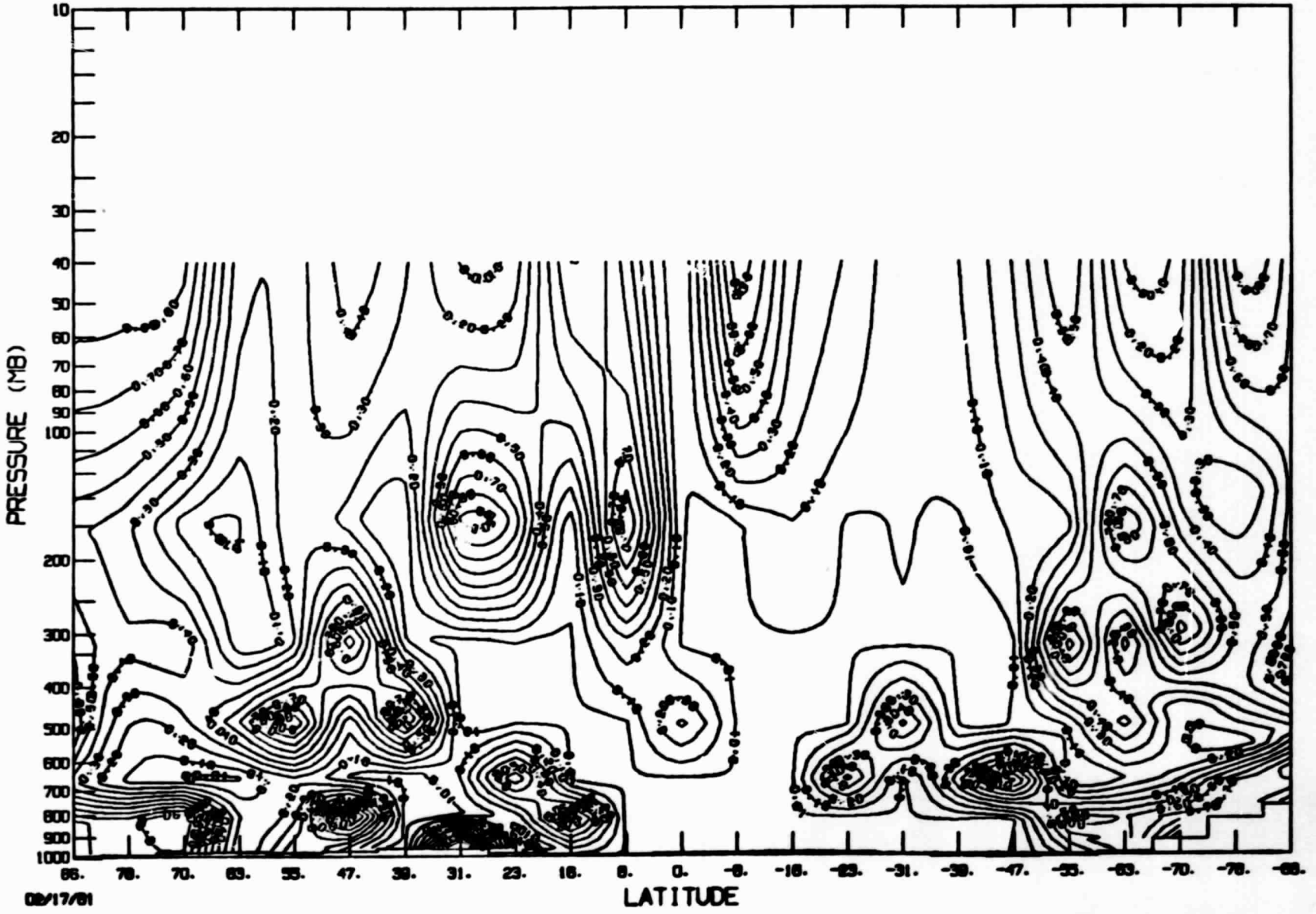

Fig. 11h

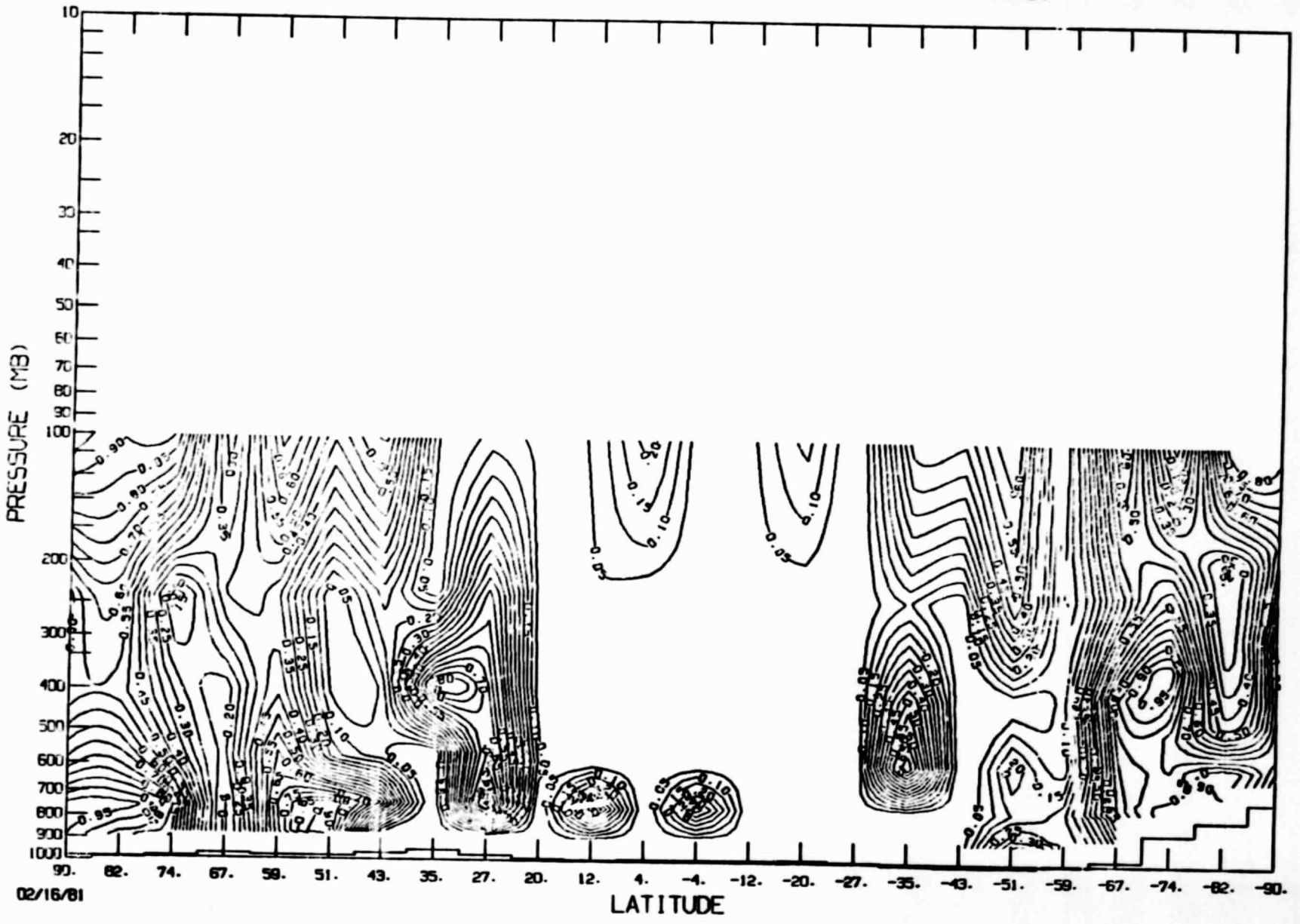
VERTICAL VELOCITY
SIGNIF.LEVELS.
RUNS 3E4
PRESSURE (MB)
10
20
30
40
50
60
70
80
90
100
200
300
400
500
600
700
800
900
1000
90. 82. 74. 67. 59. 51. 43. 35. 27. 20. 12. 4. -4. -12. -20. -27. -35. -43. -51. -59. -67. -74. -82. -90.
LATITUDE
02/16/81

Fig. 111

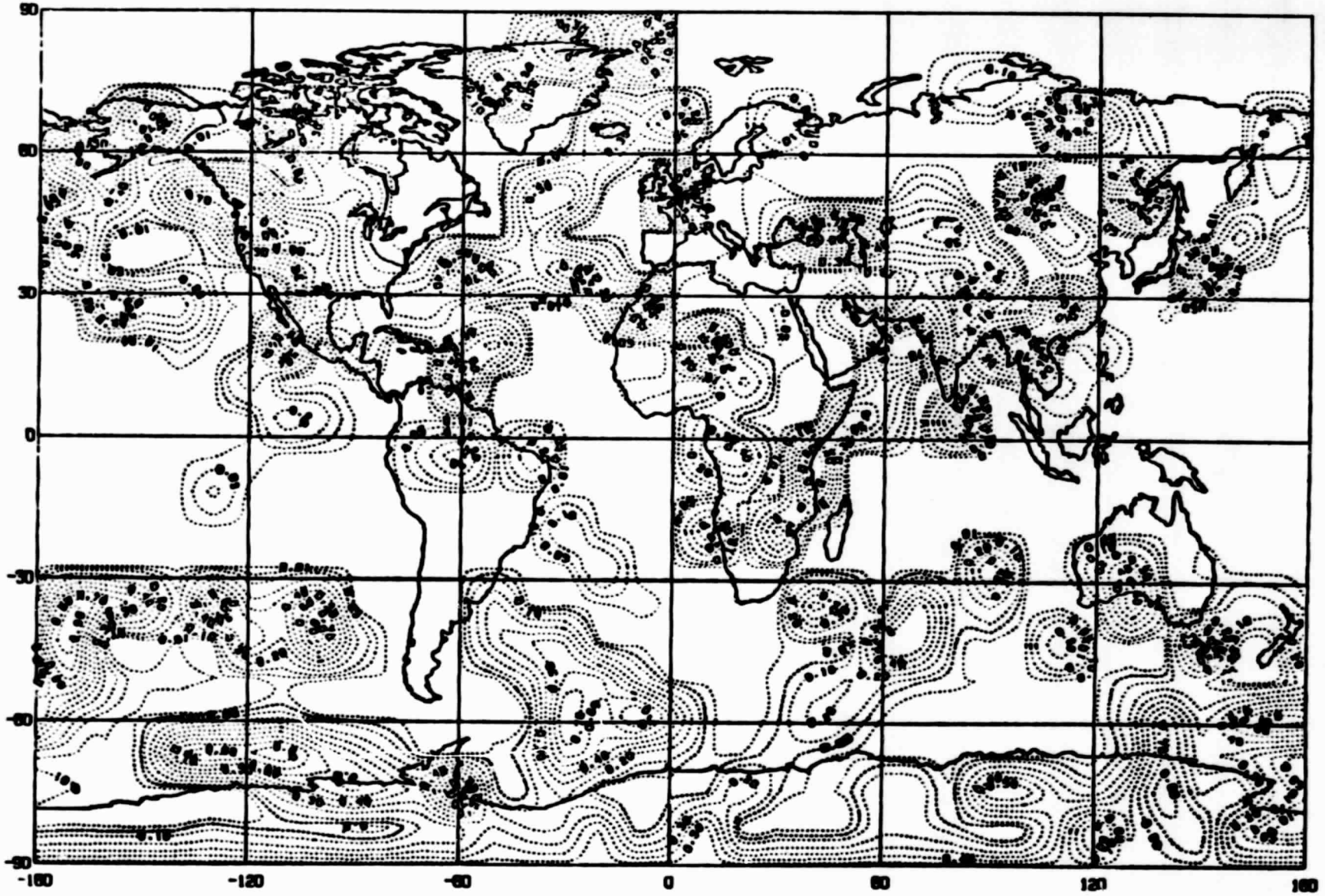

SIGNIFICANCE LEVELS OF DIFFERENCE OF MEANS: SLP. RUNS 4 & 5

Fig. 12a

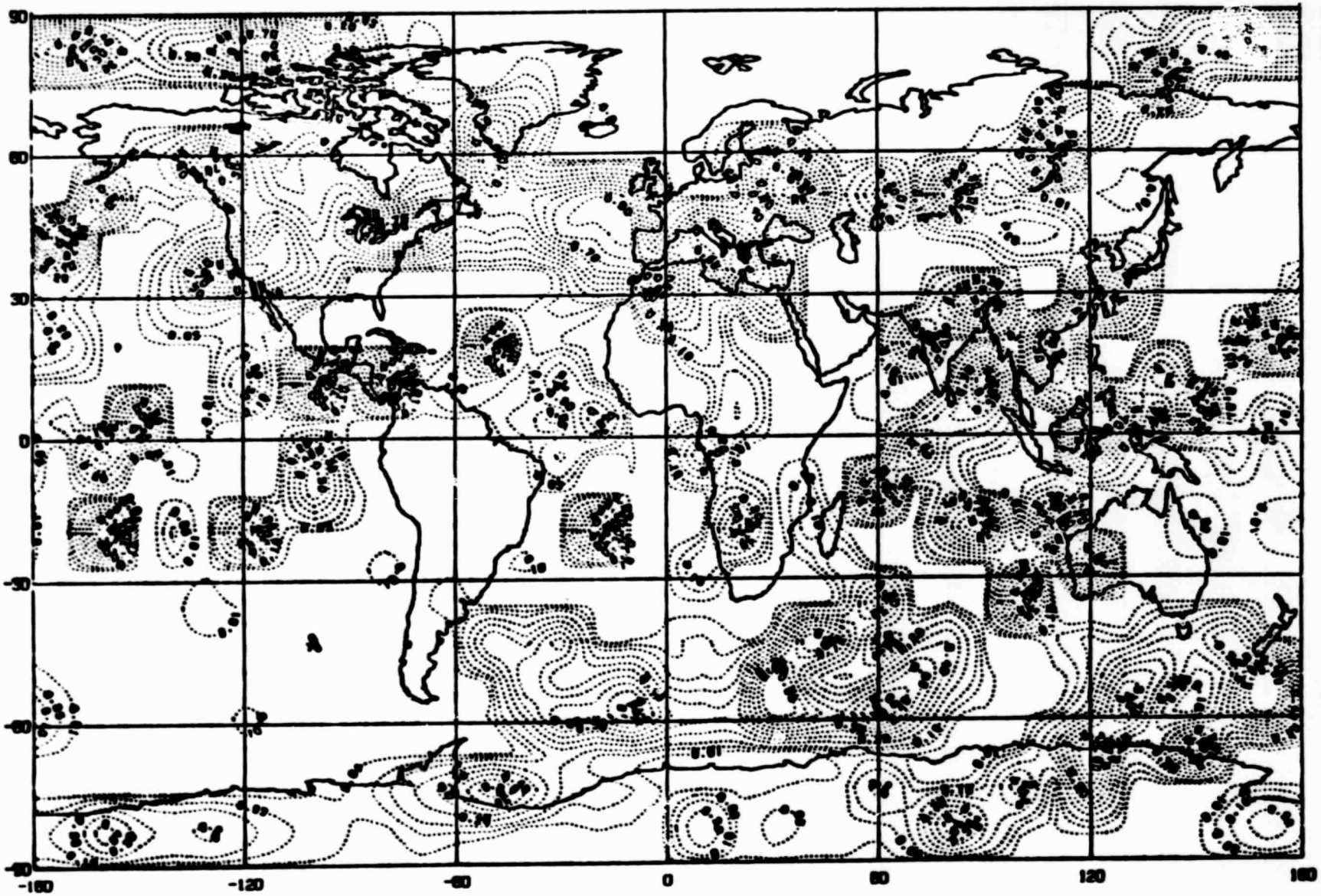

SIGNIFICANCE LEVELS OF DIFFERENCE OF MEANS: Z500. RUNS 4 & 5

Fig. 12b

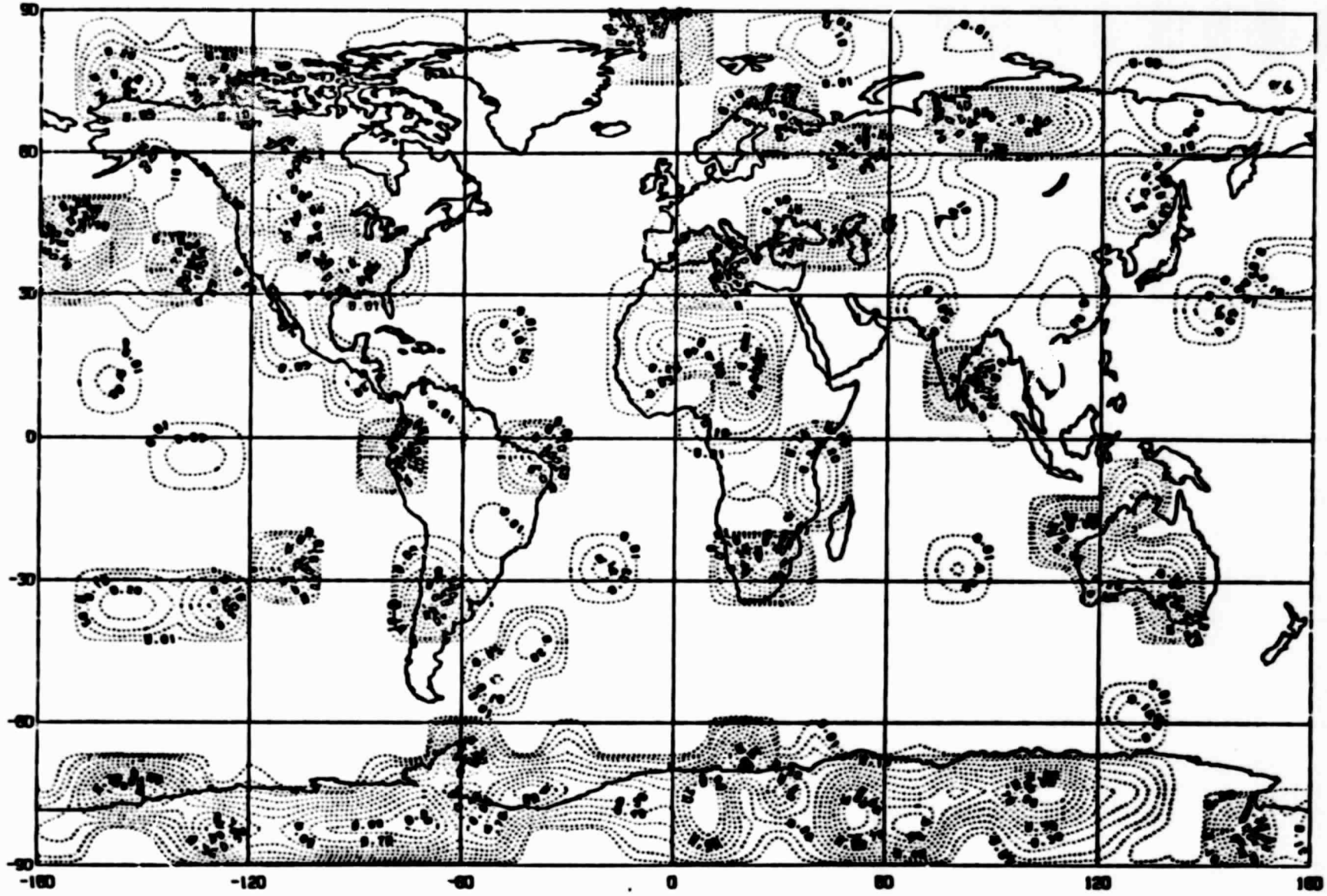

SIGNIFICANCE LEVELS OF DIFFERENCE OF MEANS: SFC. TEMP. RUNS 4 & 5

Fig. 12c

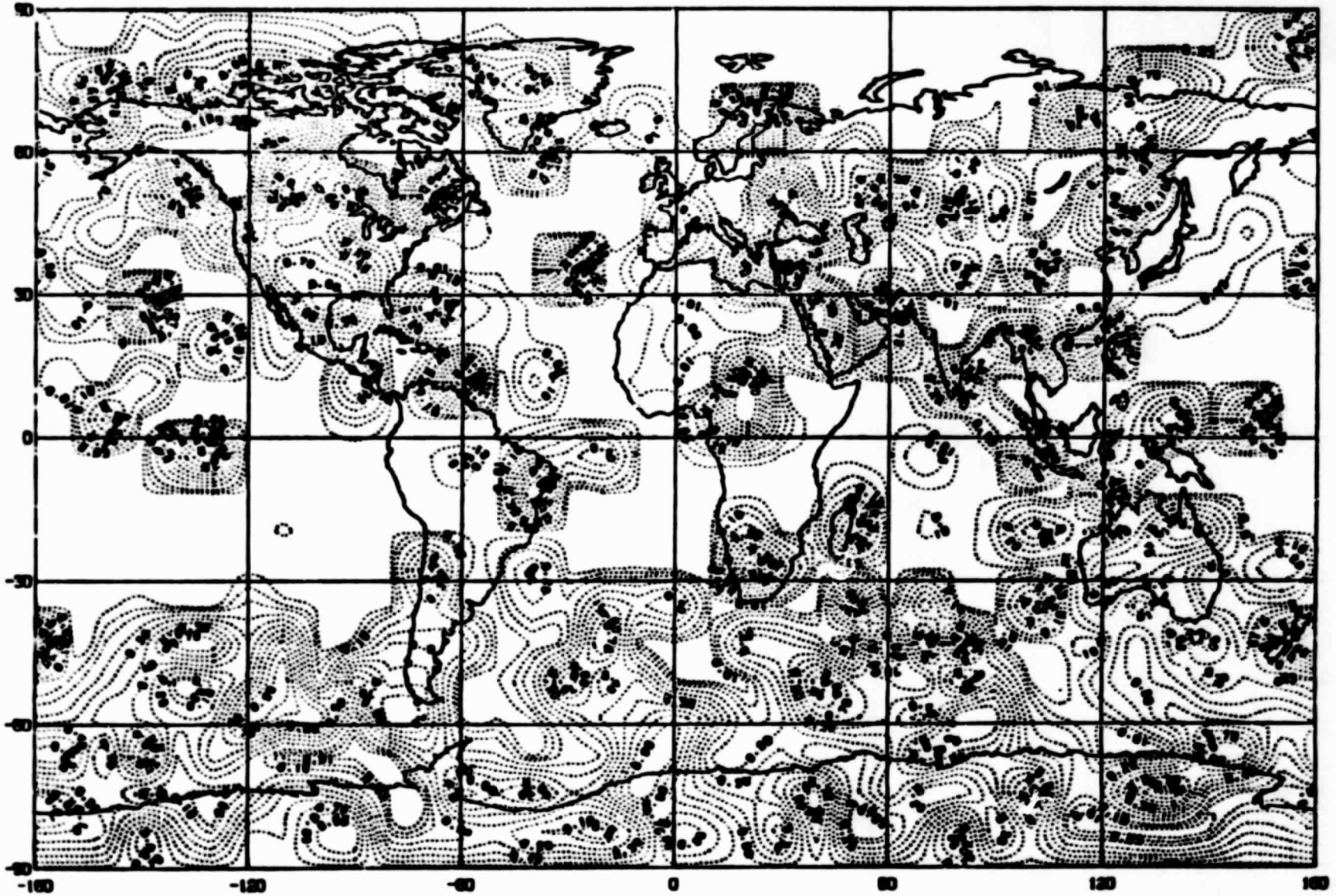

SIGNIFICANCE LEVELS OF DIFFERENCE OF MEANS: PRECIP. RUNS 4 & 5

Fig. 12d

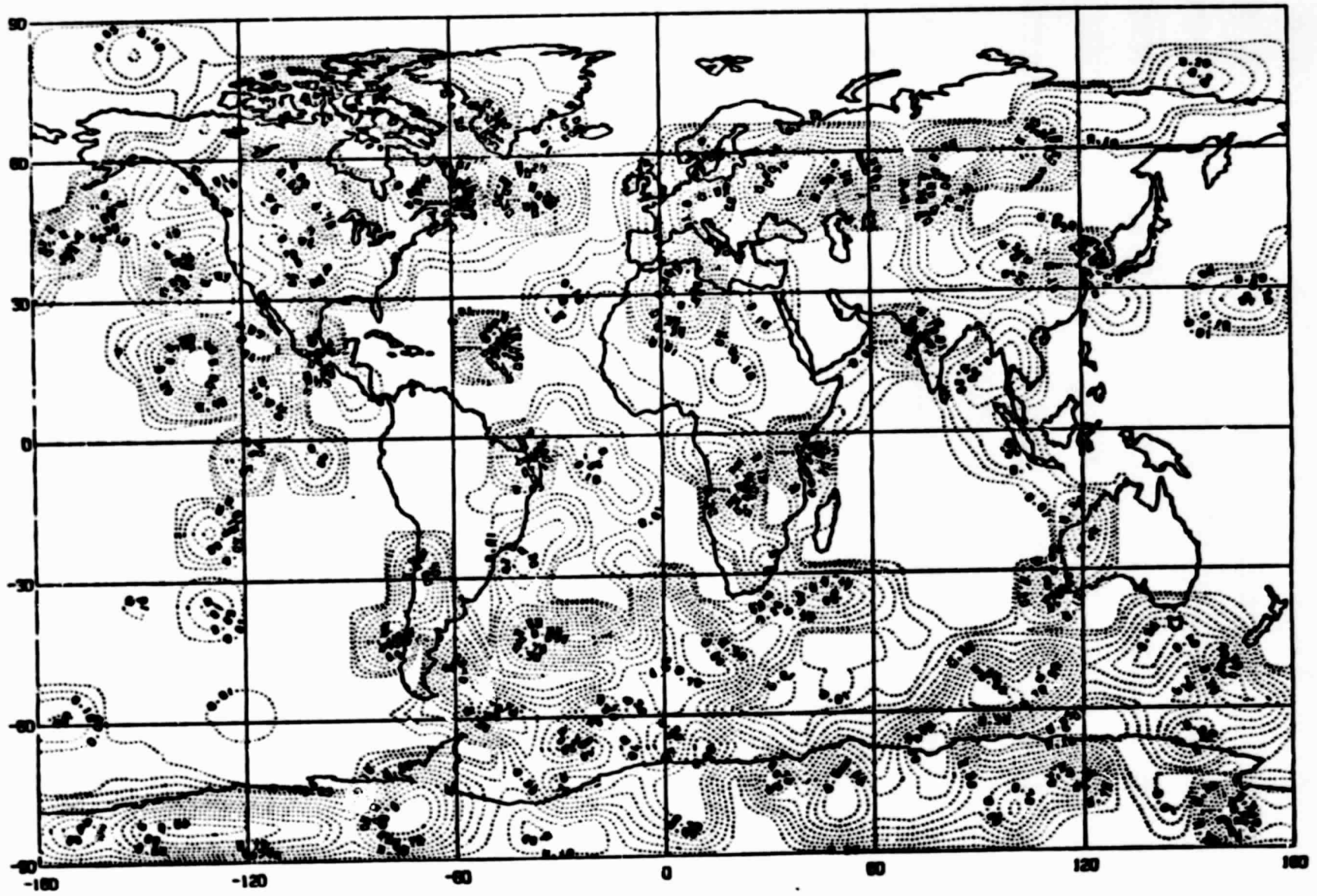

SIGNIFICANCE LEVELS OF DIFFERENCE OF MEANS: T850/700. RUNS 4 & 5

Fig. 12e

RUN#5 SPIN-UP WITH MOUNTAINS AND SURFACE PHYSICS AND REAL OCEAN TEMPERATURES SPAR.WU.COHEN RUN#5

TEMPERATURE SIGNIFICANCE LEVELS. RUNS 4&5

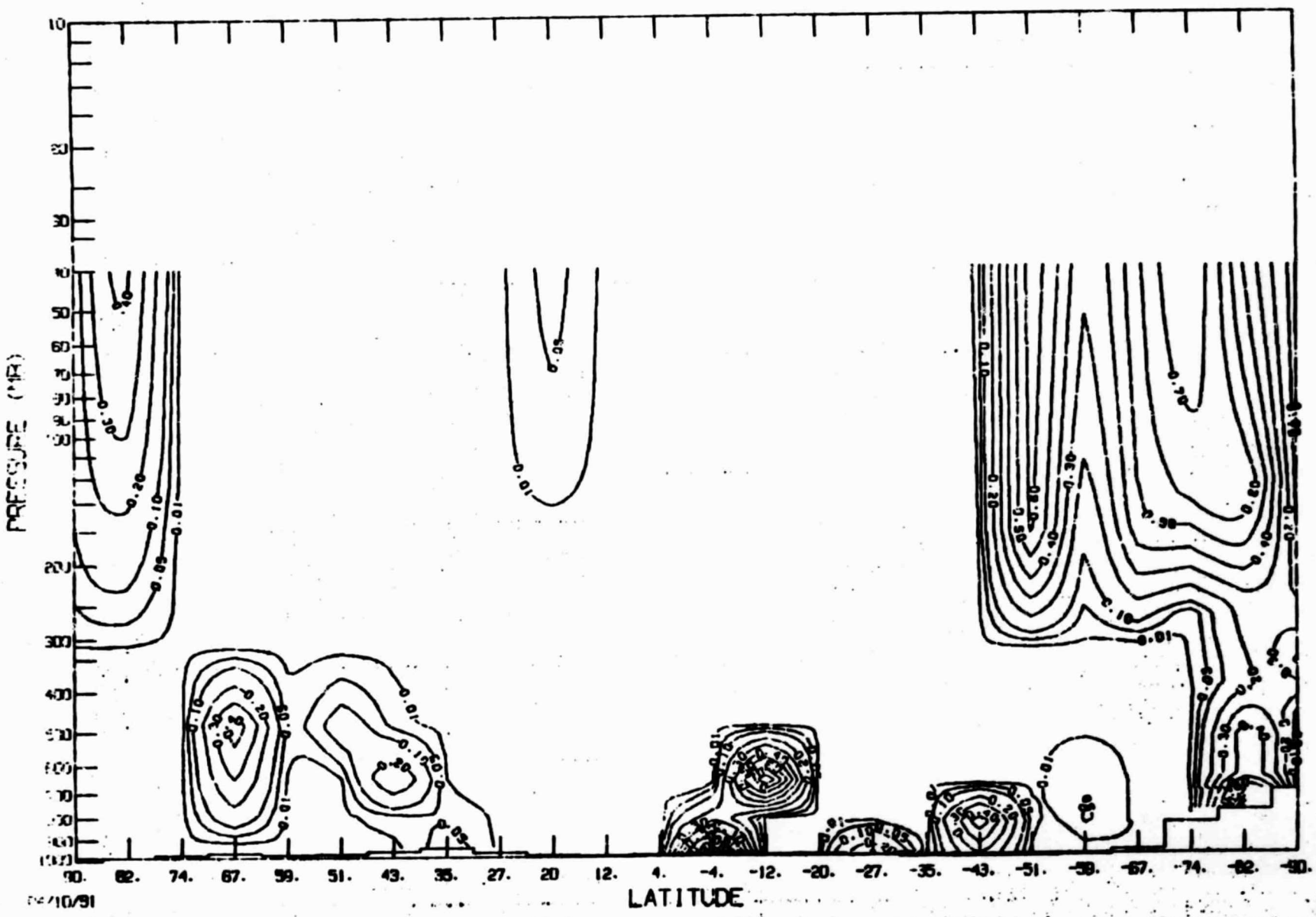

Fig. 12f

ZONAL WIND SIGNIFICANCE LEVELS. RUNS 4&5

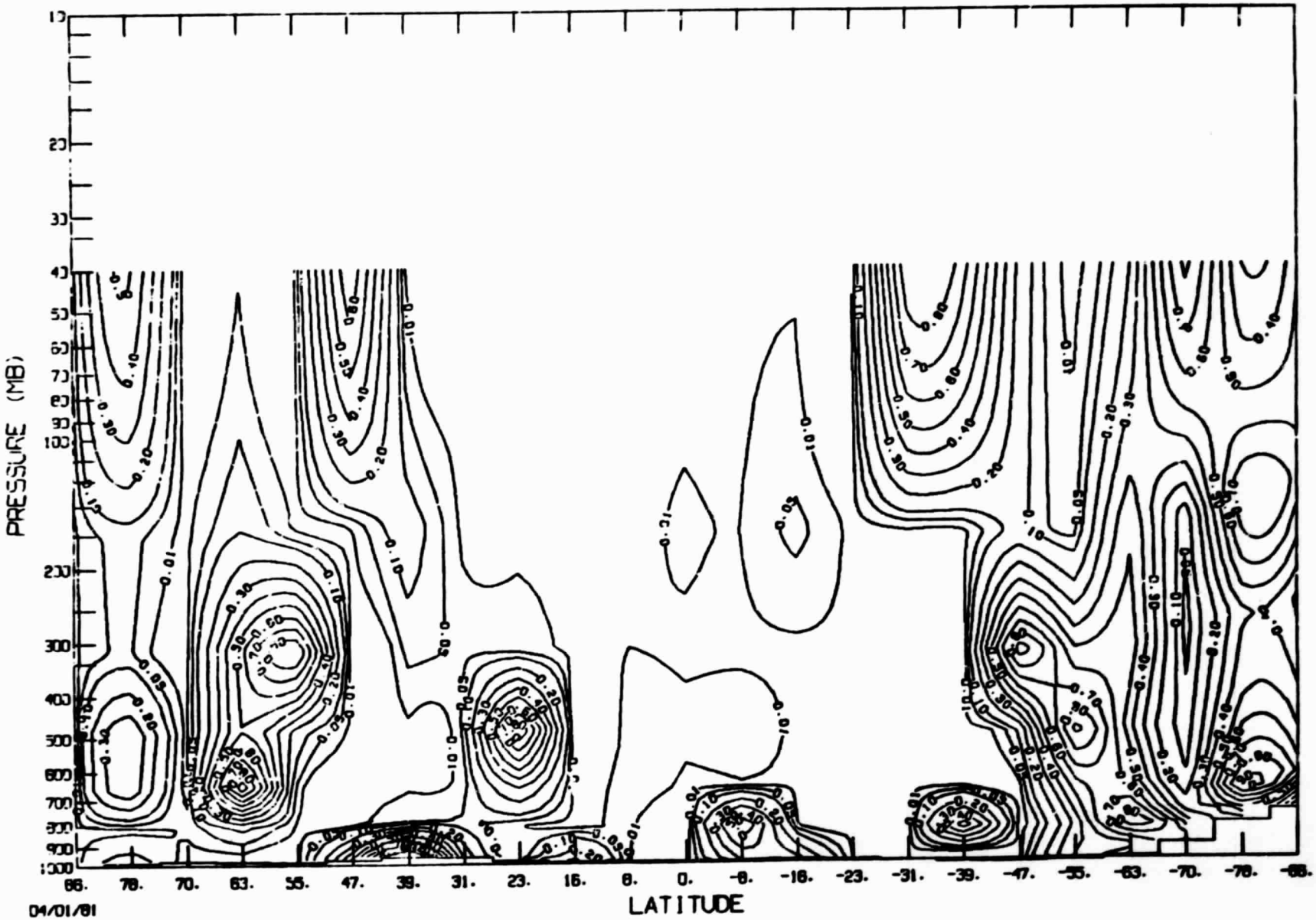

Fig. 12g

RUN#5 SPIN-UP WITH MOUNTAINS AND SURFACE PHYSICS AND REAL OCEAN TEMPERATURES SPAR.WU.COHEN RUN#5

MERIDIONAL WIND SIGNIFICANCE LEVELS. RUNS 4&5

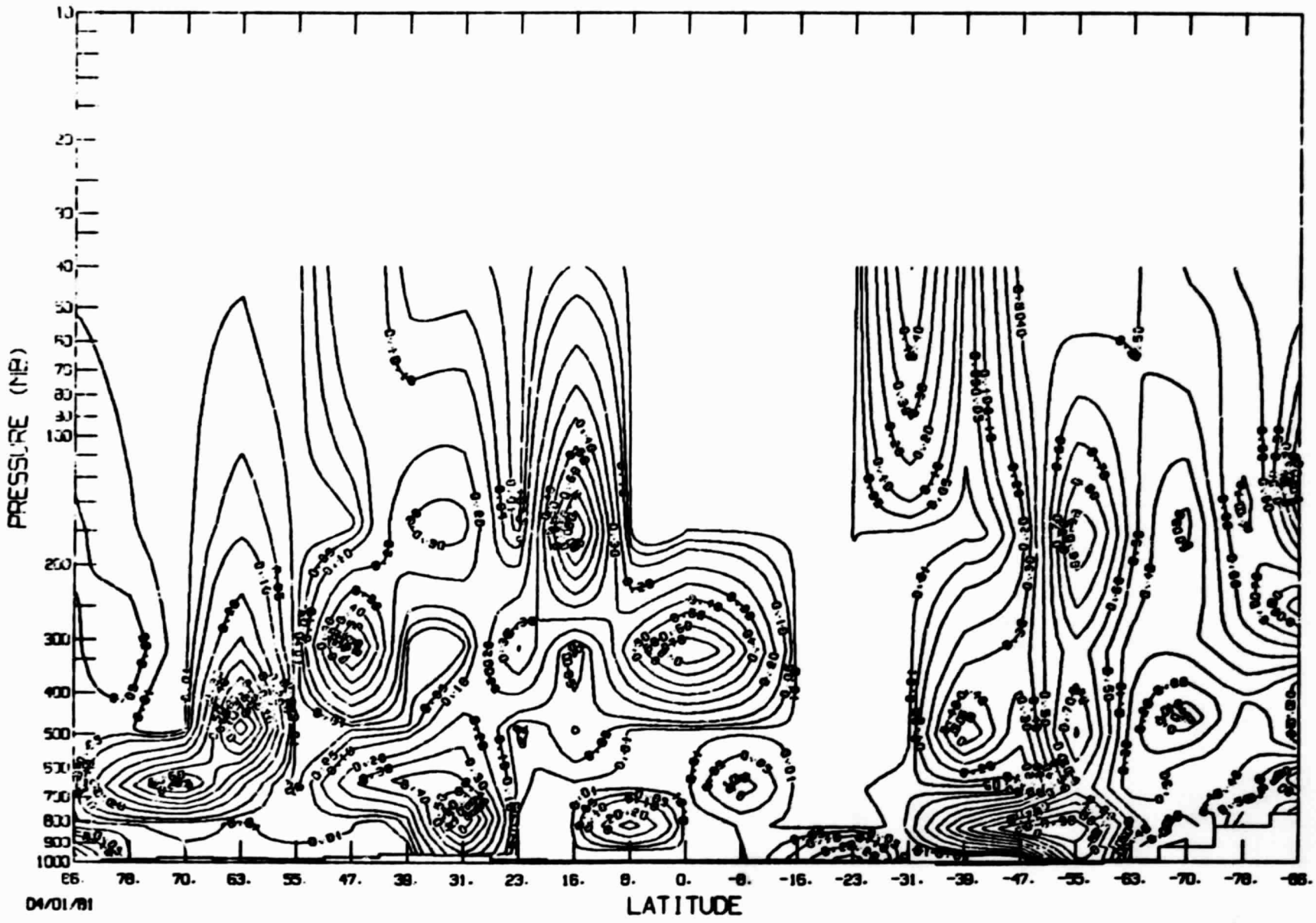

Fig. 12h

RUN#5 SPIN-UP WITH MOUNTAINS AND SURFACE PHYSICS AND REAL OCEAN TEMPERATURES SPAR.WU.COHEN RUN#5

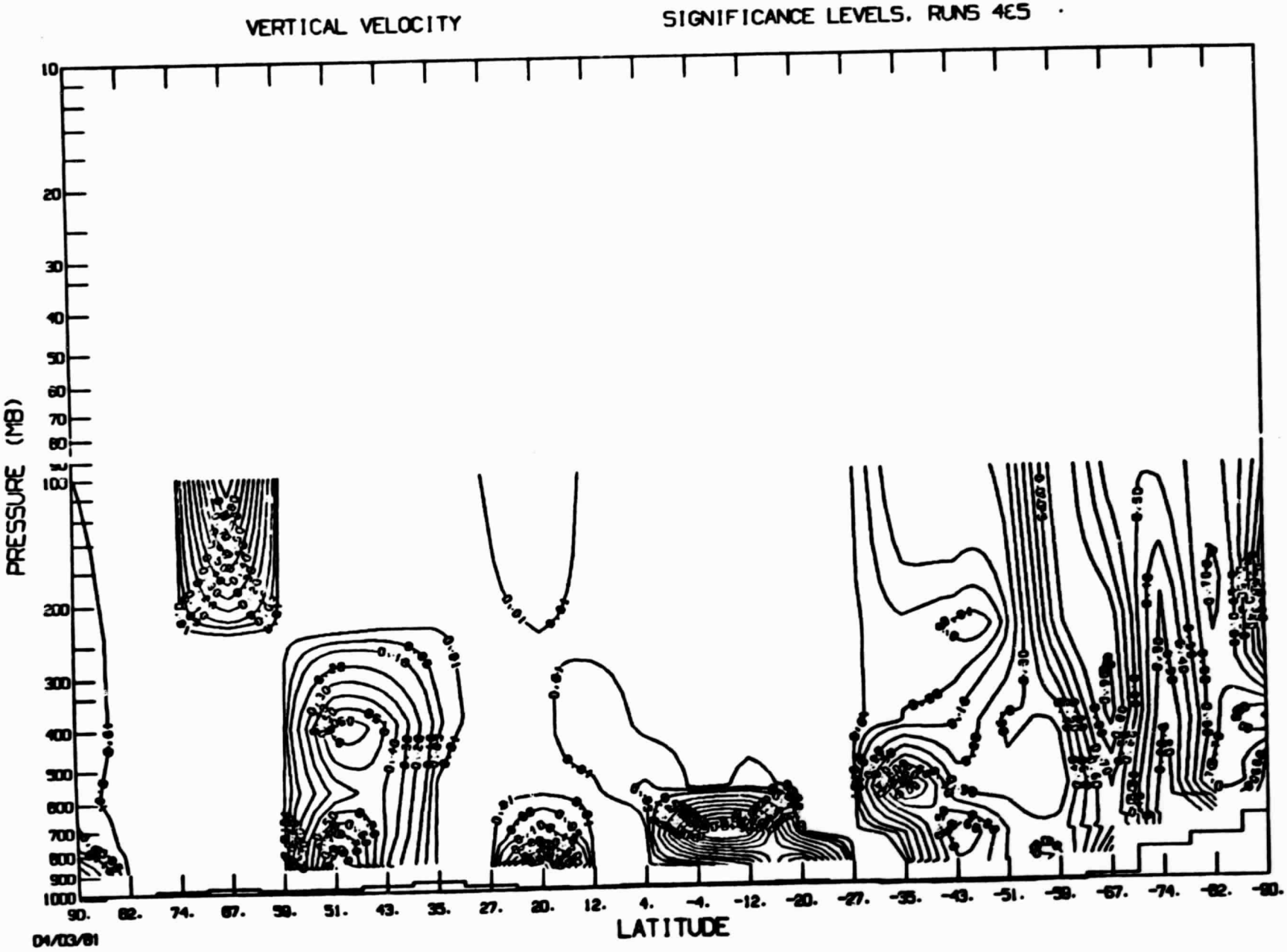

Fig. 12i